1

Elaboration of Nanoparticles

Many methods have been developed for the preparation of metal powders depending on their desired basic characteristics, such as size, size distribution, morphology and specific surface area, to which other properties can be added, such as chemical reactivity and electrostatic stability. These methods for producing powders can be grouped in three large families. The first group is based on solid-phase methods, which consist essentially of mechanical milling and mechanosynthesis or reactive milling.

The second one is based on methods by which powders are elaborated in the liquid phase:

– sonochemical synthesis;

– microemulsion synthesis;

– solvothermal synthesis;

– sol-gel synthesis.

The third group includes methods for elaborating powders in the gas phase:

– inert gas condensation;

– explosion of metal wires;

– thermal plasmas;

– laser ablation;

– pyrotechnic synthesis.

This chapter does not claim to provide an exhaustive approach to all of the nanoparticle synthesis methods, as it more specifically focuses on various implementations for obtaining nanosized metal or metal oxide particles that may present an interest for the mixture-based formulation of nanothermites.

1.1. Solid-phase elaboration

1.1.1. *Mechanical milling*

For thousands of years, man has resorted to various milling methods in order to reduce the particle size of materials. However, in the 1960s, Benjamin developed a new method, high energy milling, which allowed for obtaining materials with nanoscale organization [BEN 70, BEN 74].

Starting from the 1980s, this technique was rapidly developed, as it allowed for obtaining structural states that are difficult to obtain by other synthesis methods, and even impossible to obtain by classical methods, such as melting solidification.

As an example, the preparation of the amorphous alloy type of compounds [WEE 88] can be mentioned. The works of Gaffet *et al.* showed that injected mechanical power was the parameter controlling the crystalline to amorphous transition in nickel alloys. This is obtained in a planetary mill by independently varying the rotation speeds of the disc and satellites [GAF 91]. A further example is to obtain supersaturated solid solutions from immiscible elements at thermodynamic equilibrium [YAV 92] or metastable crystalline phases [KOC 96, KOC 93].

Two terms are commonly employed in the literature to refer to high energy milling. The term mechanosynthesis is used when powders of different nature are milled together to finally obtain materials presenting new alloy compositions and/or new structures, or when chemical reactions are activated by the mechanical energy transferred during the phenomena triggered by milling [SUR 01, GLU 08].

The term mechanical milling or mechanomilling is employed when high energy milling is used not only to reduce the size of powder grains but also to modify the structure and/or microstructure of powders.

1.1.1.1. *Principle*

High energy milling is a method that permits us to obtain in solid phase ultrafine and homogeneous powders by exerting mechanical stress on a material. This

consists of introducing one or several materials in a sealed chamber that contains one or several impactors, which are generally spherical, and shake everything in a more or less forceful manner. Under the effect of the mechanical energy transferred during collisions, the powder grains are subjected to very strong plastic deformations and go through a sequence of fractures and cold welding.

The plastic deformation rate increases enormously under milling [DEL 97], which leads to a significant increase in the hardness of the material with milling duration [KIM 95].

Nevertheless, a material's toughness cannot increase indefinitely with decreasing grain size because the reinforcement mechanism relies on the pile-up of dislocations at the level of obstacles, such as grain boundaries. Therefore, Hall–Petch law is valid as long as the grain size of the nanocrystalline material can sustain the dislocation pile-up.

$$\sigma_c = \sigma_0 + \frac{k}{\sqrt{d}} \text{ (Hall–Petch law)} \qquad [1.1]$$

where σ_c is the yield strength, d is the size of crystal grains and σ_0 and k are material-dependent constants.

Nieh and Wadsworth [NIE 91] propose a mechanism that describes the dislocation pile-up at grain boundaries and carry forward a relation that allows us to estimate the critical distance between two dislocations.

$$Lc = \frac{3Gb}{\pi(1-\nu)H} \qquad [1.2]$$

where G is the shear modulus, ν is Poisson's ratio, b is the Burgers vector, h is the material's hardness and Lc is the critical distance between two dislocations.

Nevertheless, the decrease in grain size is also limited by the rate of dislocation recombination during milling. Fetch *et al.* [FEC 90] have shown that dislocations induced by mechanical milling combine and annihilate starting from a certain level of constraint, which results in a decrease in dislocation density. This effect is all the more important for the materials with low melting points, such as aluminum. Thus, for these materials, dislocation density is instead controlled by the recombination rate rather than by the deformation energy as a result of milling. The opposite is observed for materials with high melting point. Grain size is instead controlled by plastic deformation. When equilibrium is reached, the new deformations that can occur are grain boundary slidings that do not influence nanostructure [KIM 95, ZHA 01].

Eckert *et al.* have shown that the minimal grain size induced is inversely proportional with the melting temperature for the group of metals with face-centered cubic crystal structure. This seems quite clear for the four metals with the lowest melting points (Al, Ag, Cu and Ni) [ECK 92]. The other metals having a face-centered cubic crystal structure and higher melting points, which were studied (Pd, Rh, Ir) along with the metals with centered cubic and hexagonal close packed crystal structure [FEC 90], seem to have a grain size that is constant with the melting temperature.

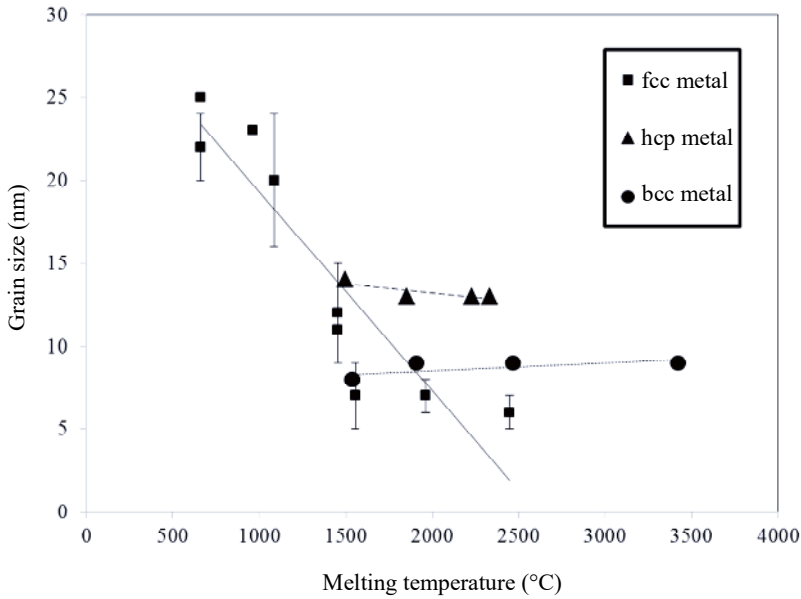

Figure 1.1. *Grain size as a function of melting temperature according to data from [ECK, 92, FEC 90, OLE 96]*

Ball milling and associated methods provide effective means for producing particles from bulk starting materials, and in the case of brittle materials it is possible to obtain a size reduction in a range below 100 nm.

Works conducted by Svrcek *et al.* aimed at the fragmentation of crystalline silicon by means of a planetary mill have allowed us to obtain particles of sizes between 2 and 6 nm, as well as silicon clusters of around 16 nm. The latter are disassembled by adding several drops of 30% ammonia, the size of particles then

being brought to around 4 nm [SVR 05]. Russo *et al.* have obtained nanoparticles with a mean diameter of 55 nm, but also in a small quantity [RUS 11].

In the case of surfactant-assisted direct milling of metal particles, Chakka *et al.* have milled iron and cobalt for 50 h in the presence of around 10% by weight mixture of oleic acid and heptane, thus obtaining more or less spherical particles with sizes between 3 and 9 nm [CHA 06]. In slightly different milling conditions (milling duration of 20 h, same surfactant, but with a concentration of 50% by weight), Poudyal *et al.* have obtained mainly nanoplatelets with a diameter ranging between 5 and 30 µm and a thickness ranging from 20 to 200 nm, but also a small fraction of nanoparticles of the order of 6 nm [POU 11].

This approach may prove ineffective for ductile and malleable materials because the particles are not easily fractured and are cold welded. However, by using a surfactant (oleic acid) diluted at 3 or 5% in a polar solvent (acetonitrile), during milling under argon atmosphere in a planetary ball mill (Retsch PM 400) for 3 h, McMahon *et al.* obtained nanoparticles of aluminum, iron and copper with sizes indicated in Table 1.1 [MCM 14].

Metal	Type of balls	Size of particles
Al	Aluminum balls 8 mm diameter	bimodal 5–10 nm (24% by weight) 20–50 nm
Fe	Mild steel balls 3 mm diameter	10–20 nm
Cu	Copper cylinder 6.35 mm diameter, 6 mm length	Bimodal 250 nm (7% by weight) 500–900 nm

Table 1.1. *Size of nanoparticles obtained by mechanical milling of ductile metals*

1.1.1.2. *The main types of mills*

In order to decrease grain size by mechanical milling or mechanosynthesis, various types of mills can be employed, such as:

– vibratory mill;

– attritor;

– ring mill;

– planetary mill.

1.1.1.2.1. Vibratory mill

Vibratory mills consist of a vial that is set in vibration motion at high frequency. Among them, we can distinguish a type of mill with only one vibration axis and only one milling ball and another type of mill with high-frequency vibration along the three axes. There are many models, which are marketed by several companies such as Fritsch (Pulverisette 0 or 23, for example) or Spex, with the 8000 M shaker mill model.

In this type of mill, mechanical effects are essentially obtained by the balls' collisions with powder. It operates at oscillation frequencies ranging from several dozen to several thousand hertz, and it can mill powder quantities ranging from 10 to 20 g, and within quite short periods of time (of the order of 24 h) [SUR 01]. This type of mill is highly energetic in comparison with the attritor.

1.1.1.2.2. Attritor

The attritor was the first mill used by Benjamin [BEN 70] to obtain metal alloys by milling. It can be vertical [GIL 83] or horizontal [ZOZ 97]. It is composed of a cylinder body that contains balls and a central shaft equipped with paddles perpendicular on the shaft axis. The rotation of this shaft sets balls into motion. A characteristic of this device is the large number of balls used (around 1,000 balls with diameters ranging from 0.2 to 1 cm). The rotation speeds are relatively low and can reach 250 rpm. In this type of mill, powder milling is essentially carried out by frictions among balls or with the body wall [SUR 01].

1.1.1.2.3. Ring mill

The ring mill is a variant of the attritor. It was developed by the team of Senna [HAM 96] and marketed by the Japanese company Nara Machinery Co under the brand name Micros. Its operation relies on a pile-up of zirconium oxide rings on six vertical axes fixed on a rotating disc. The diameter of the central hole of the rings is larger than that of the axis, thus during the rotation of the assembly the off-centered rings rub the wall of the recipient due to the centrifugal force developed. Similarly to the (vertical or horizontal) attritor with balls, the milling of powders is essentially obtained here by friction. Depending on its size, the capacity of this type of device ranges from 0.4 to 33 L and rotation speed varies between 250 and 3,000 revolutions per minute [AVV 01].

1.1.1.2.4. Planetary mill

This mill consists of a rotating platform featuring one to four spinning vials. This device owes its name to the planet-like movement. Due to the simultaneous rotation

of platform and vials, centrifugal forces are induced inside the vials, and they act alternatively in the same and opposite directions. This results in collisions and frictions between balls and the powder.

This type of mill is used for the laboratory synthesis of materials, as it allows for controlling various milling parameters. The capacity of this type of mill ranges from several grams to a hundred grams. The rotation speed of the main disc can vary between 100 and 1,100 revolutions per minute. The main planetary mills are marketed by Retsch company, with the PM range of products or by the Fritsch company with the "Pulverisette" range, some of which were developed starting from the G5 and G7 mills conceived by Gaffet *et al.* [GAF 95].

1.1.1.3. *Milling parameters*

Each milling depends on many parameters that directly influence the morphological and microstructural characteristics of the final product [GAF 04, SUR 01]. The main parameters that can be subjected to variation are the following:

– energy transferred during milling;

– milling duration;

– nature of the milling media;

– size of balls;

– balls-to-powder mass ratio;

– filling ratio;

– milling atmosphere;

– control agents;

– temperature.

1.1.1.3.1. Transferred energy

A mill's energy varies from one type of mill to another. In principle, high energy leads to more rapidly obtaining the final product.

Several teams have taken an interest in the study of modeling and simulation of phenomena that occur during milling. It is in particular worth citing the works of McCormick *et al.* [HUA 97a, DAL 96, HUA 97b], Gaffet *et al*. [ABD 95, CHO 97, ABD 96], Courtney *et al.* [MAU 94, MAU 95a, MAU 95b, MAU 96a, COO 95, MAU 96b, MAU 92, COU 96, RYD 93] or those of Hashimoto and Watanabe [WAT 95, HAS 90].

Modeling the phenomena that are happening in a mill, such as kinematics, mechanisms through which mechanical energy is transferred to the material to be milled, as well as its reaction to this transfer, is a particularly complex task. It is however possible to distinguish phenomena occurring at the local and global level. The first level refers to interactions between balls and powder, while the second relates to the mill's dynamics and kinematics. Gaffet *et al.* have added a third level, which takes into account the structural evolutions of materials subjected to mechanical stress and their evolutions as an energy of energy transfer [CHO 97].

In the vertical vibratory mills with one ball, impacts are frontal, at normal incidence; as for the vibratory mills with several balls, their kinematics are more complex, being characterized by quasi-normal impacts to the walls.

Studying a Ni_xZr_y alloy, Chen has defined milling intensity as the momentum transferred ($M_b \times V_{max}$) to the unit mass of powder (M_p) per unit time (f):

$$I = \frac{M_b V_{max}}{M_p} f \qquad [1.3]$$

with

$$V_{max} = 2\pi A f_{bol} \qquad [1.4]$$

where M_b is the mass of the ball, M_p is the mass of powder, V_{max} is the ball velocity relative to the vial at the moment of impact, f is the frequency of the collisions, A is the amplitude of vibration and f_{bol} is the frequency of vial vibration [CHE 92].

The kinetics of the planetary or horizontal mills depends on a significant number of parameters such as the speed of rotation of vials and platform, load ratio and filling ratio.

Mio *et al*. have studied the influence of various parameters, and in particular the effect of the speed ratio and rotational direction on the balls' impact energy [MIO 02]. The latter increases with platform speed and reaches an optimal value beyond which impact energy decreases.

This so-called critical speed V_c for which impact energy is optimal can be written as:

$$V_c = \sqrt{\frac{R_p}{R_b - r_b} - 1} \qquad [1.5]$$

where R_p is the platform radius, R_b is the vial radius and r_b is the ball radius.

This evolution of impact energy as a function of speed ratios can be explained by balls moving in various modes. Four modes can be distinguished as the speed ratio increases. The "balancing" mode means that balls and powder are moving as a whole. The "cascade" mode means a rolling of balls that leads to a relative movement of balls arriving in the "high" section of the pot, which cascade back to the "low" section of the pot by successive small scale collisions. In addition to this impact mechanism, balls are also sliding on the pot walls. This sliding phenomenon has a direct effect on the balls' starting frequency [DAL 96].

The "cataract" mode describes the situation where balls fill the whole space of the pot and collide with one another. This results in a high number of collisions and the sliding phenomenon is almost absent.

The "rolling" mode occurs at high speeds. Due to the centrifugal effect, balls remain glued to the inner wall of the pot, no ball gets away from the wall to strike the opposite side of the pot and friction effects are weak.

Another important point highlighted by the works of Mio *et al.* is that impact energy is much higher when the pots and platform rotate in opposite directions [MIO 02].

1.1.1.3.2. Milling duration

This parameter defines the minimum time needed for the system to reach a state of equilibrium. It depends on the type of mill used, the way balls act upon powder (collision or friction) and for metals that are sensitive to hydrogen-induced brittle fracture, on the atmosphere [ECK 92]. In effect, Eckert *et al.* have reported that face-centered cubic metals have a tendency to stick to the milling tools during milling under an argon atmosphere, and thus milling effectiveness decreases [FEC 90]. Finally, milling duration depends on the temperature at which it takes place [BOR 97]. At the beginning of the process, cold welding will predominate and can lead to an increase in the particle size [SUR 01]. Then, the fracturation phenomenon will become dominant, and as a result the size of particles will decrease. This will rapidly take place, then will slow down and will finally stop, thus reaching a state of equilibrium [SUR 01, LEE 98]. It generally takes several hours, but it may also take several dozen hours of milling to reach equilibrium [KHA 06, KHA 10, REV 05]. It is also worth noting that the longer the duration, the higher the contamination of powders by the milling media. On the other hand, it is possible to obtain undesirable phases if milling continues beyond what is researched, as shown, for example, by Suryanarayana [SUR 95] on a titanium and aluminum alloy.

During the milling phase, the balls' collisions or frictions with powder generate local heating of the material. In order to minimize heating, a cycle-based approach is often adopted by alternating milling and pause phases [KHA 08, KLE 05].

1.1.1.3.3. Nature of media

The choice of hardness, and therefore of the nature of the material that balls and vials are made of, needs to take into account the powder to be milled. The use of low-hardness material will not allow for the powder milling, while using material with too high hardness will lead to premature wear of the balls and vials, and consequently to a contamination of the milled powder. Materials currently employed are steel nuances [ELE 15, CHE 99] or chromed steel [CUK 01], yttrium oxide stabilized zirconium for the jars [YEN 96] and yttrium oxide or magnesia partially stabilized zirconium [YEN 96] for the balls [BEG 97], agate [TON 91, STU 01, LI 03], corundum [BIL 07], tungsten carbide [PAB 99], WC-Co tungsten carbides [STU 01] and sapphire [ELE 05]. Uses of other materials such as titanium, copper or copper-berylliums, ceramics or silicon nitride are also reported by Suryanarayana [SUR 01].

When a ductile material such as aluminum is milled, balls and vials are generally made of steel [ECK 92, KHA 08, REV 05].

1.1.1.3.4. Size of balls

In most cases, the balls used have the same diameter and are of the same nature [PAB 99]. Shin *et al.* have studied the effect of the size of balls with a constant load ratio on the size of powder particles obtained after milling. They have shown that the optimum diameter of the ball decreases as the rotation speed increases. At a given rotation speed, this is interpreted as an incidence of two opposite effects: the first effect, unfavorable to milling efficiency, is that kinetic energy is lower for smaller size balls. The second effect is that an increase in the number of balls, and thus of collisions, favorably influences milling efficiency [SHI 13].

Vaezi *et al.* have shown that using a mix of balls with various diameters (here, 5 and 10 mm) is more efficient than using balls of the same diameter (5 or 10 mm) at constant load ratio [VAE 12]. The explanation they propose for this phenomenon is that in a mix, the smaller balls can fill the space between the larger ones. Due to this rearrangement of balls, the number of collisions increases. Moreover, as the load ratio is constant, the weight of each large ball equals that of eight smaller balls. This means a higher number of collisions take place, while the balls' kinetic energy is not significantly reduced. This leads to an optimized number of collisions to collision energy ratio for the considered range (rotation speed, load ratio, filling ratio, etc.).

Another hypothesis can be proposed based on the works of Takacs and Pardavi-Horvath [TAK 94], who have shown that during the mechanosynthesis of iron particles produced by the reaction of iron oxide with zinc, the latter, due to its ductility, is deposited on the surface of milling media. Such behavior facilitates cold

welding phenomena. To solve this problem, they have used a mix of balls of various diameters. Even though this may effectively enable us to avoid zinc deposits on walls and balls, no explanation is proposed. In light of these results, Suryanarayana suggests that various sizes of balls generate shear forces. These forces would facilitate powder removal from the surface of vials and balls and would therefore favor fragmentation to the detriment of cold welding, thus improving milling yield [SUR 01].

1.1.1.3.5. Balls-to-powder mass ratio

Balls-to-powder mass ratio, sometimes called load ratio, is an important variable in the milling process. It is defined as the ratio between the balls' mass and powder mass. In the literature, we can equally find low ratios of 1:1, and very high values such as 220:1 [SUR 01]. Generally speaking, a ratio between 10 and 20 to 1 is more commonly used for powder milling in a low capacity mill, such as a SPEX mill or a planetary mill of the Fritsch Pulverisette type [PAB 99, AVE 03].

Load ratio influences the time needed to reach a particular phase state and/or size of the milled powder. The higher the load ratio, the shorter the time needed. An increase in the load ratio is equivalent to an increase in the number of balls, if their mass is on average identical, which involves an increase in the number of collisions per time unit. A higher quantity of energy is transferred to the powder, which more rapidly reaches its final state. We should, however, be aware of the fact that a high quantity of energy transferred within a short period of time can lead to an increase in temperature, which can influence the material's final state.

1.1.1.3.6. Filling ratio

The filling ratio of the pot with balls is another important factor in mechanical milling. A low level of filling will result in low milling yield, while on the other hand, if the filling ratio is too high, there will not be enough space for the balls to move freely. This will reduce the impact energy and will thus decrease process efficiency. An optimal filling ratio is obtained when 50–60% of the pot volume is filled [SUR 01, GAF 04].

1.1.1.3.7. Milling atmosphere

Milling can be performed under various atmospheres, either of neutral gas (argon, helium) or reactive gas [SUR 01, GAF 04], in order to obtain hydrides in a hydrogen atmosphere or to embrittle some metals [ECK 92], oxides under atmospheres of air or oxygen diluted in a neutral gas, or even nitrides when milling takes place under ammonia or nitrogen atmosphere [MIK 92].

The type of atmosphere can also influence the material's final structure. To take an example, Ogino *et al.* have shown that in the case of Cr-Cu alloys milled under

nitrogen or argon atmosphere that contains air, nitrogen atoms were absorbed by the alloy, thus increasing the thermodynamic stability of grain boundaries and amorphous phases compared with the centered cubic phase. Absorption thus facilitates grain refining and causes amorphization. No alloy amorphization is observed in the case of pure argon atmosphere [OGI 90].

Similar works conducted by Li *et al.* highlight the fact that oxygen accelerates the titanium amorphization kinetics [LI 07].

1.1.1.3.8. Control agent

As previously noted, powder particles are alternately cold welded and then fragmented during milling. A control agent can be added during milling in order to modify the welding/fragmentation ratio under given experimental conditions [SUR 01]. The agent acts to lower the surface energy of the powder particles and thus to reduce the cold welding phenomenon, to the benefit of fracturing, the intention being to reduce the size of the grains resulted after complete milling [GAF 04, ECK 92].

Control agents can be solid, liquid or gas [SUR 01, ECK 92]. When liquid agents are added, the particles obtained will have a more homogeneous size distribution compared to adding a solid agent [SUR 01]. The main agents used are stearic acid [LIU 15, WOL 96, RAM 12], alcohols [HUA 97c, LEE 96, RAM 12] or even saturated hydrocarbons (paraffin, hexane, etc.) [AME 95, SUZ 95] or unsaturated hydrocarbons (benzene [IMA 96, LEE 96] and toluene [PAB 99, PAB 96]).

Other more exotic agents are employed as control agents, such as mineral or organic salts of sodium [SHI 99], classical solvents such as tetrahydrofuran [IMA 96] or solid substances such as graphite [MOR 90]. As far as graphite is concerned, it may be interesting not to eliminate it upon milling completion, and to incorporate everything in the formulation of a nanothermite, for the purpose of reducing its sensitivity to electrostatic discharge, for example.

The agent to powder mass ratios is normally within the range from 0.5 to 3% [KHA 06, KHA 08, KLE 05] but in some cases they may reach several hundreds of percent [REV 05] in relation to the load to be milled.

1.1.1.3.9. Milling temperature

Another important parameter in determining the material's final state is the milling temperature. When temperature is high, the size of crystallites increases, but their constraints and solubility in solid state are reduced [HON 94]. The works of Zhou *et al.* referring to aluminum milled at 90 K temperature have shown that grain size reaches an average value of 26 nm after a milling duration of only 8 h, while it

took nearly 100 h of milling at 298 K for the size of the grains to become stabilized at around 25 nm. This shows that, for a similar level of milling energy, cryomilling is more efficient than milling at ambient temperature [ZHO 04].

1.1.1.4. *Mechanosynthesis*

Chemical reactions may take place during mechanical milling. In this case, the process is called reactive milling, mechanochemistry or mechanosynthesis.

Chemical reactions take place at the interface of particles that are subject to continuous renewal during milling. This technique presents the major advantage that the reaction takes place at a much lower temperature (it may often reach ambient temperature) than the thermodynamic equilibrium temperature. Reactions can occur either in stable state or during self-propagated combustions. When the latter is the case, due to the strong increase in local temperature, the resulting particles' diameters are often in the micrometer range, while the particles resulted from self-combustion have diameters in the nanometer range. In order to prevent autoignition of the mixture during milling, experimental milling parameters can often be adjusted so that the impact energy decreases and/or an inert diluent can be added to slow down reaction kinetics.

As previously described in section 1.1.1.3.7, during mechanosynthesis reactions solid matter can react with the milling atmosphere when gases are reactive. To take an example, Liu *et al.* have used mechanosynthesis to obtain tantalum and niobium nitride by milling either pure tantalum or pure niobium grains of around 100 µm in size. They have used for this purpose a planetary mill with a pot and balls (d = 17 mm) made of stainless steel, a balls-to-powder load ratio of 20:1, under nitrogen atmosphere at 2.5 atmospheres. After a milling duration of 80 h, the result was the formation of an NbN phase whose grain size ranged from 10 to 30 nm. By comparison, Ta_2N forms more rapidly than niobium nitride, as the reaction is nearly completed after a milling duration of 16 h. Even though an amorphous phase emerges when milling duration exceeds 30 h, Ta_2N is the only crystalline phase formed throughout milling. The authors advance the hypothesis that in the Ta-N system the amorphous phase emerges due to iron contamination originated in the milling medium [LIU 99].

Solid–liquid reactions may occur when a solid is milled in a reactive liquid, for example, in the case of the synthesis of nanosized crystallized silicon particles by reaction between liquid silicon tetrabromide and magnesium pellets in a Spex 8000 mill, under argon atmosphere [SAN 07] or by the reaction of silicon tetrachloride with lithium pellets in the presence of lithium chloride used as control agent to avoid a combustion reaction [CHA 14b]. The silicon obtained in this latter example is amorphous. It has been recently shown that mechanochemically induced solid–solid reactions could also be used to produce nanosized metal and metal oxide particles.

When adequate conditions in terms of chemical reaction, the stoichiometry of initial reagents and milling parameters (rotation speed or collision frequency, size and number of balls, load ratio, nature and quantity of control agent, etc.) are chosen, mechanochemical treatment can be used for the synthesis of nanosized particles dispersed in a soluble salt matrix. It is possible to obtain weakly agglomerated nanoparticles in the desired phase by selectively eliminating the matrix phase by washing the obtained powder with appropriate solvents.

Reports of the syntheses of nanosized metal and oxide particles obtained by mechanosynthesis are presented in Table 1.2.

Metal	d (nm)	Conditions	Reference
Al	25–40	$AlCl_3 + 3\ Li \rightarrow Al + 3\ LiCl$ Control agent: LiCl load/agent mass: 0.25 Glen Mills Turbula T2C, B/P load ratio: 35/1 Atmosphere: argon, 3 h, steel balls, Washing nitromethane + $AlCl_3$	[PAS 09]
	40–50	$AlCl_3 + 3\ Na \rightarrow Al + 3\ NaCl$ Control agent: NaCl load/agent mass: 0.3 Glen Mills Turbula T2C, B/P load ratio: 55/1 Atmosphere: argon, 4 h 40, steel balls	
Cu	30	$CuCl_2 + 2\ Na \rightarrow Cu + 2\ NaCl$ Control agent: NaCl load/agent mass: 1 SPEX 8000, B/P load ratio: 3/1 Atmosphere: argon, 16 h, steel balls (d = 4.8 mm) Washing with deionized water, then methanol under ultrasounds	[DIN 96a]
Co	10–50	$CoCl_2 + 2\ Na \rightarrow Co + 2\ NaCl$ Control agent: NaCl load/agent mass: 0.5 SPEX 8000, B/P load ratio: 3/1 Atmosphere: argon, 10 h, steel balls (d = 4.8 mm) Washing with deionized water, then methanol under ultrasounds	[DIN 96b]
Fe	15–20	$FeCl_3 + 3\ Na \rightarrow Fe + 3\ NaCl$ SPEX 8000, B/P load ratio: 3/1 Atmosphere: argon, 16 h, steel balls (d = 4.8 mm) or 24 h (d = 3.2 mm) or 3.3 h (d = 6.4 mm) Washing with deionized water, then methanol under ultrasounds	[DIN 96c]
	30–35	$FeCl_3 + 3/2\ Ca \rightarrow Fe + 3/2\ CaCl_2$ 8 h, steel balls (d = 9.5 mm) $FeCl_3 + Al \rightarrow Fe + AlCl_3$	
	50–60	90 h, steel balls (d = 6.4 mm) Control agent: NaCl load/agent mass: 1	

Ni	10–20	$NiCl_2$ +2 Na → Ni + 2 NaCl Control agent: NaCl load/agent mass: 0.5 SPEX 8000, B/P load ratio: 3/1 Atmosphere: argon, 16 h, steel balls (d = 4.8 mm) Washing with deionized water, then methanol under ultrasounds	[DIN 96b, DIN 99]
	10–500	$NiCl_2$ + Mg → Ni + $MgCl_2$ SPEX 8000, B/P load ratio: 10/1 Atmosphere: argon 3 h, steel balls (d = 4 mm) Washing with deionized water, then methanol under ultrasounds	[BAB 97]
Si	20	$SiBr_4$ + 2 Mg → Si + 2 $MgBr_2$ SPEX 8000, B/P load ratio: 10/1 Atmosphere: argon 20 h, steel balls (2 of d = 11.1 mm and one of 14.3 mm) washing 40 mL of HCl (37%) and heated at 70°C for 30 min, then ethanol.	[SAN 07]
	51 13	$SiCl_4$ + 4 Li → Si + 4 LiCl Glen Mills Turbula T2C, B/P load ratio: 90/1 Atmosphere: argon, 24 h, steel balls (d = 7.9 mm and 12.7 mm), washing, tetrahydrofuran, Without control agent With control agent: LiCl load/agent mass: 10	[CHA 14b]
	2.5	3 SiO_2 + 4 Al → 3 Si + 2 Al_2O_3 SPEX 8000, B/P load ratio: 23/1 Atmosphere: argon 15 h, stainless steel balls (total weight 24.87 g)	[ARA 03]
	5	SiO_2 + C → Si + CO_2 Planetary mill, B/P load ratio: 10/1 Atmosphere: argon, 240 h, stainless steel balls (d = 7.5 mm)	[LAM 00]
Sb	19	Sb_2S_3 + 3 Fe → 2 Sb + 3 FeS Fritsch Pulverisette 6, B/P load ratio: 120/1 Atmosphere: argon, 3 h, 50 balls WC (d = 10 mm)	[BAL 07]

Table 1.2. *Mechanosynthesis of nanosized metal particles*

Oxide	d (nm)	Conditions	Reference
Al_2O_3	10–20	$2\ AlCl_3 + 3\ CaO \rightarrow Al_2O_3 + 3\ CaCl_2$ SPEX 8000, B/P load ratio: 8/1 Atmosphere: argon, 24 h, balls (d = 9.5 mm) Annealed at 400°C, 1 h Washing with deionized water under ultrasounds	[DIN 96d]
CeO_2	10	$CeCl_3 + 3\ NaOH \rightarrow Ce(OH)_3 + 3\ NaCl$ Control agent: NaCl 12 equivalents SPEX 8000, B/P load ratio: 10/1 Atmosphere: argon, 4 h, steel balls (d = 6.4 mm), annealed at 500°C, 1 h Washing with deionized water under ultrasounds	[TSU 01c]
	19	$CeCl_3 + 3/2\ CaO + 1/4\ O_2 \rightarrow CeO_2 + 3/2\ CaCl_2$ SPEX 8000, 24 h, annealed at 400°C, 6 h	[GOP 00]
	40–70	$2\ CeCl_3 \cdot 6H_2O + 3\ Na_2CO_3 \cdot 10H_2O \rightarrow Ce_2(CO)_3 \cdot n\ H_2O + 6$ NaCl + (42-n) H_2O SPEX 8000, B/P load ratio: 5/1 24 h, annealed at 900°C, 1 h Washing with deionized water under ultrasounds	[LI 05]
Cr_2O_3	3 50 10–100 10–80	$Na_2Cr_2O_7 + S \rightarrow Cr_2O_3 + Na_2SO_4$ Control agent: NaCl 187% SPEX 8000, B/P load ratio: 10/1 Atmosphere: argon, 6 h, steel balls (d= 12.7 mm), annealed at 450°C, 1h or Annealed at 500°C, 1 h or Annealed at 600°C, 1 h Washing with deionized water under ultrasounds With Na_2SO_4 as control agent and annealed at 800°C, 1 h	[TSU 00]
Fe_2O_3	10–30	$2\ FeCl_3 + 3\ CaO \rightarrow Fe_2O_3 + 3\ CaCl_2$ Control agent: $CaCl_2$: load/agent mass: 1 SPEX 8000, B/P load ratio: 5/1 Atmosphere: argon, 24 h, steel balls (d = 4.8 mm), annealed at 150°C, 1 h Washing with methanol under ultrasounds	[DIN 97b]
	20–50	$2\ FeCl_3 + 3\ Ca(OH)_2 \rightarrow Fe_2O_3 + 3\ CaCl_2 + 3\ H_2O$ Same conditions except annealed at 200°C, 1 h	
	5 50–100 Hexagonal platelets D: 50–200 E: 20–40	$Fe_2(SO_4)_3 + 3\ Na_2CO_3 \rightarrow Fe_2(CO_3)_3 + 3\ Na_2SO_4 \rightarrow$ $Fe_2(CO_3)_3 \rightarrow Fe_2O_3 + 3Na_2SO_4 + 3\ CO_2$ SPEX 8000, B/P load ratio: 10/1 Atmosphere: air, 4 h, 6 steel balls (d = 12.7 mm), annealed at 350°C, 1 h or Annealed at 500°C, 1 h or Annealed at 700°C, 1 h Washing with deionized water under ultrasounds	[TSU 11]

Gd_2O_3	5–50 Platelets length 20–150 E: 5–20	$GdCl_3 + 3\ NaOH \rightarrow Gd(OH)_3 + 3\ NaCl$ Control agent: NaCl load/agent mass: 0.1 SPEX 8000, B/P load ratio: 10/1 Atmosphere: argon, 24 h, balls (d = 6.4 mm), annealed at 500°C, 1/2 h Washing with deionized water under ultrasounds $2\ GdCl_3 + 3\ CaO \rightarrow Gd_2O_3 + 3\ CaCl_2$ SPEX 8000, B/P load ratio: 40/1 Atmosphere: argon, 8 h, balls (d = 12.7 mm) Washing and then annealed at 800°C, 1 h	[TSU 99] [TSU 98]
Nb_2O_5	10–100 200–1,000	$2\ NbCl_5 + 5\ Na_2CO_3 \rightarrow Nb_2O_5 + 10\ NaCl + 5\ CO_2$ Control agent: NaCl 8 equivalent SPEX 8000, B/P load ratio: 10/1 Atmosphere: argon, 6 h, steel balls (d = 12.7 mm), annealed at 550°C, 1/2 h Washing with deionized water under ultrasounds $2\ NbCl_5 + 5\ MgO \rightarrow Nb_2O_5 + 5\ MgCl_2$ Same condition, milling duration 8h Annealed at 400°C	[TSU 01a]
SnO_2	5–30	$2\ SnCl_2 + 2\ Na_2CO_3 \rightarrow 2\ SnCO_3 + 4\ NaCl$ $SnCO_3 \rightarrow SnO + CO_2$ $SnO + ½\ O_2 \rightarrow SnO_2$ Control agent: NaCl: 100% equivalents B/P load ratio: 10/1 Atmosphere: argon, 6 h, chromed steel balls (d = 6.4 mm), annealed at 400°C, under air Washing with deionized water under ultrasounds	[CUK 01]
TiO_2	37	$TiOSO_4\ xH_2O + Na_2CO_3 \rightarrow TiO_2 + Na_2SO_4 + xH_2O + CO_2$ TB-1 Kadan ltd, B/P load ratio: 20/1 Atmosphere: argon, 6 h, corundum balls (d = 11 mm), annealed at 700°C, 1 h under air Washing with deionized water under ultrasounds	[BIL 07]
Y_2O_3	28	$2\ YCl_3 + 6\ LiOH \rightarrow Y_2O_3 + 6\ LiCl + 3\ H_2O$ SPEX 8000, Atmosphere: argon, 4 h, 20 steel balls (d = 9.5 mm), annealed at 500°C, 1 h Washing with deionized water then methanol under ultrasounds	[DOD 01a]
ZnO	10–40	$ZnCl_2 + NaCO_3 \rightarrow ZnCO_3 + 2\ NaCl$ $ZnCO_3 \rightarrow ZnO + CO_2$ Control agent: NaCl 8.6 equivalents SPEX 8000, B/P load ratio: 10/1 Atmosphere: argon, 6 h, steel balls (d = 6.4 mm), annealed at 400°C, 1/2 h under air Washing with deionized water under ultrasounds	[TSU 01b]

ZrO_2	5–10	$ZrCl_4 + 2\ CaO \rightarrow ZrO_2 + 2\ CaCl_2$ SPEX 8000, B/P load ratio: 5/1 Atmosphere: argon, 20 h, steel balls (d = 9.5 mm), annealed at 350°C, 1/2 h Washing with methanol under ultrasounds	[DIN 97a]
	14	$ZrCl_4 + 4\ LiOH \rightarrow ZrO_2 + 4\ LiCl + 2\ H_2O$ SPEX 8000, Atmosphere: Argon, 4 h, 20 steel balls (d = 9.5 mm), annealed at 500°C, 1 h Washing with deionized water then methanol under ultrasounds	[DOD 01a]
	7	$ZrCl_4 + 2\ MgO \rightarrow ZrO_2 + 2\ MgCl_2$ SPEX 8000, Atmosphere: argon, 12 h Annealed at 500°C, 1 h Washing with deionized water under ultrasounds	[DOD 01b]
	32	$ZrCl_4 + 2\ Li_2O \rightarrow ZrO_2 + 4\ LiCl$ Control agent: LiCl, 4 equivalents SPEX 8000, B/P load ratio: 10/1 Atmosphere: argon, 6 h, 20 steel balls (d = 9.5 mm), annealed at 400°C, 1 h Washing with deionized water then methanol under ultrasounds	[DOD 01c]

Table 1.3. *Mecanosynthesis of nanosized metal oxide particles: D: diameter, E: thickness, L: length*

1.1.1.5. *Conclusion*

It is possible to obtain nanosized particles through the direct milling of metals of oxides by mechanical milling of brittle materials, and as well of ductile materials such as copper or aluminum, provided that a surfactant is employed during the milling.

The same applies to reactive milling, which offers the possibility to obtain metals or metal oxides in the form of crystallites or nanosized amorphous particles. This often requires the use of a control agent, which will act as a diluent by preventing or delaying autoignition reactions, and due to its dilution effect, it will also strongly reduce the effects of agglomeration between nanosized grains. The drawbacks of the mechanosynthesis technique are, on the one hand, the low quantities produced and, on the other hand, the duration of the process, which is often of several hours. However, the most important problem is the contamination of powders by the milling media.

It is worth noting that oxides manufactured by this method have low "reactivity" when they are used for the preparation of nanothermites. Examples of the most reactive oxides for this application include WO_3, MoO_3, CuO, Bi_2O_3, I_2O_5 or Ag_2O.

1.2. Liquid-phase elaboration

1.2.1. *Sonochemistry*

1.2.1.1. *Principle*

Sonochemistry is a technique that uses ultrasonic waves to activate or accelerate chemical reactions. This simple method is recommended in particular for organizing nanoscale structures. The use of this method allows us to obtain amorphous or crystalline particles or even metal or metal oxide colloidal suspensions. The ultrasounds used in sonochemistry are essentially in the range of low frequencies (between 16 and 100 kHz) [PIN 08, KOL 96, KOL 12] and high frequencies (between 100 kHz and 1 MHz) [ABU 14, REY 15, FUJ 14]. Very high frequency ultrasounds (above 1 MHz) are generally used for diagnostic purposes, even though frequencies above 1 MHz may sometimes be used in sonochemistry [REY 15].

1.2.1.2. *Effects of implementation parameters*

1.2.1.2.1. Power of emission

A second criterion for differentiating ultrasonic waves is the power of emission. When this is below 1 W, ultrasounds induce no modification of the medium. In this case, there is only vibratory interaction between the wave and the matter it passes through. Such low powers are employed in the non-destructive testing of materials or structures, or in medical diagnosis. When the wave has higher levels of power, its passing through matter is accompanied by nonlinear physics phenomena and associated chemical reactions. In contrast with photochemical phenomena, the chemistry associated with acoustic waves does not depend on the wave–matter direct interaction. It is essentially due to acoustic cavitation. A characteristic of the cavitation phenomenon is the formation of vapor bubbles in a liquid. This phenomenon emerges when hydrostatic pressure decreases below the value of the liquid vapor tension for a given temperature. A cavitation bubble's evolution depends on its initial volume, the field of pressure it is subjected to and the liquid surface tension. Small size bubbles that are subjected to low pressure fields disappear by rapidly dissolving in the surrounding liquid.

At high values of the pressure field, the bubbles' volume fluctuates. During depression, the bubble's volume increases under the influence of vaporization and gas diffusion. When the bubble is compressed, its gas content is dissolved in the liquid and vapor condenses at the liquid/gas interface. The implosion of the

cavitation bubble results in a very sharp increase in temperature, which can reach values above 5,000°C, pressures above 500 atmospheres, local accelerations above 10 g, photon emissions and shockwaves over a duration of less than a microsecond [SUS 89]. These extreme conditions enable the development of chemical reactions that occur only at high energies [SUS 91]. Moreover, due to the rapid cooling of vapors in contact with the liquid interface, metallic glasses can be obtained, such as amorphous iron powder [SUS 91].

Volatile precursors, such as metal carbonyls, are to a large extent thermally decomposed inside the cavitation bubble and lead to the formation of metal nanoparticles [SUS 96, KOL 96], oxides [KOL 12, ABU 05], carbides [SUS 96] or sulfides [LOP 14].

As far as non-volatile precursors are concerned, chemical reactions take place in the vicinity of the liquid/gas interface of the cavitation bubble. On the one hand, they take place by the interaction of radicals formed during solvent pyrolysis in the cavitation bubble with ions in solution, and on the other hand, as a result of temperature, which, despite being lower in the vicinity of the interface, it is however high enough to trigger thermal decomposition of the present solutes and to generate radicals that will also interact with the species that are present in solution. Several other experimental parameters have an influence on the nature and size of the particles produced.

1.2.1.2.2. Frequency of emission

Reyman *et al.* have shown that the rate of Fe^{3+} sonochemical production from Fe^{2+} decreased linearly as a function of frequency. By contrast, the size of iron oxide particles formed does not seem to depend on frequency [REY 15].

1.2.1.2.3. Amplitude of emission

In their works on the sonochemical synthesis of lead dioxide, Ghasemi *et al.* have shown that the size of the particles formed depended on the amplitude of the wave. For an amplitude of 36 µm, lead oxide particles take the form of aggregates of 300–350 nm. For an amplitude of 60 µm, the size of aggregates ranges between 50 and 100 nm. Thus, an increase in the amplitude of ultrasonic waves reduces the particles' growth rate [GHA 08].

1.2.1.2.4. Duration of emission

The impact of the duration of ultrasonic emission on the reaction medium was most notably analyzed by Aslani and colleagues, in relation with the production of nickel oxide (NiO) nanoparticles. For a power in the range from 12 to 18 W, the mean size of particles goes from 60 nm, for a 2 h emission time, to a mean size of 20 nm, for a 3 h emission time [ASL 11].

1.2.1.2.5. Impact of solvent

There are other solution-dependent parameters that can influence wave propagation, such as the viscosity of solution, which depends on the solvent's nature and temperature. The increase in the viscosity of a liquid increases the power threshold for reaching the cavity. Compared to low viscosity liquids, viscous liquids require higher variations of acoustic pressure in order to allow the cavitation phenomenon.

The energy provided by acoustic emission is partly dissipated as heat, which leads to an increase in the medium's temperature. Therefore, it is sometimes necessary to exert thermal control of the medium by a heat transfer fluid to ensure constant temperature during work. The impact of temperature increase during reaction is a complex issue, as temperature influences the viscosity of the reaction medium, vapor pressure and concentrations of dissolved gases, but also the reaction kinetics involved [GHA 08].

Reports of several examples of sonochemical production of metal oxide and metal nanoparticles are provided by Tables 1.4 and 1.5.

Oxide	*d* (nm)	Conditions	Reference
Bi_2O_3	40–100	$Bi(NO_3)_3$, PVP, H_2O, pH 11 US: 600 W, 20 kHz, 75 min, 60°C	[ZHA 06a]
	<23	$Bi(NO_3)_3$, PVP, H_2O, pH 1 US: 200 W, 24 kHz, 1 h, 80°C Annealed at 300°C, under air, 1 h	[AZI 15]
Cr_2O_3	200	$Cr_2O_7(NH_4)_2$, H_2O US: 100W, 20 kHz, 3 h	[DHA 97]
CuO	15–40	$Cu(NO_3)_2$, NaOH aq. (0.1–0.3M) US: 20 kHz, 600 W, 90°C, 0.5–2 h, Annealed at 100–300°C	[PEN 14]
	Nanorods 70 × 350	$CuSO_4$, NaOH aq. (0.05 M), polyvinyl alcohol US: 80°C, 30 min, then maturing at 25°C, 12 h	[SHU 13]
	50–70	$Cu(NO_3)_2$, H_2O, NaOH aq. (0.05 M) US: 20 kHz, 750 W, 1/2 h Annealed at 700°C	[WON 11]
Fe_2O_3	20 nm 5–10	$Fe(acac)_3$, tetraglyme, 2% vol. H_2O $Fe(acac)_3$, tetraglyme, 6% vol. H_2O US: 20 kHz, 13 W, 8 h	[PIN 08] [BAN 07]
Amorphous hollow spheres	6 <20	$Fe(CO)_5$, hexadecane C (4–12 nm), $Fe(CO)_5$, hexadecane and annealed at 450°C, 2 h	[REY 15]
	21–23	US: 20 kHz, 50 W, 20°C, 3 h, atm. Ar. $FeSO_4$, NaOH aq. (0.2 M), ethylene glycol US: 581 kHz, 29W, 20°C, 35 min	

Fe_3O_4	3–14	$Fe(CO)_5$, SDS (0.02M), H_2O US: 20 kHz, 25°C, 3 h, atm. Air.	[ABU 05]
HfO_2	14–25	$HfCl_4$, NaOH aq. US: 500W, 1 h Annealed at 500°C, 2 h	[AMA 12]
In_2O_3	15–30	$In(acac)_2$, H_2O, pH : 9–10 US: 20 kHz, 750 W, 1 h, 80–90°C	[HAF 14]
MnO_2	50–150 200–1,000	$KMnO_4$, H_2O, US: 200 kHz, 13 W, 20°C, pH 6.0, 9 min US: 200 kHz, 13W, 20°C, pH 9.3, 8 min	[ABU 14]
Mn_2O_3	50	$KMnO_4$, H_2O US: 100 W, 20 kHz, 3 h	[DHA 97]
Mn_3O_4	60 10–40 30–40 20–70	$MnSO_4$ $Mn(NO_3)_2$ $Mn(CH_3COO)_2$ Mn(acetylacetonate) US: 180 W, 12 h	[KUM 03]
NiO	20–150	$Ni(CH_3COO)_2$, NaOH aq. (0.1 M), H_2O Ethanol, polyethylene glycol US: 6–18 W, 30 kHz, 0.5–3 h, then calcination 500°C, 1/2 h	[ASL 11]
PbO_2	50–150	PbO, $(NH_4)_2S_2O_8$, H_2O US: 20 kHz, 600 W, 75°C, 1 h	[GHA 08]
SiO_2	60	$Si(OC_2H_5)_4$, methanol, H_2O, BS, US: 20 kHz, 100 W, 1/2 h, 25°C, atm. Air then ethylene diamine, washing with methanol, calcination 600°C, 2 h.	[MAS 14, MAS 16]
SnO_2	23–30	$SnCl_2$, PEG, H_2O, 1,2-ethylene diamine US: 10 min Then calcination, under air, 500°C, 3 h	[WAN 15a]
TiO_2	17	$Ti(OC_2H_5)_4$, ethanol, H_2O, acetic acid US: 38 kHz, 30 W Calcination 530 K	[AWA 03]
$WO_3 \cdot H_2O$ WO_3	Nanoplates L:250 E: several dozens 50–70	WCl_6, H_2O US : 20 kHz, 1,000 W, 200°C $W(CO)_6$, Diphenylmethane US: 20 kHz, 100 W, 90°C, 3 h, atm Ar/O_2 (8/2), then annealed at 1,000°C, under air	[CHA 11a] [KOL 12]
ZnO	4–7	$Zn(CH_3COO)_2$, LiOH, Ethanol, US: 20 kHz, 900 W, 1–120 min	[QIA 03]

Table 1.4. *Sonochemical synthesis of metal oxide nanoparticles acac, acethylacetonate; BS, Schiff base; bis(acethylacetonato) propylene-1,3 diimine or bis (acethylacetonato) butylene-1,4 diimine; SDS, sodium dodecylsulfate; PVP, polyvinylpyrrolidone*

Element	d (nm)	Conditions	Reference
Fe	10	$Fe(CO)_5$, decane US: 20 kHz, 100 W, 0°C, 3 h, atm. Ar	[SUS 91]
	8	$Fe(CO)_5$, octanol, PVP (M_w 40,000), US, 20°C, 1 h, atm. Ar	[SUS 96]
	8	$Fe(CO)_5$, octanol, oleic acid US: 30°C, 3 h, atm. Ar	
Cu	50–70	$Cu(N_2H_3CO_2)_2$, H_2O US : 20 kHz, 100 W, 2–3 h, 80°C, atm. Ar/H_2 (95/5)	[DHA 98]
Ni	10	$Ni(CO)_4$, decane US: 20 kHz, 100 W, 3 h, 0°C, atm. Ar	[KOL 96]
C	150–400	Toluene / H_2O (1/100 in volume) US: 480 kHz, 2.5 W, 6 h, 20°C	[FUJ 14]

Table 1.5. *Sonochemical synthesis of metal and carbon nanoparticles*

1.2.1.3. *Conclusion*

Sonochemical synthesis proves to be a technique that is easy to implement. Nevertheless, the quantities manufactured are low, of the order of several grams per experiment. Sonochemistry therefore remains a laboratory technique. It is worth noting that pollution problems may occur due to the erosion of metals in the probe alloy when waves are generated by an emission probe immersed in the solution.

1.2.2. *Microemulsion synthesis*

1.2.2.1. *Definition*

The term microemulsion was introduced by Schulmann *et al.* [SCH 59] and it denotes a thermodynamically stable dispersion of two immiscible liquids. Adding a surfactant stabilizes the system. At low concentration, the surfactant is dissolved and is present as a monomer. When its concentration in solution reaches a critical value, the spontaneous self-assembly of monomers into various structures and aggregates takes place.

The phase diagrams of microemulsions are very rich, exhibiting a very wide variety of structures. These result from geometrical constraints, curvature energy, interface tension and solubility of surfactant in the continuous phase. Thus, it is possible to obtain oil-in-water or water-in-oil dispersions and also bicontinuous

structures. The form taken by dispersed structures, called micelles, is generally spherical. This form is the most frequent because, due to its surface/volume ratio, it is the most advantageous for minimizing the contribution of interface tension to the system's overall energy. Cylindrical forms have nevertheless been experimentally observed [SVE 00].

Micelles emerge when surfactant concentration exceeds critical micelle concentration. "Micelles" are referenced when the polar side of the surfactant is at the outer surface of the micelle in contact with the continuous polar phase and the lipophilic organic phase inside the micelle. On the contrary, a "water in oil" microemulsion is formed when water is dispersed in a continuous organic phase. In this case, the surfactant molecules self-assemble to form aggregates called "reverse micelles", the polar parts of the surfactant being directed toward the inner part of the micelle.

These emulsions can be used to carry out chemical reactions and they most notably permit the synthesis of metal or metal oxide nanoparticles.

In 1982, Boutonnet *et al.* obtained noble metal (Pt, Pd, Rh and Ir) nanoparticles of very small sizes (from 2 to 5 nm) by reduction of chloride salts with either hydrazine or a hydrogen bubbling in an emulsion consisting of water, octanol and cetyltrimethylammonium bromide (CTAB), or by using a microemulsion composed of water, hexane and pentaethyleneglycol dodecylether (PEDGE) [BOU 82].

1.2.2.2. *Preparation of nanoparticles*

The most widespread methodology for the synthesis of nanoparticles consists of mixing two identical inverted microemulsions (water: oil: surfactant) each containing a different reagent dissolved in the aqueous phase confined in the micelles [KIM 01]. The second method consists of adding a reagent in pure state [BOU 82] or dissolved in the aqueous phase [PAN 02, QIU 99] directly to a solution of inverted micelles containing the other reagent. There are numerous syntheses in micellar phase, and only those reactions leading to the production of solid nanoparticles will be developed here.

1.2.2.3. *Mechanisms involved*

There are several works that attempt to explain the mechanisms of formation of nanoparticles in microemulsions. Destrée and Nagy [DES 06] propose a mechanism that is based on LaMer diagram [LAM 50] representing the concentration of dissolved species as a function of time during crystal formation. In the case of emulsion synthesis, nucleation occurs at the beginning of the reaction in micelles that, on the one hand, have sufficient ion concentration, allowing for the nucleation

to generate a stable nucleus and, on the other hand, have been in contact with the second reagent. According to this model, the first stage in nanoparticle formation is the nucleation, followed by the growth of particles, in the second stage. Growth kinetics being faster than nucleation kinetics, the latter can be neglected and only growth of nanoparticles takes place. When the reaction is completed, a population of quasi-monodisperse particles will be obtained.

According to a second model, the reagent will thermodynamically stabilize the formed nanoparticles. The size of particles will thus remain constant, although nucleation goes on simultaneously with the particle growth stage. The particles having reached a certain size cease to grow due to the surfactant stabilizing effect, irrespective of the micelles' concentration in metal salts or size.

These mechanisms seem to be supported by the works of Concha. Tojo *et al.* conducted a simulation-based study of nucleation and particle growth processes [TOJ 97]. Their works show that separation in time of the nucleation and growth stages is clearly facilitated by a high concentration of reagent in the droplets. When concentration is low, nucleation and growth phenomena take place simultaneously.

These works also show that the growth of particles may be due to the "Ostwald ripening" process, which consists of the solubilization of a small particle that afterward redeposits on a larger particle. Because of the difference in free energy between small and large particles, they cannot be in equilibrium at the same concentration in solution. Due to Gibbs–Thomson effect, smaller particles having higher solubility than the large ones, they are slowly dissolved. Thus, larger particles end up within a slightly supersaturated solution and the solute precipitates on their surface. In the case of microemulsions, this mechanism develops inside the micelles and by exchange among micelles when they interact. The second process of growth of particles is the autocatalytic process [BES 05].

For the classical synthesis path involving the mixture of two emulsions, Fletcher has proposed two limit cases describing the exchanges of compounds solubilized in water inside micelles [FLE 87]. First of all, the reactive species should remain confined inside the droplets, which excludes the possibility to diffuse in another droplet by passing through the continuous phase formed by the organic solvent. In effect, given the low solubility of salts in organic media, a dynamic exchange of reagents among the droplets through the continuous organic phase is not favorable. Second, the exchange of solutes inside the micelle has to be the key stage in the reaction kinetics.

The first limit case involves the two droplets getting closer and in contact, but without coalescing. The solubilized species diffuse through the surfactant bilayer at the point of contact between the droplets.

The second limit case involves the fusion of the two droplets and formation of one "dimer" droplet, a structure whose lifetime is below one microsecond, and which afterward breaks up into two new droplets that contain a mixture of solutes of the two initial droplets.

The simulation works of Bandyopadhyaya *et al.* referring to the method of classical synthesis with two emulsions corroborate previous works. The mechanism proposed for obtaining nanoparticles requires that micelles exchange by coalescence the reagents under soluble form, thus triggering the formation of nuclei, followed by the growth of nanoparticles, supplied by the reagents in solution in the micelles when they come into contact [ETH 06a, ETH 06b, BAN 97, BAN 00]. In order to be able to predict the size of particles, Bandyopadhyaya *et al.* have added a stage of nuclei coagulation during the coalescence of two micelles, each containing a nucleus. The threshold for taking this mechanism into account becomes important when the resulting particle is larger than the micelle issued from the two micelles' fusion [ETH 07].

1.2.2.4. *Influence of implementation parameters*

The diameter of the synthesized particles depends on several implementation parameters. Correlations have been observed between the form of the micelles present in the microemulsion and the form of the particles produced [BUR 05, PIL 03].

1.2.2.4.1. Concentration of surfactant

When water and oil concentrations are constant, an increase in the concentration of surfactant leads to an increase in the number of micelles, but their mean diameter will be smaller. This results in a reduction of the number of metal ions present in a micelle, a fact less favorable to nucleation. By contrast, when there are more micelles, they will collide more frequently, and this can favor the growth process by Ostwald ripening. On the contrary, the quantity of ions in aqueous solution provided at each micelle's contact is lower than it would have been if its size were higher, and thus growth by autocatalysis slows down. This suggests that the growth of particles is subjected to conflicting effects. The work carried out by Lopez-Quintela and Rivas on the control of iron particles' size shows that the size of particles is higher when the concentration of surfactant is low, compared to high surfactant concentration [LOP 93].

1.2.2.4.2. Nature of surfactant

Surfactants are amphiphilic molecules whose hydrophilic part can consist of ions (anions or cations). Their solubilization in water leads to the release of a counterion and the presence of a charge on the polar head: CTAB [CHE 11], sodium dodecylsulfate (SDS) [QIU 99] and even didodecyldimethylammonium bromide [BUM 11] are part of it. There are amphoteric surfactants that, depending on the pH, simultaneously act as anionic and cationic molecules.

Some nonionic surfactants that are commonly used in the microemulsion synthesis of nanoparticles are sorbitan esters (sorbitan monolaurate; SPAN®) or polyethylene glycol esters (TWEEN 80®) [DIC 15], ethers such as IGEPAL co-520® (polyoxomethylene nonylphenylether) [ARR 99],Triton X-100® (4-(1,1,3,3 tetramethylbutyl) phenyl-polyethylene glycol) [WAN 14a, PAN 02] or the PEDGE [BOU 82].

There are also surfactants that have a double hydrophobic chain such as AOT (bis (2-ethylhexyl) sulfosuccinate sodium salt) [LU 15, OH 01] or ammonium carboxylates perfluoroether [MEZ 05] or even perfluorothiols [FER 07]. These are used for the synthesis of metal particles, especially when supercritical carbon dioxide is employed as solvent.

The use of a surfactant for a particular water–oil mixture is not trivial, as besides the resulting phase diagram, micellar exchanges are affected by the very nature of the surfactant. Lopez-Quintea *et al.* have proposed an explanation that involves the flexibility of the surfactant film. This parameter influences the curvature of the film that is at the origin of the creation of a channel between two micelles that are in contact. The more rigid the film, the more reduced the channel, which will induce a decrease in intermicellar exchanges, whereas a more flexible film will facilitate the transfer of reactants through the interdroplet exchange zone [LOP 03, DE 05].

Finally, the charges carried by the surfactant and also by the counterion can trigger modifications of local concentration of reactants, inducing a modification of the nucleation rate.

1.2.2.4.3. Reaction rate

Depending on the nature and concentration of the reduction agent used, the reduction process can be more or less rapid. The higher the reaction rate, the sharper the decrease in particle size. It is possible to prepare metal nanoparticles by the reduction of metal salts, using agents such as sodium borohydride [QI 97] or potassium borohydride [CHE 11], hydrazine [BOU 82] or dihydrogen [LU 15]. Thus, in the case of platinum salts, the reduction with hydrazine is faster than the reduction with bubbled hydrogen [BOU 82]. In order to decrease the time of

reaction, the reducing agent is often added in excess relative to the concentration of metal salt [WAN 01]. The simulation works conducted by Lopez-Quintea *et al.* indicate that the final size of particles is inversely proportional to the reaction rate. They also show that a high reaction rate results in the distribution of particle size being narrower than the one for lower rates [DE 05, BAR 05].

1.2.2.5. *Conclusion*

This method offers a simple way to obtain metal or metal oxide particles of very small size (several nanometers) while allowing for very good control of the particle size and narrow size distribution, and even getting near-monodisperse particles. A weak distribution of particle size is needed for obtaining uniform properties. This is all the more so in the case of mixtures intended for the manufacturing of nanothermites. This will enable us to obtain a more homogeneous mixture of constituents. This control is readily achieved by modifying experimental parameters such as the reactant concentrations and the water:surfactant concentration ratio. In some cases, it is also possible to control the form of particles depending on the ternary system employed (water–oil–surfactant).

One drawback of this technique is the low quantity of product obtained, in comparison with the reaction volume. This is due to the low concentrations of dissolved reactants and to the fact that a significant part of the reaction volume (the organic phase) is reduced to the role of liquid that separates micelles. This synthesis method is not adapted for the production of significant quantities of metal or metal oxide particles and in particular for producing nanothermites, therefore it is recommended for laboratory use.

1.2.3. *Solvothermal syntheses*

The first hydrothermal synthesis related works were conducted by Schafhäult in 1845 starting from silicic acid present in the water heated for 8 days in Papin's steam digester in order to obtain quartz crystals [SCH 45]. Starting from the 1890s, this methodology was developed on corundum. A significant number of metal oxides are today obtained by this method.

1.2.3.1. *Principle*

The term solvothermal is used to describe the technologies in which a heterogeneous chemical reaction occurs under conditions of pressure above one atmosphere and temperature above ambient temperature, irrespective of the solvent used. When water is used as solvent, then the synthesis is "hydrothermal".

These methods can be divided into two different categories, depending on the temperatures and pressures involved:

– the classical or subcritical solvothermal synthesis corresponds to reactions conducted at temperatures above the solvent's boiling point, but below its critical temperature, and within a range of pressures below the critical pressure of the solvent [YAN 07c, QIN 11];

– the supercritical solvothermal route corresponds to reactions conducted at pressures and temperatures above the critical values of pressure and temperature of the solvent.

Critical temperatures and pressures of the main solvents used in the synthesis of metal oxide and metal nanoparticles are provided in Table 1.6.

Solvent	T_c (°C)	P_c (MPa)
Water	374	22.10
Carbon dioxide	31.2	7.38
Methanol	240	8
Ethanol	243	6.39

Table 1.6. *Common solvents used in the solvothermal synthesis of metal and metal oxide nanoparticles (Tc: critical temperature, Pc: critical pressure)*

Solvothermal reactions can be conducted in discontinuous mode in a closed reactor or in continuous mode. The first works related to the continuous synthesis of nanoparticles in supercritical medium were conducted in the 1990s by Adchiri and Arai [ADS 92b]. These works refer to the hydrolysis of a dozen metal salts in order to obtain the corresponding oxides by continuous injection of aqueous solutions of salts in a flow of water in the supercritical phase. The time of reaction is of the order of 2 min and the size of the particles obtained ranges between 20 and 600 nm, depending on the nature and concentration of salts [ADS 92a].

The main advantage of carrying out reactions in subcritical or supercritical aqueous medium is that the properties of the reaction medium can vary within a wide range by modifying pressure and/or temperature. Thus, subcritical and supercritical water were used as reaction medium for the synthesis of crystalline

particles, in particular of metal and metal oxide nanoparticles. This method also allows us to control morphology, size and size distribution of particles by relatively slight variations of temperature and pressure [JUN 01].

In the case of metal oxide formation, a hydrothermal synthesis method can be described according to two chemical reactions: hydrolysis of salts in solution, followed by dehydration as follows:

$$M(L)_x + xH_2O \rightarrow M(OH)_x + xHL \quad \text{Hydrolysis} \qquad [1.6]$$

$$\mathrm{M(OH)}_x \rightarrow \mathrm{MO}_{x/2} + \frac{x}{2}\mathrm{H_2O} \quad \text{Dehydration} \qquad [1.7]$$

When these reactions take place in supercritical water, it is possible to obtain metal particles by adding a reducing agent such as formic acid [ARI 11], formaldehyde [ZHO 15a] or glycerol [KIM 14].

The following mechanisms come into play: in supercritical medium, the formic acid decomposes [YU 98, YOS 04] either by decarbonylation (or dehydration):

$$\mathrm{HCO_2H \rightarrow H_2O + CO} \qquad [1.8]$$

or by decarboxylation (or dehydrogenation):

$$\mathrm{HCO_2H \rightarrow H_2 + CO_2} \qquad [1.9]$$

Formaldehyde decomposes into:

$$\mathrm{HCOH \rightarrow H_2 + CO} \qquad [1.10]$$

and glycerol decomposes into:

$$\mathrm{C_3H_5(OH)_3 \rightarrow 4H_2 + 3CO} \qquad [1.11]$$

In turn, carbon monoxide can react according to the gas reaction to water:

$$\mathrm{H_2O + CO \rightarrow H_2 + CO_2} \qquad [1.12]$$

Then, hydrogen reacts with the metal oxide resulting from the hydrolysis and dehydration reactions [ARI 11, SEO 11, KUB 14].

$$\mathrm{MO}_x + x\,\mathrm{H_2} \rightarrow \mathrm{M} + x\,\mathrm{H_2O} \qquad [1.13]$$

While the vast majority of solvothermal reactions are conducted in water for the fabrication of metal particles, these can also be obtained in other media.

Titanium oxide nanoparticles were obtained either by the hydrolysis of titanium (IV) isopropoxide [STA 03] or by the hydrolysis of titanium (IV) diisopropoxide bis(acetylacetonate) [ALO 07] solubilized in an aqueous phase and injected in supercritical carbon dioxide. The particles obtained are spherical, but their size distribution is wide, ranging between 20 and 800 nm in the first case, and somewhat narrower in the second case (between 100 and 600 nm).

Alumina nanoparticles have been obtained by oxidation of aluminum particles in a medium of water/supercritical carbon dioxide. This leads especially to producing particles with sizes ranging between 300 and 500 nm, composed of crystallized alumina in its alpha form, and smaller particles of crystallized alumina in the gamma phase, with sizes between 20 and 70 nm [VOS 10].

Various works show that it is possible to use supercritical methanol or ethanol for the continuous or discontinuous synthesis of metal oxide nanoparticles and influence the form of the particles obtained. For example, the use of supercritical methanol allows us to elaborate spherical ZnO nanoparticles [VER 10b, HAN 11], while particles obtained with supercritical water take the form of nanorods [KIM 15c].

Depending on the implementation conditions, the use of supercritical alcohol allows us to obtain also metal particles [KIM 09, CHO 10].

In Choi *et al.* [CHO 10, KIM 09], it has been shown that it was possible to form nickel, silver and copper nanoparticles with supercritical methanol without reduction agent above a certain temperature threshold, which was specific for each metal. Below this threshold oxide and hydroxide formation can be observed. The presence of oxides and hydroxides was equally noticed during the continuous synthesis, when the residence time is too short. According to the explanation advanced, at high temperature, supercritical methanol acts as a hydroxylation agent. In effect, the hydroxyl ions are dissociated from the methanol molecules, when in the supercritical phase [BUL 08, AND 06]. The “free” hydroxyl ion can thus participate in the reduction by transfer of electrons to the metal precursor or to a metal intermediary [ZHO 15a].

The examples reported hereafter refer predominantly to the synthesis in water in subcritical or supercritical conditions. Several examples using an alcohol [KIM 09] or carbon dioxide [VOS 10] are reported in the tables below.

Oxide	d (nm)	Conditions	Reference
Bi_2O_3 nanowires	D: 40 L: several µm	$Bi(NO_3)_2$, Na_2SO_4, NaOH aq., H_2O, 120°C, 12 h	[WU 14b]
CeO_2 particles	13–17	$Ce(NO_3)_2$, hexamethylene tetramine, H_2O, PVP, 180°C, 100 min	[XIE 15]
Co_3O_4 nanocubes	20	$Co(NO_3)_2$, H_2O_2 aq., pH 8–9, PEG (M_w 20 000), H_2O n-butanol, 160°C, 10 h	[YAN 07c]
Cr_2O_3	29–60	CrO_3, ethanol, H_2O, 190°C, 1 h, calcination 500°C 1 h	[PEI 09]
CuO platelets	L: 250–300 l: 50-100	$Cu(NO_3)_2$, NaOH AQ., sodium citrate, H_2O, 160°C, 12 h	[SON 15]
CuO nanotubes	L: 20–120 D: 7	$Cu(NO_3)_2$, ethylene diamine, NaOH aq., H_2O, 100°C, 24 h, calcination 400°C, 5 h	[IPE 14]
α-Fe_2O_3 nanocubes	100–200	$Fe(NO_3)_3$, triethylamine, H_2O, 160°C, 24 h	[QIN 11]
α-Fe_2O_3 polyhedrons	90–110	$FeCl_3$, NH_3 aq., H_20, 180°C, 8 h	[MA 10]
α-Fe_2O_3 polyhedrons	20–50	$FeCl_3$, CH_3CO_2Na aq., PVP, H_20, 200°C, 18 h	[ZHU 12]
In_2O_3 platelets	15–35	$In(NO_3)_3$, Triton X-100, hexamethylene tetramine, H_2O, 180°C, 8 h, calcination 400°C, 3 h	[SEL 14]
α-MnO_2 nanowires	D: 15–20 L: several micrometer	$KMnO_4$, $(NH_4)_2S_2O_8$, H_2O, HNO_3, 180°C, 15 h	[TOU 14]
MoO3 nanoribbons	l: 100–300 L: several µm	H_2MoO_4, oxalic acid, H_2O, HNO_3, 180°C, 24 h	[ZEN 13]
α-MoO_3 nanorods	L: 3 µm D: 200	Na_2MoO_4, HCl, H_2O, 120°C, 18 h	[WAN 13c]
MoO_3	<100	Na_2MoO_4, cyclohexane, sc CO_2, 35°C, 150 bars	[REV 10]
NiO particles	100–3,000	$Ni(NO_3)_2$, H_2O, 400°C, 300 bars 10 min	[KIM 14]
Sb_2O_3 polyhedrons Sb_2O_3 nanoribbons	100 L: 4 µm, l: 400, E : 20	$SbCl_3$, pH 7–9, 150°C, 16 h, CTAB butanol-1/ethanol Water/butanol-1/ethanol	[LIU 10]
Sb_2O_3 nanorods	L: 1–2 µm, l: 50–150	$SbCl_3$, H_2O, pH 8–9, 120–180°C, 12 h	[CHE 05b]
SiO_2 spheres	2–14	Na_2SiO_3, H_2O, AOT, sc CO_2, 5.60 MPa, 308.2 K	[ZHA 06b]
SnO_2 nanorods spheres	7–27 10–15	$SnCl_4$, NH_3 aq., H_2O, pH 10.0, 180–250°C, 40 atm. without surfactant, calcination 600°C, 4 h with CTAB	[JAI 06]

SnO_2 nanorods nanoflower aggregate	270 for the nanorods	$SnCl_4$, polyacrylamide, NaOH aq., H_2O, 200°C, 12 h	[TIA 14]
SnO2	19	$Sn(Cl)_4$ CTBA, urea, pH 8, H_2O, 100°C, 24 h, calcination 600°C, 2 h	[BLE 14]
SnO_2 platelets	2–19	$SnCl_4$, CTAB, urea, H_2O, 100°C, 24 h	[FAR 10]
WO_3 hexagonal nanorods	*L*: 500–1,000 *D*: 50–60	$(NH_4)_6H_2W_{12}O_{40}.nH_2O$, Na_2SO_4, citric acid, H_2O, pH 1.5, 180°C, 24 h	[WAN 14b]
WO_3	*D*: 80 *L*: >2.5 µm	Na_2WO_4, Na_2SO_4, K_2SO_4, H_2O, pH 1.5–2, 180°C, 24 h	[MIA 15]
WO_3 nanowires	*D*:15 *L*: >5µm	Na_2WO_4, H_2O, glycine, pH 1.3, 180°C, 12 h	[LIN 15]
WO_3 Particles agglomerate	500 20–50	Ammonium tungstate, HNO_3, pH 3, 180°C, 30–60 min, assisted by microwaves (200W), annealed at 250°C, 10 min under air	[HER 14]
WO_3 nanorods	<50	Na_2WO_4, H_2O, pH 2.0, 180°C, 0.75–3 h, assisted by microwaves (200 W)	[CHA 11b]
h-WO_3	*D*: 100–150 *L*: 1–2 µm	Na_2WO_4, H_2O, pH 1–1.2, 180°C, 4–12 h,	[HA 09]
ZnO particles	<300	$Zn(CH_3COO)_2$, NaOH aq., pH 9, H_2O, 120°C, 12 h	[BAM 14]

Table 1.7. *Hydrothermal synthesis of metal oxide nanoparticles in closed reactor and in subcritical medium; L, length; l, width; D, diameter; E, thickness; CTAB, cetyltrimethylammonium bromide; PVP, polyvinylpyrrolidone; sc, supercritical*

Materials	*d* (nm)	Conditions	Reference
Al_2O_3	20–400	Al, H_2O, sc CO_2, 446–723 K, 0.85–38.03 MPa	[VOS 10]
WO_3	25–100	Na_2WO_4 cyclohexane, sc CO_2, 35°C, 150 bars	[REV 10]
TiO_2 spheres	20–800	TTIP, Zonyl® FSP fluoro surfactant–2-propanol–water (35–20–45), sc CO_2, 20–30 s	[STA 03]

Table 1.8. *Hydrothermal synthesis of metal oxide nanoparticles in closed reactor and in supercritical carbon dioxide medium; TTIP, titanium tetraisopropoxide*

Materials	*d* (nm)	Conditions	Reference
α-Fe_2O_3 particles	30–60	$Fe(NO_3)_3$, H_2O, pH 1.8, 250–350°C, FW/FS: 3/2, flow rate 50–100 mL/min	[KRI 15]
ZnO particles	20–25	$Zn(NO_3)_2$, NaOH aq., H_2O, 210°C, 260 bars, flow rate 10 mL/min	[SON 11]
TiO_2 spheres	200 ± 100 (a) 270 ± 125 (b)	DIPBAT (a) or TTIP (b), ethanol, sc CO_2, 300°C, 20 MPa, residence time: 2 min	[ALO 07]

Table 1.9. *Continuous hydrothermal synthesis of metal oxide nanoparticles in subcritical medium: FW, subcritical fluid flow; FS, solute solution flow; DIPBAT, diisopropoxititanium bis (acetylacetonate); TTIP, titanium tetraisopropoxide*

Materials	*d* (nm)	Conditions	Reference
γ-Al_2O_3 spheres		$Al(NO_3)_3$, H_2O, 585°C, FW: 24-43.5 g/min, FS: 3.5–20 g/min, 25–35 MPa	[NOG 08]
CeO_2	30–50	$Ce(NO_3)_3$, sc methanol, 400°C, 30 MPa, residence time 40 s	[VER 09]
Co_3O_4 nanocubes	9–90	$Co(CH_3COO)_2$, H_2O_2 aq., 430°C, 240 bars, residence time 2s	[LES 12]
CuO	8–14.8	$Cu(NO_3)_2$, H_2O, 400°C, 30 MPa, residence time: 0.129–2.08 s	[SUE 11]
Fe_3O_4 particles aggregate	16–25 90–150	$Fe(NO_3)_3$, methanol, 400°C, 30 MPa, residence time: 38 s	[VER 10a]
α-Fe_2O_3 spheres	37 ± 6	$Fe(NO_3)_3$, H_2O, 400°C, 30 MPa, residence time: 38 s	[VER 10a]
Fe_2O_3	4–6.7	$Fe(NO_3)_3$, H_2O, 400°C, 30 MPa, residence time: 0.129–2.08 s	[SUE 11]
Fe_3O_4 sphere	21 ± 2	$Fe(NO_3)_3$, sc methanol, 400°C, 30 MPa, residence time 38 s	[VER 10a]
NiO particles	20–55	$Ni(NO_3)_2$, H_2O, 400°C, 30 MPa, total flow rate: 30–60 g/min	[KAW 10]
NiO	6.6–9.7	$Ni(NO_3)_2$, H_2O, 400°C, 30 MPa, residence time: 0.129–2.08 s	[SUE 11]
TiO_2 particles	13–30	$Ti(SO_4)_2$, KOH, H_2O, 400°C, 30 MPa, residence time 1.7 s	[KAW 09]
ZnO nanorods agglomerates particles	*D*: 200–500 *L*: 1–5 µm 200–1000 5–10	$Zn(NO_3)_2$, FW: 9 g/min, FS: 2 g/min, sc H_2O, 400°C, 30 MPa sc methanol, 270°C, 20 MPa	[KIM 15c]
ZnO particles	20–25	$Zn(NO_3)_2$, NaOH aq., H_2O, 210°C, 260 bars, flow rate 10 mL/min	[SON 11]
ZnO nanorods	*L*: 22–166 *D*: 20–331	$Zn(NO_3)_2$, KOH, H_2O, 410°C, 305 bars, FW = FS = 20 mL/min	[DEM 14]

Table 1.10. *Continuous hydrothermal synthesis of metal oxide nanoparticles in supercritical medium: L, length; D, diameter; FW, flow of supercritical fluid; FS, flow of solute solution*

Metals	*d* (nm)	Conditions	Reference
Ag particles	390 ± 114 320 ± 73	$AgNO_3$, CH_3OH, 400°C, 300 bars, 5 min $AgNO_3$, C_2H_5OH, 400°C, 300 bars, 5 min	[KIM 09]
Co cubes	30	$Co(NO_3)_2$, CH_3OH, oleic acid, 400°C, 300 bars, 15 min	[SHI 10]
Co agglomerates	200-400	$Co(CH_3COO)_2$, H_2O, CH_3OH, HCHO, 340–420°C, 22.1 MPa, 10 min	[SEO 11]
Cu particles	420 ± 119	$Cu(NO_3)_2$, CH_3OH, 400°C, 300 bars, 5 min	[KIM 09]
Cu particles	14-,85	$CuSO_4$, $EDTA(Na)_2$, NaOH aq., H_2O, HCHO, 400°C, 25 MPa, 3 min	[ZHO 15a]
Cu particles	100-1,000	$Cu(NO_3)_2$, glycerol, H_2O, 400°C, 300 bars, 10 min	[KIM 14]
Ni particles	50 ± 10	$Ni(NO_3)_2$, CH_3OH, 400°C, 300 bars, 5 min	[KIM 09]
Ni particles	100–1,000	$Ni(NO_3)_2$, glycerol, H_2O, 400°C, 300 bars, 10 min	[KIM 14]

Table 1.11. *Discontinuous hydrothermal synthesis of metal nanoparticles in supercritical medium ($EDTA(Na)_2$, disodium ethylenediamine tetraacetate dihydrate)*

Materials	*d* (nm)	Conditions	Reference
Ag spheres	148 ± 32	$AgNO_3$, 150°C, 30 MPa, FS 6 mL/min, sc methanol	[CHO 10]
Cu particles	14–85	$Cu(SO_4)$, $EDTA(Na)_2$, NaOH aq., sc H_2O, HCHO, 400°C, 25 MPa, residence time: 3 min	[ZHO 15a]
Cu spheres	240 ± 44	$Cu(NO_3)_2$, 250°C, 30 MPa, FS 6 mL/min, sc methanol	[CHO 10]
Ni spheres	119 ± 19	$Ni(NO_3)_2$, 400°C, 30 MPa, FS 6 mL/min, sc methanol	[CHO 10]

Table 1.12. *Continuous hydrothermal synthesis of metal nanoparticles sc, supercritical; FS, flow of solute solution*

The characteristics of the particles (mean size, size distribution, forms, etc.) are governed by numerous parameters, such as temperature, pressure, concentration of precursor solution, its nature, the nature of the solvent, purity of the raw materials, design of the reactor, duration of reaction in the case of continuous reactions, time of residence in the flow, etc.

1.2.3.2. *Effect of temperature*

Several works have shown that an increase in temperature leads to an increase in the size of the resulting particles, when hydrothermal reactions are conducted at various temperatures [LES 12].

To give an example, Patzke *et al.* use temperature as a parameter when adjusting the diameter of the molybdenum oxide nanorods that they manufacture. For a temperature between 90 and 12°C, they obtain thin nanorods, with a mean diameter of 40 nm. For a temperature of 150°C, nanorods nearly reach their maximal diameter of 150 nm [PAT 04]. Kolen'ko and colleagues obtain anatase nanoparticles of 8 and 26 nm at 423 and 523 K, respectively [KOL 03].

A further effect of temperature was observed by Choi *et al.* during the continuous hydrothermal reactions of metal nitrates in supercritical methanol. When temperature increases above a certain value that depends on the metal ion, the particles obtained are metals and not oxides. Reduction takes place starting from 150°C for silver, 300°C for copper and 400°C for nickel. In this case, an increase in the reaction temperature activates a mechanism of metal oxide reduction by supercritical methanol [CHO 10].

1.2.3.3. *Effect of precursor concentration*

Several authors have shown that the size of particles formed was directly influenced by the concentration of precursor salt. The higher the precursor concentration, the larger the particles. Furthermore, strong concentrations facilitate the formation of aggregates [LES 12, ZHU 12, JAI 06].

For example, Søndergaard and colleagues obtained an increase in the size of zinc oxide particles from 29 to 34 nm for a precursor concentration of 0.005 mol/L and from 49 to 59 nm for a concentration of 0.5 mol/L [SON 11]. Similarly, Zhou *et al.* have varied the size of copper particles from 14 to 50 nm by varying the concentration of copper sulfate from 0.05 to 0.5 mol/L. Above this value, the size of particles slightly changes. However, their size distribution becomes more heterogeneous. At low concentration, nuclei are rapidly generated, and the low concentration of ions still present does not allow for further growth. The low density of nuclei generated prevents or in any case significantly slows down aggregation-induced growth. This results in small particles with low polydispersity. On the contrary, at high concentration, nucleation can extend over a longer period, which results in larger particles with higher polydispersity [ZHO 15a].

1.2.3.4. *Effect of surfactant presence*

The effect of surfactant on the solvothermal synthesis of nanoparticles is manifested along two axes. The first consists of preventing or reducing aggregate

formation [XIE 15]. The use of non-ionic surfactant such as polyethylene glycol facilitates proper dispersion of Co_3O_4, while the use of an ionic surfactant such as sodium dodecylbenzenesulfonate does not allow us to prevent the formation of aggregates [YAN 07c].

The second is to induce morphological modifications of the particles. These are due to a preferential mechanism of growth of particles alongside privileged crystallographic directions that depend on the material's structure. As crystallographic planes have different surface energies, surfactant molecules show preference for the interaction with the surface of certain planes. The surfactant molecules that are thus interacting prevent the deposition of solute molecules on these planes, which prevents their growth. Besides the absence of particles' aggregation in the presence of surfactant, Jain *et al.* obtained a change in the morphology of tin oxide particles generated, going from nanorods to spheres with a diameter ranging from 10 to 15 nm [JAI 06].

1.2.3.5. *Effect of pH*

The influence of base concentration, which is linked to the pH of a solution, has also been highlighted. Yang *et al.* have shown that pH influences the morphology of the particles obtained during cobalt oxide formation. For a pH of 8–9, regular nanocubes of 20 nm are obtained, while for a pH of 11–12, irregular nanocubes are observed [YAN 07c].

In the case of CeO_2 particle elaboration, Xie *et al.* have used hexamethylenetetramine to facilitate the growth of a structure according to a particular crystalline plane for particles' size ranging between 13 and 17 nm. When the base is absent, the particles have sizes between 200 and 300 nm and a spherical form [XIE 15].

Finally, the works of Søndergaard *et al.* relating to the zinc oxide synthesis, in which morphology variations are obtained depending on pH, should be cited. Large nanorods are obtained in acid medium, small particles are obtained in neutral medium, while in basic medium platelets and nanorods are formed [SON 11].

1.2.3.6. *Effect of solvent*

Depending on the solvent nature, it is possible to influence the morphology of the final structures. Liu *et al.* modify the form of antimony oxide particles by using mixtures of alcohol and water. The use of a butanol-1/ethanol mixture results in polyhedral oxide particles with cubic crystalline structure. When water is added to the alcohol mixture, nanoribbons with a mean length of 4 μm, width of 400 nm and thickness of 20 nm are obtained. These nanoribbons have an orthorhombic crystalline structure [LIU 10]. Using subcritical (120–180°C) hydrothermal

synthesis, Chen *et al.* obtain orthorhombic Sb_2O_3 nanorods with a length ranging from 1 to 2 μm and width ranging from 50 to 150 nm [CHE 05b].

1.2.3.7. *Effect of anion*

The modification of counterions (nitrate, sulfate, acetate) in the precursor solutions can lead to modifications in the morphology of particles. Yang *et al.* have shown during the formation of Co_3O_4, the existence of irregular nanocubic forms, quasi-spherical forms or regular nanocubes when nitrate, sulfate or acetate was respectively employed [YAN 07c].

1.2.3.8. *Effect of duration*

It has repeatedly been shown in the literature that when solvothermal reactions are carried out in closed reactor, the increase in the reaction duration typically facilitates the increase in size of formed particles [QIN 11, MA 10]. Similarly, in continuous synthesis, the increase in residence time leads to an increase in the size of formed particles [LES 12].

Duration influences first of all the rates of conversions of solubilized salts into particles. For example, the works of Lester *et al.* on cobalt oxide show that when residence time (T_s) varies from 0.5 to 2 sec for a reaction conducted at 430°C, conversion rate goes from 89% to 99%. At 200°C, due to slower kinetics, conversion rates go from several percent to less than 30% after 20-sec residence time. As for the size of particles, it goes from 28 to 47 nm for residence times of 1 and 7 sec, respectively [LES 12].

1.2.3.9. *Microwave-assisted synthesis*

The literature mentions the use of microwave sources to assist hydrothermal reactions, as a means to accelerate reactions by efficiently providing radiation energy. This allows us to take into consideration larger-scale syntheses due to more rapid and uniform heating. Furthermore, radiation effects of microwaves allows uniform seeding of the solution. This assistance may also be useful in certain cases when there is an interest not to use additives [HER 14], surfactants or model agents, and it has allowed Hu *et al.* to obtain hematite nanorings with outer diameter of the order of 100 nm and inner diameter between 20 and 60 nm depending on the duration of irradiation [HU 07].

1.2.3.10. *Conclusion*

Hydrothermal synthesis, either classical or in supercritical medium, has several advantages in terms of control of size, distribution and morphology of the formed particles. The vast majority of solvothermal reactions are conducted in water. A supercritical medium is preferred for the reactions, as in this state the decrease in the

dielectric constant improves the hydrolysis and dehydration stages. The most important drawback resides in the discontinuous fabrication. In effect, it is important to have a good management of the reaction time, which should be relatively short in order to obtain nanosized particles. Very rapid increases in temperature are therefore needed and can be obtained easily in smaller reactors, and this, combined with low concentrations, which are also required when nanometric sizes are aimed at, leads to obtaining low quantities of product. The continuous method allows us to avoid this obstacle, provided that the injection of the solute phase in the sub- or supercritical fluid stream is brought under control. The mixture should be carried out very rapidly, as residence times range from several seconds to several dozen seconds. But the injection nozzles should not be clogged by a sudden deposit of particles formed when the reaction takes place in the mixture area due to rapid precipitation of metal species. Geometries of continuous reactors have been modified in order to mitigate these problems [RUI 13]. This allows us to consider the synthesis of quasi-monodisperse small size nanoparticles of metal oxides that are of interest for nanothermites.

1.2.4. *Sol-gel syntheses*

The first works in the field of sol-gel synthesis were carried out by the French chemist Jacques-Joseph Ebelmen in 1846. He brought tetraethyl orthosilicate to react in the presence of water and form gelatin-silica [EBE 46]. The first patents related to sol-gels were issued at the end of the 1930s for surface treatments of rearview mirrors [GEF 39]. In the 1950s, colloidal silica spheres obtained by the sol-gel method were commercialized under the trade name Ludox® by Dupont de Nemours [ILE 52, BEC 51]. A very large number of works on this subject have been published since then.

The sol-gel method allows us to elaborate a wide variety of oxides in various forms (dense monolithic structures or, on the contrary, extremely porous structures, thin films, fibers, powders). Due to the wide diversity both in terms of materials and implementation technique, this method has become very attractive for a large number of industries.

1.2.4.1. *Principle*

Sol-gel methods rely on the solution-gelation method as their basic principle. This consists of preparing a stable solution (sol) that contains the molecular precursors and initiating hydrolysis-condensation reactions to obtain a gel.

The sol-gel method can be approached based on two synthesis paths. The inorganic or colloidal path resorts to metal salts (chlorides, nitrates, sulfates, etc.) in aqueous solution. It has the advantage of being less expensive, but controlling it may

prove a complex task, due to the high number of reaction parameters (pH, temperature, mixture method, rate of hydrolysis, condensation, oxidation, etc.). When adopting this path, the counterion may influence the morphology, structure and even chemical composition of the chemical phase obtained. Finally, eliminating the counterion may prove problematic. This is why the organometallic method is preferred. The most frequently used precursor in the organometallic method is a metal alcoholate that can be easily converted into oxide. The sol-gel method is based on two chemical reactions: hydrolysis and condensation of precursors.

The hydrolysis stage consists of the following reactions:

$$[M(H_2O)_x]^{y+} + H_2O \rightarrow [(HO)M(H_2O)_{x-1}]^{(y-1)+} + H_3O^+ \xrightarrow{H_2O} M(OH)_y \quad [1.14]$$

$$M(OR)_x + H_2O \rightarrow HO-M-(OR)_{x-1} + ROH \xrightarrow{H_2O} M(OH)_x \quad [1.15]$$

The condensation stage consists of the following reactions:

– olation, in which a hydroxy bridge is formed, and a metal hydroxide is generated:

$$M-OH + H_2O - M \rightarrow M-OH-M + H_2O \quad [1.16]$$

– oxolation in which an oxo bridge is formed and a metal oxide is generated:

$$M-OH + HO-M \rightarrow M-O-M + H_2O \quad [1.17]$$

1.2.4.2. *Influence of operating conditions*

The synthesis of metal oxide nanoparticles can be influenced by many parameters, among which the most important are the pH and ratio of the water to metal precursor concentration.

1.2.4.2.1. Effect of temperature

Temperature usually accelerates the reaction kinetics, and this influences the reaction duration. On the contrary, the effect on the particle size seems much more complex. In effect, Kojima and Sugimoto have not observed a significant effect of temperature on the size of titanium oxide particles synthesized from titanium butoxide in the presence ammonia in aqueous medium, for temperature variations between 25 and 80°C. The size of the particles obtained is of the order of 450 nm [KOJ 08]. However, Qiu *et al.* have observed a complex effect of temperature during the synthesis of silica particles. There is an increase in particle size when temperature goes from 26 to 28°C and then a decrease from 28 to 32°C [QUI 13].

Finally, during the zirconium oxide synthesis Santos *et al.* have observed an increase in the size of particles, which in their view is caused by an increase in temperature. Zeta potential may vary when temperature increases, and this may affect the stability of particles in solution and facilitate size increase [DOS 14].

1.2.4.2.2. Effect of solvent

Water is commonly used as solvent when inorganic salts are used as precursors [WAH 07], but if the salt is soluble, it is also possible to employ alcohols [MBA 15, CAM 08]. Alcohol or a water–alcohol mixture is generally employed when using alcoholate-type precursors, as they only slightly miscible or non-miscible with water [SON 15, DEM 15, DOS 14, QUI 13].

When water concentration increases compared with metal precursor concentration, a decrease in the size of the particles obtained is observed [WAN 14c, KOJ 08].

1.2.4.2.3. Effect of pH

During sol-gel reactions under acid catalysis, hydrolysis kinetics is favored over condensation reactions, which start in general when hydrolysis is completed. Condensation reactions in basic medium are more rapid than hydrolysis reactions, which results in the precipitation of agglomerated thin particles.

The influence exerted by pH on the size of particles has been particularly studied by Pottier *et al.* in relation to the formation of anatase nanoparticles produced by hydroxylation of titanium tetrachloride. The size of particles was measured for a pH range between 2 and 6. The results indicate that the more acidic a solution is, the smaller the size of particles will be. Their mean diameter varies in the range between 5 nm, for pH of 1, and 8.6 nm, for pH of 5. This size variation is explained by a decrease in interfacial tension due to the protonation of groups at the surface of particles [POT 03]. Works on the synthesis of magnetite particles have also shown, though for a basic medium, that the higher the pH, the smaller the size of particles [VAY 98]. This indicates that the further the pH gets from the zero charge point, the smaller the size of particles [JOL 04].

1.2.4.2.4. Effect of salt addition

Several teams have shown that size and polydispersity of metal oxide particles obtained by sol-gel methods were highly sensitive to the presence of salt being added during reaction. Using electron microscopy, Eiden-Assmann *et al.* have observed perfectly spherical TiO_2 colloids obtained during the synthesis in the presence of alkaline chloride or nitrate (LiCl, NaCl, KCl, CsCl, KNO_3). When using alkaline chlorides, the size of particles decreases when the zeta potential and the ionic radius of cation increase. The size of particles goes from 2,500 nm in the

presence of LiCl (zeta potential of 9 mV) to approximately 200 nm in the presence of CsCl (zeta potential of 25 mV). The same behavior is observed when the chloride anion is replaced by a bromide or iodide one. It appears that the size of particles is also correlated to the ionic force of the solution. When KCl concentration is 4×10^{-4} mol/L, the size of particles is in the range between 500 and 900 nm. For a concentration of 8×10^{-4} mol/L, the size drops down to nearly 50 nm and when concentration doubles, no particles are observed [EID 04]. The conclusions of these works are similar to those of Vayssiere *et al.* on the formation of magnetite nanoparticles in basic medium, when the ionic force of the solution evolves. When it increases, the size of particles decreases [VAY 98]. It had already been shown by the works conducted in 1991 by Bogush and Zukoski that the ionic force had an influence on the size of silica particles formed, but in this case the increase by two orders of magnitude of the concentration of electrolyte resulted in a doubling of particle diameter [BOG 91].

Cai *et al.* observed an increase in the polydispersity of silica particles synthesized when the concentration of electrolyte increases to a certain value. According to the explanation proposed, colloidal silica particles are negatively charged due to the presence on their surface of silanol groups. However, given that the surface charge of particles is weak, the forces of repulsion between colloidal silica particles are generally weak, which facilitates particle coagulation and consequently an increase in polydispersity. When interactions are very weak, especially when salts are absent or their concentration is low, the reaction medium generates very few free silica particles, as it instead produces agglomerated spheroids. The increase in zeta potential of the solution would lead to an increase in the force of repulsion between silica colloidal particles, which might be beneficial to monodispersity in a certain range, as an effect of competing forces of attraction and repulsion [CAI 12].

1.2.4.2.5. Effect of surfactant

An increase in the concentration of surfactant generally leads to a decrease in the size of particles and less agglomerates are formed [MIR 10, EID 04].

Adding surfactant during sol-gel synthesis can also influence the crystalline structure of the particles obtained. For example, in their works on the preparation of alumina nanoparticles, Mirjalili *et al.* and Park *et al.* have shown that the addition of surfactants resulted in the formation of an amorphous phase of boehmite coupled with surfactant hydrates. This further generated amorphous alumina, while in the absence of surfactant, crystalline alumina particles had been obtained [MIR 10, PAR 05b].

1.2.4.3. *Conclusion*

The sol-gel method allows the elaboration of materials as nanoparticles at temperatures close to ambient value and at atmospheric pressure. The fact that many synthesis parameters can be influenced allows us to control the size and form of oxide and metal hydroxide particles. As for the latter, a stage of calcination will be required to obtain the desired oxide. The same is applicable for obtaining particular crystalline phases. This methodology also allows us to obtain very intimate mixtures of mixed oxides that are definitely more homogeneous than those resulting from other techniques [TOB 94, AND 97a, AND 97b]. It is also possible to carry out continuous synthesis of nanoparticles [GIE 94]. The main drawbacks of this technique are the costs of alcoholate precursors and the significant volumes of solvent required for all the operations (synthesis, washing, etc.).

1.3. Gas-phase elaboration

1.3.1. *Condensation in inert gas*

1.3.1.1. *Principle*

This method consists of setting a high purity (>99%) metal sheet, wire or pellet either in a pot made up of ceramic material such as alumina [REC 94] or metal such as tungsten [SAN 98] or on a metal wire [FUK 74]. The assembly is then placed in a vacuum chamber, in which an atmosphere of low pressure neutral gas is generated (helium or argon [BOW 81, WAD 67, KIM 63, YAT 73], xenon [FUK 74, WAD 68] or nitrogen [SAN 98]). The metal is then resistively heated to a temperature that is specific to the metal to be evaporated. The atoms of the evaporated material lose kinetic energy due to their collisions with the gas molecules. They condense in small particles that grow both by the addition of vapor atoms to particular clusters and by aggregation due to collisions between clusters. These are afterward collected on a cold finger. For metals that are highly sensitive to oxidation, such as aluminum, the nanoparticles thus formed are subsequently passivized by small quantities of oxygen diluted in a neutral gas before being exposed to air [SAN 98].

1.3.1.2. *Influence of operating conditions*

The modification of various experimental parameters allows for the variation in the size of metal nanoparticles synthesized:

– the increase in the evaporation temperature leads to an increase in the size of particles [PAN 95];

– the size of particles increases with the distance between the target and the recovery device [PAN 95, GLE 89];

– the increase in the pressure of inert gas generates an increase in the size of nanoparticles formed [PAN 95, KIM 63];

– the increase in molar mass of the inert gas leads to an increase in the size of nanoparticles [WAD 67, WAD 68].

Many metal nanoparticles can be obtained by this method (see Table 1.13).

Metal	Mean diameter or size range (nm)	Experimental conditions	Reference
Ag	1–15 5–20, 20–60, 70–300 100–300	He, P = 30 kPa, V = 25 m/s T = 1000°C Ar, P = 0.13, 0.67, 2.0, 4.0 kPa Xe, P = 0.27, 2 kPa	[IWA 92] [KIM 63] [WAD 68]
Al	10–40 24–100 5–20, 20–60, 70–300 100–400 100–2,300	N_2, P = 0.13 kPa, T = 1350°C Ar, 1.3 kPa < P < 6.7 kPa, 1,400°C < T < 1600°C Ar, P = 0.13, 0.67, 2.0, 4.0 kPa Xe, P = 0.27, 2 kPa He, P = 6.67 kPa, 1,100°C < T < 1,500°C	[SAN 98] [PAN 95] [KIM 63] [WAD 68] [YAT 73]
Au	5–20, 20–60, 70–300 30–200	Ar, P = 0.13, 0.67, 2.0, 4.0 kPa Xe, P = 0.27, 2 kPa	[KIM 63] [WAD 68]
Be	100–400	Xe, P = 0.27, 2 kPa	[WAD 68]
Bi	5–20, 20–60, 70–300	Ar, P = 0.13, 0.67, 2.0, 4.0 kPa	[KIM 63]
Cd	5–20, 20–60, 70–300 100–400	Ar, P = 0.13, 0.67, 2.0, 4.0 kPa Xe, P = 0.27, 2 kPa	[KIM 63] [WAD 68]
Co	5–20, 20–60, 70–300 10–20	Ar, P = 0.13, 0.67, 2.0, 4.0 kPa Xe, P = 0.27, 2 kPa	[KIM 63] [WAD 68]
Cr	5–20, 20–60, 70–300 >20 50–100	Ar, P = 0.13, 0.67, 2.0, 4.0 kPa Ar, P = 0.67 kPa Xe, P = 0.27, 2 kPa	[KIM 63] [NIS 74] [WAD 68]
Cu	5–20, 20–60, 70–300 10–200 2–5	Ar, P = 0.13, 0.67, 2.0, 4.0 kPa Xe, P = 0.27, 2 kPa He or Ar, 26.66 kPa < P < 53.33 kPa, 1,727°C < T < 2127°C	[KIM 63] [WAD 68] [BOW 81]
Fe	30 5–20, 20–60, 70–300 50–200 6	Xe or Ar, 1;33 kPa < P < 2.67 kPa Ar, P = 0.13, 0.67, 2.0, 4.0 kPa Xe, P = 0.27, 2 kPa He, P = 2 kPa	[FUK 74] [KIM 63] [WAD 68] [BIR 84]
Mg	5–20, 20–60, 70–300 500–3,000 2–6	Ar, P = 0.13, 0.67, 2.0, 4.0 kPa Xe, P = 0.27, 2 kPa He, P = 1.3 kPa	[KIM 63] [WAD 68] [KIM 87]

Mn	5–20, 20–60, 70–300 20–300	Ar, P = 0.13, 0.67, 2.0, 4.0 kPa Ar, P = 2.0 kPa, T = 1,500°C, V = 6 m/s	[KIM 63] [IWA 95]
Nb	10	Ar, 2.0 < P < 6.67 kPa, 2,500°C < T < 2,600°C	[SAIT 80]
Ni	5–20, 20–60, 70–300 5–60	Ar, P = 0.13, 0.67, 2.0, 4.0 kPa Xe, P = 0.27, 2 kPa	[KIM 63] [WAD 68]
Pb	5–20, 20–60, 70–300	Ar, P = 0.13, 0.67, 2.0, 4.0 kPa	[KIM 63]
Sn	5–20, 20–60, 70–300	Ar, P = 0.13, 0.67, 2.0, 4.0 kPa	[KIM 63]
Sb	20	Ar, P = 0.8 kPa, T = 750°C, V = 4.2 m/s	[IWA 95]
V	10–100	Ar, 0.03 kPa < P < 5.33 kPa, 2,000°C < T < 2,300°C	[SAIT 80]
Zn	5–20, 20–60, 70–300 50–200 10–20	Ar, P = 0.13, 0.67, 2.0, 4.0 kPa Xe, P = 0.27, 2 kPa Ar, 13.33 < P < 26.66 kPa, T = 900°C	[KIM 63] [WAD 68] [REC 94]

Table 1.13. *Examples of sizes for various metal particles obtained by thermal evaporation techniques as a function of experimental conditions: pressure (P), temperature (T), gas velocity (V)*

There is a variant of this method that consists of heating the metal by radiofrequency (RF) induction in a cryogenic fluid in the liquid phase (argon, nitrogen or helium). This method allows for a significant nucleation rate and rapid cooling, which results in limiting the particle growth. Finally, the high vapor pressure contributes to a significant yield [CHA 98].

Nanoparticles are afterward collected by bubbling the cryogenic gas that contains them in suspension through an organic solvent such as hexane. The metal nanoparticles obtained have a granulometry between 20 and 200 nm [CHA 96a]. Starting from an aluminum block (30 g) subjected to RF induction heating (150 KHz) under argon atmosphere (used instead of liquid nitrogen, to avoid formation of aluminum nitride (AlN), Champion and Bigot [CHA 98] produce approximately 150 mg aluminum nanoparticles per minute. These are spherical particles, with a diameter of the order of 100 nm. They are passivized by an oxide layer with a thickness of 3 nm. The cryogenic fluid used for iron and copper nanoparticles is nitrogen, and size dispersion is weaker [CHA 96a, GOU 93].

1.3.1.3. *Conclusion*

This is a simple method, which can be readily implemented, though with low yields [REC 94].

This technique can also be used for manufacturing nanosized metal oxides, by evaporating metal in the presence of oxygen or air diluted in the flow of inert gas.

Zeng *et al.* [ZEN 04] have thus obtained Sb_2O_3 nanoparticles with a diameter between 50 and 180 nm.

1.3.2. *Explosion of metal wires*

1.3.2.1. *Principle*

Electric explosion of wire is one of the vapor-phase methods for the production of particles by evaporation of a thin metal wire through which a strong current flows.

Nairne was the first to describe this phenomenon in 1774 [NAI 74], when he carried out the discharge of a battery of interconnected Leyden jars through copper and silver wires.

It is in a US Atomic Energy Commission report from 1946, drafted by Abrams *et al.* [ABR 46], that the production of ultra-thin powders was for the first time described, together with the fabrication of nanoparticles of apparently non-crystalline plutonium, uranium and aluminum, with a diameter of the order of 200 nm, and whose particles form aggregates at least 1 µm in length.

In 1962, Karioris and Fish described a metal particle aerosol generator based on explosion of metal wire, and applied to about 15 metals, including aluminum and copper [KAR 62].

This method is still being developed throughout the world [KOT 03, IVA 03]. Many other metal and alloy nanoparticles have also been obtained in a gas atmosphere [NAZ 06, LEE 10, JAN 11]. The implementation parameters are the following:

– 5–30 KV high voltage source [DRE 09];

– current density above 10^{10} A/m^2 [KWO 01];

– pulse duration that can vary from several nanoseconds [ROM 06] to several microseconds [JIA 98];

– metal wire diameter that can vary from a dozen to hundred micrometers [DAS 12, BAG 11, SUE 07].

1.3.2.2. *Influence of operating conditions*

1.3.2.2.1. Effect of pressure

The influence that inert gas pressure exerts on the formation of particles has been studied by Liu *et al.* [LIU 13]. Results show that aluminum nanoparticles produced

under high pressure argon are more spherical in form and furthermore the mean diameter of aluminum nanopowders increases with argon pressure. This effect is accompanied by an increase in the size distribution of aluminum nanoparticles and in yield [SAR 07a].

1.3.2.2.2. Effect of gas nature

Sarathi *et al.* [SAR 07b, SAR 10] have shown that the nature of the inert gas (helium or argon) employed does not seem to influence the size of particles formed or their composition (aluminum and oxygen rates) for an equivalent implementation pressure. On the contrary, the use of nitrogen leads to the formation of AlN.

The aluminum nanoparticles obtained by explosion under inert gas have very high surface reactivity. Before being subjected to other treatments, these particles have to be passivated to avoid autoignition when they are exposed to air.

1.3.2.3. *Passivation*

Most of the aluminum nanoparticle powders for commercial use are passivated by inert oxide layers composed of amorphous or crystalline alumina. This air passivation can be carried out after obtaining the particles or during the fabrication process.

The works of Kwon [KWO 03] present several passivation methods for thin aluminum particles (between 200 and 300 nm) either by using argon (at a pressure of 1.1 atm) with a very low air concentration (below 0.1% in volume), or by employing mixtures based on argon and nitrogen or argon and hydrogen (10% in volume) with air traces. The table below includes several examples. The passivations carried out during particle preparation in the presence of reactive gases (oxygen or nitrogen) diluted by argon lead to an increase in the size dispersion of particles obtained [KOT 99]. Passivation by nitrogen is not stable, as AlN [KIN 03] becomes oxidized and hydrolyzed during its air storage and alumina is formed in the end. Ilyin and colleagues have in turn developed a method of passivation by boron during the fabrication process. The aluminum particles are enveloped by a compound that approximately consists of AlB_2 [KWO 02].

Passivation can also be conductive starting from organic coatings such as stearic or oleic acids or fluoro polymers [KWO 03, GRO 06].

1.3.2.4. *Conclusion*

This method is currently used for the fabrication of aluminum nanopowder for commercial use under brand names such as Elex or Alex.

It is worth noting that metal nanopowders can be produced by explosion of metal wire in liquids such as deionized water, ethanol, isopropanol or acetone [CHO 10, HA 10, GOO 09, YUN 11] when this method is used for producing non-oxidized metal powders. Cho [CHO 07] has described the process for the elaboration of silver nanoparticles in deionized water. This work notes the formation of a plasma sphere composed of atoms of vaporized material. This plasma bubble is contained in the water under pressure generated by the shockwave. By cooling, vapor condensation generates particles inside this sphere before its collapse and subsequent dispersion of particles in the liquid. There is high dispersion of the size of particles, which varies from 10 to 500 nm depending on the solvents and type of metal used.

1.3.3. *Thermal plasma synthesis*

There is a broad spectrum of plasma generation techniques, which can be classified depending on plasma temperature, gas pressure, frequency or electrode presence. The latter will be described here taking into account their excitation mode. A special section will be dedicated to plasmas generated by pulsed laser (see section 1.3.4). Plasmas generated in the gas phase can be classified into three groups:

– plasmas initiated by direct current (DC) and low-frequency (AC) discharges;

– plasmas initiated by RF;

– plasmas initiated by microwave sources.

1.3.3.1. *Direct current (DC) and low frequencies (AC) discharges*

These plasmas are obtained starting from an arc plasma torch. These can be divided into two categories depending on their design geometry: the so-called blown arc plasma and the transferred arc plasma.

1.3.3.1.1. Blown arc plasma in direct current

In 1957, Gage [GAG 57] designed the first coaxial configuration, in which the electric arc develops between a central cathode and a concentric nozzle that plays the role of the anode. The cathode is generally made up of 2% thoriated tungsten [FAU 96a]. The electrodes are powered by a direct current source and the arc is confined by the flow of cold gas established around the plasma column. Plasma jet temperatures vary between 6,000 and 15,000 K [FAU 96b]. Cold gas also prevents electrodes from overheating. A cooling system using heat transfer fluid may be needed for high power systems.

This type of system sustains injection of precursor in the form of powder [LEE 07], liquid (aqueous or organic solutions) [SIV 13, FAU 11] or gas [RAO 95] [HUA 10a]. Powder can be injected along a direction that is parallel or perpendicular to the plasma flow. It is worth noting that when injecting solvent, its nature strongly influences the temperature and the nature of species present in the plasma.

The use of this method often leads to strongly agglomerated powders [ZHO 09a]. However, by optimizing the flow rate parameters of the carrier gas and plasma gas, Im *et al.* have obtained tin oxide particles with diameters varying between 3 and 21 nm and few aggregates formed. The size of these aggregates is approximately 20 nm. They have also evidenced that a decrease in the flow rate of gas carrying the tin tetrachloride used as precursor led to a decrease in the quantity of oxide formed, and notably to a decrease in the size of the particles formed. Furthermore, by increasing the flow rate of plasma gas, the particle time of residence in plasma diminishes, which considerably reduces the particle growth time and their coalescence, and this also facilitates the formation of small particles with narrow size distribution and few aggregations of particles [IM 08].

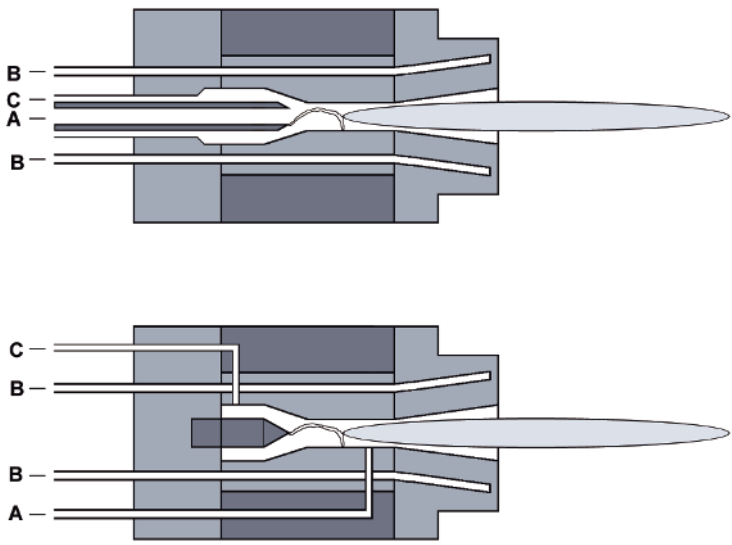

Figure 1.2. *Principle of blown arc plasma torches: top: axial injection, hollow cathode (A); bottom: perpendicular injection of precursor (A), cooling fluid (B) and plasma gas (C)*

1.3.3.1.2. Transferred arc plasma

In the case of transferred arc plasmas, the arc is initiated between two coaxial though non-concentric electrodes powered by direct current. The cathode is made up of tungsten, while the anode may consist of a metal to be vaporized in order to obtain metal or oxide nanoparticles (aluminum [CHA 06], copper [RYU 09], iron [BAR 06]), or it may be made up of tungsten or copper and sustain a pot that allows the fusion of metal to be transformed (aluminum [PAR 05a], silver [ZHO 09a], tungsten [SU 08, SU 05], bismuth [CHE 05a] and nickel [WEI 05]). The temperatures of plasmas generated by transferred arc vary between 9,000 and 25,000 K.

The arc is stable for a voltage between 15 and 20 V, and for a current between 25 and 50 A [PAR 05a]. The plasma chamber is swept by a plasma flow, generally consisting of argon. A reducing reactive gas such as hydrogen may be added during the synthesis of metal particles in order to prevent the formation of oxide [ZHO 09a]. If, on the contrary, obtaining oxides is desired, diluted oxygen or air can be added [CHA 06, BAR 06].

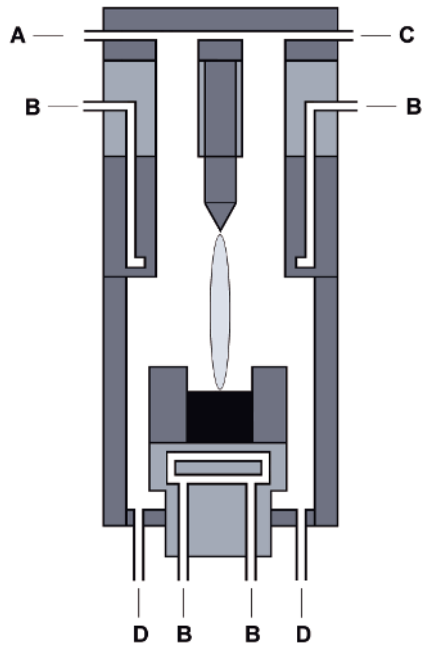

Figure 1.3. *Principle of transferred arc plasma torches: (A) quench gas, (B) cooling fluid, (C) low pressure and (D) plasma gas*

Nanopowders thus produced are highly agglomerated [VOL 07], which is not advantageous for the elaboration of particles used in the formulation of nanothermites.

1.3.3.2. *RF plasma*

Numerous studies were dedicated to RF plasma torches. The vast majority of these torches are based on inductive coupling, but there are also some torches that use capacitive coupling to generate nanopowders [MAT 06, BUS 97].

1.3.3.2.1. RF inductively coupled plasma

The first experiments on low pressure discharge without electrodes were conducted by the end of the 19th Century, but it was not until the 1940s that atmospheric pressure inductive discharge was discovered. The Russian physicist George Babat [BAB 47] was the first to report, in 1947, that once established at low pressure, a discharge can be maintained, while the pressure is brought to the level of atmospheric pressure.

The key development that led to the currently used inductive plasma originated in the works of Reed [REE 61], who in 1961 showed that an inductively coupled plasma discharge can be maintained in an open tube in the presence of a streaming gas. When exiting the discharge area, the partially ionized gas forms a low velocity plasma jet with an average temperature in the range between 6,000 and 11,000 K [BOU 95].

The design of the RF torch is relatively simple. It consists of two concentric tubes placed at a small distance from each other. These tubes are made up of quartz for low powers and ceramics for higher powers. The plasma confinement tube is cooled by compressed air when powers are below 10 kW or by circulating water when powers are up to 150 kW. The induction coil has several turns (three to five), depending on the power source [FAU 96a, FAU 96b]. The range of frequency used by this technology for generating metal or oxide nanopowder goes from 50 kHz to over 10 MHz [VOL 08].

Plasma is initiated and maintained by the RF powered helicoidal winding. As energy is transferred from the source to plasma by inductive coupling, neither the electrons nor the ions can reach the torch walls at the applied frequencies. For this reason, and provided that the wall being in contact with plasma is appropriately cooled, this method allows us to obtain powders that are free from contamination resulted from erosion of electrodes, by contrast with the production methods using direct current arc. On the other hand, this technique does not allow the use of a

sacrificial anode, it requires precursor injection. This injection is generally axial [YE 07, SAT 03, ZHA 12a], and in the direction of plasma gas propagation. Schulz and Hausner have used a plasma torch whose geometry allows for reactive precursors being injected tangentially to the plasma gases (argon) and cooling gases (air) [SCH 92]. The rate of this precursor injection varies from 10 to 30 m/s. Particles are obtained with sizes ranging between 100 and 400 nm, and in quantities of the order of 100 g/h. Optimized industrial systems produce good quality nanopowders with particles sized below 100 nm. The range of products includes metals, oxides, carbides and nitrides.

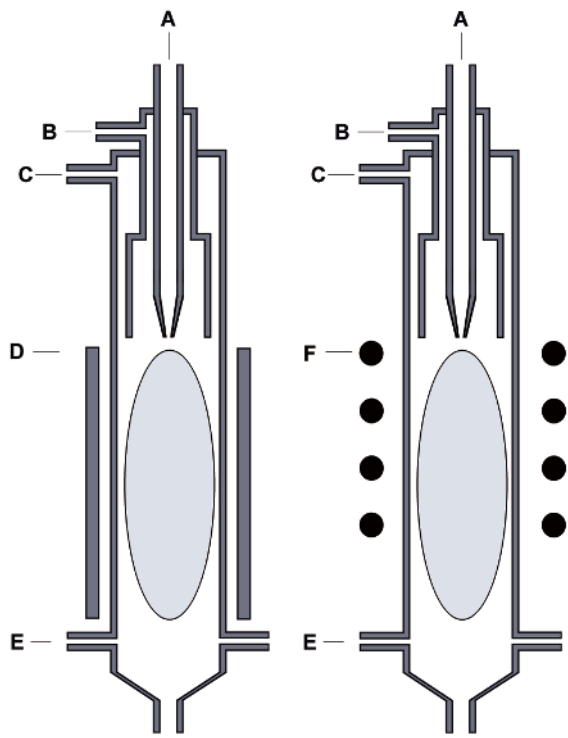

Figure 1.4. *Principle of radiofrequency (RF) plasma torches: left: capacitively coupled torch; right: inductively coupled torch. (A) Precursor and carrier gas, (B) central plasma gas, (C) sheath gas, (D) capacitive plate, (E) quench gas and (F) inductive coil*

1.3.3.2.2. RF capacitively coupled plasma

Several reactors generating capacitively coupled plasmas have been developed for the synthesis of nanopowders [MAT 06, BUS 97]. A capacitively coupled

plasma source is composed of two parallel conductive electrodes placed in a vacuum chamber. The discharge is confined by the reactor walls, which can be either conductive or insulating. The electric field that accelerates electrons is generated between the two electrodes. The alternating electric field allows the electrons present in the respective area to gain the energy required for atom ionization. The electrons thus freed contribute in turn to gas ionization. Due to the avalanche effect, the whole chamber will be filled with plasma whose density and temperature will depend on the applied RF power and also on the gas pressure. Gas sheaths separate plasma from electrodes and walls [BUS 97].

Matsui and colleagues [MAT 06] have developed a reactor with perforated stainless steel electrodes placed inside, perpendicular to the flow of plasma gas (argon) and precursor. To control the size of particles produced, a discontinuous plasma discharge cycle is chosen. The cycle duration of the plasma discharge is between 0.5 and 30 s, with a 4s duration of plasma extinction. The size of the particles thus obtained varies depending on pulse duration. The longer the pulse duration, the longer the particle residence time in the plasma, which increases their growth and coalescence time, and therefore their mean diameter increases. According to the works of Matsui and colleagues, this diameter varies between 10 and 120 nm.

1.3.3.3. *Microwave discharge plasmas*

All microwave systems operate according to the same principle. They have no electrodes: microwaves are generated by various sources such as magnetrons or klystrons. The frequencies used are within the range from 200 to 3,000 MHz [FAU 80]. In industry, the most commonly used frequencies are 0.915 GHz and 2.45 GHz. Microwaves are then guided through waveguides and transfer their energy to the electrons in the plasma gas.

Microwaves allow generation of plasmas with a variety of characteristics [TEN 06]. The gas temperature of microwave-generated plasmas can vary from 300 to several thousand kelvin [VOL 93a, PET 11] for several eV electron energy (or an equivalent electronic temperature of several tens of thousands Kelvin).

The first works on the nanopowder synthesis using microwave-induced plasma were carried out in the beginning of the 1990s by Mehta and colleagues [MEH 91], Chou [CHO 92] and Vollath [VOL 93a].

The reactor basically consists of a microwave resonant cavity connected to a waveguide supplied by a microwave generator and an impedance matching system. Plasma is confined in a quartz tube, with axial injection of plasma gas and

precursor. Sheath gases are tangentially injected to trigger a swirling type of displacement.

There are many parameters, often interdependent, that may influence the quantity and quality of the nanopowders generated.

First of all, several works have evidenced strong dependency of the size of particles obtained on the precursor concentration. This can be readily explained by the fact that, when concentration is high, there is a stronger probability that a heavy atom meets another one, and this facilitates nucleation, and then coalescence phenomena. This has most notably been studied by Szabo in relation with the size of SnO_2 particles [SZA 12] and by Schumacher [SCH 07].

For their part, Vennekamp *et al.* [VEN 11] have shown that a too high flow rate of central plasma gases leads to reaction quenching due to the rapid transfer of matter out of the plasma area. On the contrary, an increase in the microwave power leads to increase in the length of plasma jet, which results in a longer residence time and allows for growth and coalescence reactions to develop for a longer period, which in the end increases the size of particles. Finally, they have shown that the size of particles is a linear function of the logarithm of overall gas pressure, and that when precursor (tetramethylsilane) concentration is constant, the growth of SiC particles is a linear function of time.

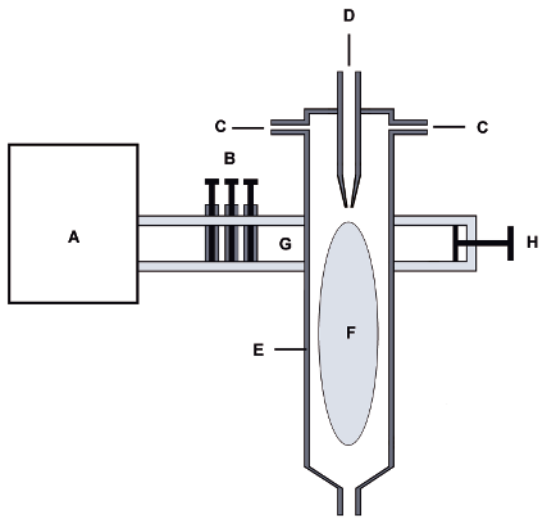

Figure 1.5. *Diagram of a microwave system; microwave generator (A), tuners (B), tangential entries for quench gases (C), entries for central plasma gases and precursors (D), discharge tube (E), plasma ((F), waveguide (G) and mobile piston (H)*

M	Precursor	Gas	Type	Generator	Diameter (nm)	Reference
Al	Al micron	Ar	MW	1.5 kW, 2.54 GHz	1–100	[PHIL 04]
	Al 50 µm	Ar	MW	1 kW	7.4–34.2	[WEI 04]
	Al pellets	Ar	DC	375–1,000 W	19	[PAR 05a]
	Al (anode)	Ar	DC	750 W	200–600	[CHA 06]
Ag	Ag_2CO_3	N_2	MW	2.45 GHz	9–10	[CHA 05]
	Ag micron	Ar, Ar/H_2	DC	7–9 kW	<100	[LEE 07]
	Ag bulk	Ar, N_2, He	DC	1.2–4.8 kW	20-100	[ZHO 09a]
B	BCl_3	$Ar/H_2/CH_4$	RF	45 kW	2–50	[MAR 05]
	BCl_3	Ar/H_2	DC	23–25 kW	50	[HUA 10a]
Co	$C_5H_5Co(CO)_2$	Ar	MW	0–6 kW, 2.45 MHz	12	[POD 04]
	$CoCl_2$	N_2/H_2	MW	2.45 GHz	41.4–21.6	[CHA 06]
Cu	Cu 40 µm	Ar/H_2	RF	28 kW, 2 MHz	50–280	[KOB 08]
	Cu bulk	Ar	DC	Unspecified	30–90	[WEI 06]
	$CuCO_3$	N_2, N_2/H_2	MW	5 kW, 2.45 GHz	60	[CHA 14a]
Fe	Fe 5–9 µm	Ar	RF	20 kW, 2.9 MHz	10–100	[GIR 93]
	$Fe(CO)_5$	Ar	MW	0–6 kW, 2.45 MHz	10	[POD 04]
	$Fe(CO)_5$	Ar	MW	0–6 kW, 2.45 MHz	10–15	[KAL 98]
	Fe bulk	Ar	MW	1.2 kW, 2.45 GHz	3–5	[HAY 90]
Mo	$Mo(CO)_6$	N_2	MW	5 kW, 2.45 GHz	20	[CHA 14a]
Mn	Mn bulk	He/H_2	DC	Unspecified	60	[PAN 07]
Ni	Ni Bulk	Ar	DC	Unspecified	20–70	[WEI 05]
	$NiCl_2$	N_2/H_2	MW	2.45 GHz	35–57.5	[CHA 07]
	$Ni(OH)_2$	Ar/H_2	RF	30 kW, 4 MHz	50–500	[BAI 09]
	$NiCO_3$	Ar/H_2	RF	30 kW, 4 MHz	50–500	[BAI 09]
Si	$SiCl_4$	N_2/H_2	MW	5 kW, 2.45 GHz	26	[KUM 12]
	SiH_4	Ar/H_2	MW	6 kW	4–50	[PET 11]
	Si 30–40 mm	Ar/H_2	RF	10–15 kW	13–37	[LEP 08]
	$SiCl_4$	Ar/H_2	RF	20–100 W, 70 MHz	2–10	[DIN 14]
	$SiCl_4$	H_2	MW	0.8 kW, 2.45 GHz	54	[WU 10]
	$SiCl_4$	Ar/H_2	DC	7.6–13 kW	<100	[RAO 95]
	SiH_4	Ar	RF	0.2 kW, 27.12 MHz	2–8	[MAN 05]
	$SiCl_4$	Ar/H_2	RF	15 W, 144 MHz	3–15	[NOZ 07]
	SiH_4	Ar	RF	200 W, 13.56 MHz	35 ± 4.7	[BAP 07]
W	APT	Ar/H_2	RF	30 kW, 4 MHz	6–48	[PLA 13]
	$W(CO)_6$	N_2	MW	5 kW, 2.45 GHz	30	[CHA 14a]
	APT	Ar/H_2	DC	13 kW	88.5	[RYU 09]

Table 1.14. *Examples of metal nanoparticles synthesized by thermal plasma, according to the literature; APT, ammonium paratungstate*

Oxides	Precursor	Gas	Type	Generator	Diameter (nm)	Reference
Al_2O_3	Al 3 µm $Al(NO_3)_3$ Al (anode)	Ar/O_2 Air Ar/air	RF MW DC	30 kW, 4 MHz 0.915 GHz 750 W	65.6–126 100–2,000 <40	[YE 07] [VOL 93a] [CHA 06]
Bi_2O_3	Bi bulk	O_2	DC	Unspecified	<1000	[CHE 05a]
Cr_2O_3	$Cr(CO)_6$	Ar/O_2	MW	0.915 GHz	7–15	[VOL 96]
Fe_2O_3	$Fe(CO)_5$ $Fe(CO)_5$ $Fe(CO)_5$ $Fe(CO)_5$ $Fe(Cl)_3$ Fe (anode) Ferrocene	Ar/O_2 $Ar/H_2/O_2$ $Ar/H_2/O_2$ Ar n.s. Ar/O_2 Ar/O_2	MW MW MW MW MW DC DC	0.7 kW, 2.45 GHz 2.45 GHz 2.45 GHz 180 W, 2.45 GHz 0.915 GHz 8.4 kW 6.7–7 kW	4.5 ± 1.3 25 <30 5.5–22 4–7 10–100 8–9	[BAU 06] [DAV 14] [DAV 13] [SYN 11] [VOL 95] [BAR 06] [LEI 12]
HfO_2	$Hf(OC_4H_9)_4$ or $HfCl_4$	Ar/O_2	MW	2.45 GHz	<5	[FOR 08]
MgO	Mg granule	Ar/O_2	MW	2.45 GHz	10–50	[HON 06]
MoO_3	$(NH_4)_6Mo_7O_{24}{\cdot}4H_2O$	n. s.	MW	700 W	100–1,000	[KLI 12]
NiO	Ni bulk	Ar/O_2	DC	Unspecified	25	[WEI 09]
SiO_2	SiO_2 µm	Ar/O_2	RF	40 kW	10–300	[GOO 06]
SnO_2	$Sn(C_4H_9)_4$ $SnCl_4$ $SnCl_4$ $SnCl_4$	Ar/O_2 Ar/O_2 Ar/O_2 $Ar/N_2/O_2$	MW MW MW DC	900 W, 2.45 GHz 2.45 GHz 2 kW, 2.45 GHz 6.6–10.2 kW	10 2–5 <10 3–20	[SZA 12] [SZA 07] [SCH 07] [IM 08]
TiO_2	$TiCl_4$ $Ti(OC_4H_9)_4$ TiN 28 µm	$Ar/O_2/SO_2$ Ar/O_2 Ar/O_2	MW MW RF	1.2 kW, 2.45 GHz 2.45 GHz 25 kW, 2 MHz	24–101 <5 50–70	[HON 11] [SCH 07] [OH 05]
V_2O_5	$VOCl_3$	$Ar/O_2/H_2$	MW	2.45 GHz	50–60	[KIM 07]
WO_3	ATP W bulk W bulk W wire $W(CO)_6$	Ar Ar/O_2 Ar/O_2 H_2O Ar/O_2	RF DC DC MW MW	30 kW, 4 MHz 2.34 kW 2.34 kW 200 W, 2.45 GHz 300 W, 2.45 GHz	100 20–30 6–18 7–13 3–4	[PLA 13] [SU 08] [SU 05] [HAT 13] [SAG 03]
ZnO	$Zn(CH_3)_2$ $Zn(CH_3)_2$ Zn powder Zn powder Zn powder	Ar/O_2 Ar/O_2 N_2/Ar or N_2 Ar/O_2 Ar/O_2	MW MW DC RF MW	Unspecified 2.45 MHz 70 kW 300 W, 13.56 MHz 2.45 GHz	3–7 4.9–10.3 30 30 100–200	[JAN 02] [KLE 02] [KO 06] [SAT 03] [KIM 07]
ZrO_2	$Zr(NO_3)_4$ $ZrCl_4$ $Zr(OC_4H_9)_4$ $Zr(OC_4H_9)_4$ or $ZrCl_4$	Ar Ar/O_2 Ar/O_2 Ar/O_2	MW MW MW MW	0.915 GHz 0.915 GHz 2.45 GHz 2.45 GHz	100–500 5 <5 <5	[VOL 93a] [VOL 93b] [SCH 07] [FOR 08]

Table 1.15. *Metal oxide nanoparticles synthesized by thermal plasma; ATP, ammonium paratungstate*

1.3.3.4. *Thermal plasma in solution*

The techniques that use discharges in liquids to obtain nanopowders can be differentiated depending on whether they are based on the conversion of liquid or components in solution or on electrode erosion. Several examples of metal or oxide nanoparticles obtained by these two options are reported in Tables 1.16 and 1.17.

In the case of the method based on erosion of metal electrodes, the latter are used as source material, and are immersed in an inert liquid, which means that its decomposition in the plasma phase does not generate solid particles. Deionized water is the most frequently used solvent, in which various salts can be dissolved in order to control ionic conductivity, pH or the oxidoreduction capacities of the medium in order to obtain metal or oxide particles. Either direct or alternating current can be used, and it can be applied in continuous, sequential or high frequency pulsed modes. To obtain the discharge arc, electrodes can be both made of the same metal or, if direct current is applied, the cathode only can be made up of a metal to be eroded. The anode is then made up of platinum. Finally, the electrodes can be placed facing each other or in parallel (Figure 1.6). Discharge-based erosion of electrodes creates a vapor starting from which nanoparticles are generated, and then condensates are formed.

A difficulty of this process relates to the control of the size of particles produced. The smaller ones, of the order of several nanometers, result from the condensation of metal vapor and are cooled by the liquid before being able to grow or coalesce with other particles. Those of intermediary size (between 20 and 30 nm) have already stayed for some time in the intermediary region between plasma discharge and the liquid. Finally, the larger particles (of the order of 100 nm) are generated by the metal droplets resulted from the fusion of the electrode during the erosion process. The nanoparticle size distribution is largely determined by how the electrical discharge is delivered [CHE 04].

Works conducted by Ashkarran *et al.* have evidenced that the size of particles produced is correlated with the intensity of the discharge current used during the production of TiO_2 [ASH 10d] and WO_3 [ASH 08] particles.

Still, some other important parameters should be taken into account. Some of these are, for example, the melting temperature of the electrode material, the time and amount of energy deposited, the distance between electrodes or the solvent nature, dielectric character, viscosity, etc. [BEL 14].

Oxide can be obtained directly by metal oxidation in the liquid phase or from the species resulted during the liquid decomposition. At breakdown voltage, besides the

evaporation of the electrode metal (copper or zinc, for example) [SAI 11, HU 14a], there is water decomposition into reactive ionized radical species that oxidize the metal atoms. A second method consists of bubbling gaseous oxygen into the liquid phase [ASH 10d].

As for metals that are sensitive to strong oxidation of the aqueous medium due to the presence of hydroxide radicals and atomic oxygen resulted from water decomposition in the plasma phase, in their case it is possible to use another solvent, such as styrene [OMU 07]. The resulting metal particle is coated with a thin layer of polystyrene [SUL 09]. As described by Yao *et al*. a further method consists of modifying the aqueous medium by adding a reducing agent such as hydrazine hydrate [YAO 05] or by using a citric acid buffer solution (pH 4.8) as per Saito *et al.* study [SAI 11]. In the example mentioned, these researchers obtained metallic copper nanoparticles in porous spherical form. The proposed mechanism involves the transformation of molten copper nanoparticles containing oxygen resulted from water decomposition, via the formation of hydroxylated species, followed by a phase of solidification of a Cu-Cu_2O eutectic. The oxide is dissolved by the buffer solution, and non-oxidized copper emerges in porous spherical form.

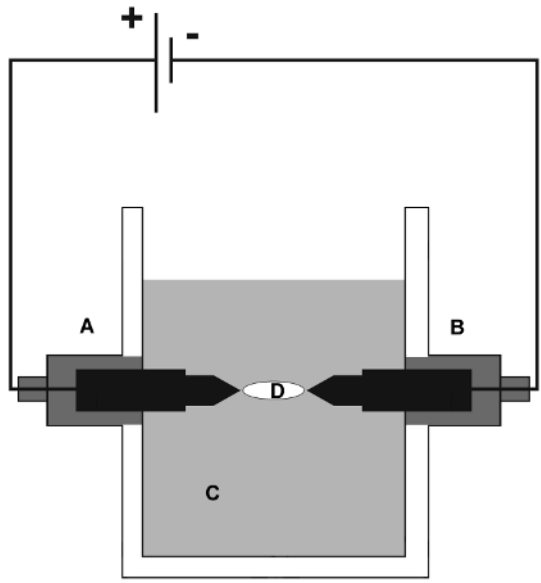

Figure 1.6. *Diagram of a plasma arc system in liquid medium: anode (a), cathode (b), liquid (c) and plasma (d)*

A second method is to transform metal ions in solution in the liquid by generating plasma between two tungsten or platinum electrodes [LEE 14a, BRA 11]. When nanoparticles are fabricated by plasma in liquid medium, a surfactant such as SDS or CTAB is often added. The surfactant generally facilitates the dispersion of particles and eliminates or strongly reduces particle aggregation. This results in slower growth of particles [LEE 14b]. Moreover, surfactant molecules tend to preferentially bond to certain crystal faces, if they are characterized by significant differences in the surface energy, which results in anisotropic growth of the particle. Surfactants are thus perceived as contributors to the generation of non-spherical particles [KIM 13a].

NP	Liquid	Precursor	Electric conditions	Diameter (nm)	Reference
Ag	H_2O	$AgNO_3$	DC 15A	27 ± 14	[ASH 10a]
	H_2O	Ag electrodes	DC 4 A, 135 V	5–55	[TIE 09]
Al	H_2O, CTAB	$AlCl_3{\cdot}6H_2O$	DC 250 V, 5 µs, 30 kHz, W electrodes	10–100	[KIM 15a]
Au	H_2O, CTAC	$HAuCl_4$	DC, 250 ns, 10 kHz, Pt electrodes	1–10	[BRA 11]
	H_2O	Au electrodes	DC, 70–100 V, 2–3 µs	15–30	[LUN 07]
	C_2H_5OH	Au electrodes	DC, 135V, 6.4A, 50 µs	4–15	[TSE 09]
Co	H_2O, SDS	$CoCl_2$	DC 250V, 5 µs, 30 kHz, W electrodes	10–30	[KIM 13a]
Cu	styrene	Cu electrode	AC 200 V, 5A	3	[OMU 07]
	H_2O, CTAB	$CuCl_2$	DC 250 V, 5 µs, 30 kHz, W electrodes	1–5	[LEE 14b]
	H_2O, citric buffer	Cu cathode	DC 105–130 V Pt anode	100	[SAI 11]
	H_2O Hydrazine	Cu electrodes	AC 150 V	30–50	[YAO 05]
Fe	H_2O CTAB	$FeCl_2$	DC 250 V, 5 µs, 30 kHz, W electrodes	5–20	[HEO 15]
Mn	H_2O, CTAB	$MnCl_2$	DC 250 V, 5 µs, 30 kHz, W electrodes	50–150	[KIM 13b]
Ni	H_2O, SDS	$NiCl_2$	DC 250 V, 5 µs, 30 kHz, W electrodes	20	[KIM 15b]

Table 1.16. *Examples of metal nanoparticles (NP) synthesized by plasma in liquids; SDS, sodium dodecylsulfate; CTAB, cetyltrimethylammonium bromide; CTAC, cetyltrimethyl ammonium chloride*

NP	Liquid	Precursor	Electric conditions	diameter (nm)	Reference
CoO	H_2O	Co acetate	AC 20 kHz, 15 kV, 10 A, 2 µs	2.5	[CHE 12]
Cu_2O	H_2O, ascorbic acid	Cu electrodes	AC 150 V	4–10	[YAO 05]
CuO	H_2O K_2CO_3			<100	[SAI 11]
CuO nanowires	H_2O, $NaNO_3$	Cu cathode Cu electrodes	DC 105–130 V Pt anode AC, 150 V	D = 1– 3 L = 4–10	[YAO 05]
CuO nanowires	H_2O, NaCl	Cu cathode	DC 10–20 kHz, 1–2 µs,	D = 15–25 L = 50–60	[HU 14a]
TiO_2	H_2O	Ti electrodes	AC 200 V, 5 A	7	[OMU 07]
	H_2O, O_2	Ti electrodes	DC, 20–40 A, 2–3.5 V	5–31	[ASH 10d]
WO_3	H_2O, SDS	WCl_6 ethanol	DC 250 V, 5 µs, 30 kHz, W electrodes	50–70	[LEE 14a]
	H_2O	W electrodes	DC, 10 V, 25 A	30 ± 12	[ASH 08]
WO_3. H_2O	H_2O	W electrodes	DC 100 V, 50 A, 15 µs	5	[CHE 14]
ZnO nanowires	H_2O	Zn electrodes	DC 3.5 kV, 100 Hz, 30 µs	D = 30 L = 80–100	[TAR 10]
ZnO	H_2O	Zn electrodes	DC, 5–15 A, 2-3.5 V	100–260	[ASH 09]
	H_2O	Zn electrodes	DC, 5A, 2–3.5 V	15–20	[ASH 10c]
ZrO_2	H_2O	Zr electrodes	DC 10–20 A, 2–3.5V	7–52	[ASH 10b]

Table 1.17. *Examples of metal oxide nanoparticles (NP) synthesized by plasma in liquids; SDS, sodium dodecylsulfate; CTAB, cetyltrimethylammonium bromide; CTAC, cetyltrimethylammonium chloride*

1.3.4. *Laser ablation*

Reports on the use of a laser beam to ablate a solid target date from the 1960s, when ruby lasers were developed [SMI 65].

Nanopowders can be obtained by using various types of laser, which operate in continuous or pulsed mode. Referring to the latter, they differ depending on the pulse duration: there can be nanosecond or ultrashort (pico- or femtosecond) pulse lasers, since ablation mechanisms differ.

In a classical approach, processes resulting from the interaction of a laser beam with the surface of a material are strongly dependent on laser parameters such as pulse duration, wavelength or fluence, on the one hand, and on material's physical properties, especially melting and evaporation temperature, latent heat, thermal diffusivity, etc., on the other hand.

From the perspective of using laser ablation to obtain nanopowders, it is worth taking into account a new parameter related to the nature of the environment in which the plasma plume formed during ablation will expand. The expansion can take place in a "free" medium, which means in the presence of high vacuum or vacuum with low gas concentration or even in a confined medium, such as a liquid. This will significantly influence the formation mechanisms, size, dispersion or the nature of particles obtained, if there is chemical interaction between them and the surrounding medium (gas or liquid).

Laser ablation systems presently feature Nd:YAG or excimer lasers. The first systems are inexpensive and require little maintenance. As for excimer lasers, they are based on gas-filled laser cavities, so their use requires precaution. On the other hand, in comparison with Nd:YAG lasers, these lasers allow us to obtain higher output power and have a more homogeneous beam profile. The target can be a sheet of very high purity metal or metal alloy or a tablet of micron-sized metal or oxide particles. Particles obtained by laser ablation of solid targets result directly from the condensation of the plasma plume generated by the laser pulse irradiating the solid target surface.

1.3.4.1. *Long pulse*

When long pulses (ranging from continuous to nanosecond) are used, particle formation is essentially dominated by thermal transfer. The photons in the laser beam have their energy absorbed quasi-instantaneously by the valence electrons, then electronic thermalization takes place by collisions of electrons with each other over a duration from 10 to 100 fs, depending on the nature of the material and laser fluence [RET 02]. In a next stage, energy is transferred within picoseconds from hot electrons to the ion network in the form of phonons. Throughout this thermalization phase, the system is out of equilibrium, its electronic temperature being higher than its ionic temperature. Complete thermalization of the material is normally reached within several picoseconds from the laser energy deposit.

Since the pulse duration is longer than the duration of the thermal mechanisms involved, the ion network becomes heated during the laser pulse.

The process of ablation taking place during a long pulse irradiation is governed by hydrodynamics and heat conduction, since the pulse duration is longer than both

the electron-phonon thermalization time (1–10 ps) and the thermal diffusion time (~10 ns).

When applied fluence exceeds the ablation fluence threshold of the material, matter is ejected in the form of vapor or fragments composed of ions, electrons, neutral atoms, aggregates and droplets of molten material. This fluence threshold depends on the material and laser parameters. The ejected particles remain at first confined near the target surface and form the Knudsen layer [KEL 98]. This layer has the same surface dimensions as the laser spot and its thickness corresponds to the optical penetration length δ, which depends on the laser wavelength and the material's extinction coefficient (n_2) according to the relation: $\delta = \lambda\ 4\pi\ n_2$. The particle density within this layer is close to solid density (10^{19}–10^{21} cm^{-3}) [SIN 90].

When the target stops being able to diffuse the absorbed energy into the network, the Knudsen layer is subjected to vaporization [MIO 95, WIL 00].

Since ablation starts well before the end of the laser pulse, the forming vapor and the laser interact, and plasma will be generated. This will be formed through two different mechanisms [CHA 96, SCH 98]. The first one consists of photoionization, which involves ionization of an atom which is neutral or in an excited state, following the absorption of one or several photons. It is worth noting that this process proves more efficient when lasers operate at short wavelengths [AMO 99, MAO 07] rather than at visible or infrared light wavelengths. The second mechanism involves primary electrons emitted either as result of the absorption of several photons by a neutral atom that thus reaches its ionization potential (multiple photon ionization), or due to electron emission by the heated material (thermionic effect), or finally by ionizing collision between vapor atoms. These free electrons absorb the photons emitted by the laser through inelastic collisions with vapor ions and neutral atoms. Called inverse Bremsstrahlung (or inverse braking radiation), this phenomenon enables electrons to gain kinetic energy that, when reaching sufficiently high values, will allow them to ionize vapor atoms through collisions.

Finally, when electron density increases too much, plasma becomes highly opaque to the laser beam and reflects it [MAO 97, AGU 98]. As a result, the material gains less and less energy, and this slows down ablation phenomena and therefore plasma growth, until the end of the laser pulse.

1.3.4.2. *Ultrashort (picoseconds and femtoseconds) pulses*

In the case of a femtosecond pulse, whose duration is shorter than the time needed for a material to thermalize, energy is transferred to the ion network only after the pulse has ended. Depending on the deposited energy, two major

phenomenologies can be observed. If the intensity is strong enough to rapidly excite a significant number of carriers, then non-thermal phenomena will cause ablation. On the other hand, thermal phenomena will predominate: the solid is then composed of a gas of hot electrons surrounding a network of ions that are still cold. Then, electron network thermalization takes place (several picoseconds). Ablation can be produced as follows:

– by evaporation [LOR 06]: when the energy level is below the ablation threshold, only the layers at the surface of the material are ejected through vaporization. Should a thick (several micrometers) material be considered, which is often the case of targets employed for producing nanoparticles, and if this target is irradiated by pulses with fluence above the ablation threshold, this will result in several distinct types of ablation products for one unique irradiation. The energy deposited decreases as it penetrates the solid and thus it is the more in-depth layers that will evaporate;

– by phase explosion [LOR 03]: phase explosion or explosive boiling takes place when the energy deposit allows to obtain at the surface, and in its vicinity, a level of temperature close to the critical value. This triggers homogeneous nucleation of gas bubbles within the overheated liquid layer and the material is subjected to rapid transition from overheated liquid to a mixture of vapor and liquid drops. Contrary to the phase explosion mechanism for long pulses (of the order of 1 ns), material heating induced by a femtosecond pulsed irradiation is carried out at constant volume;

– by spallation fracture [WU 14a, DEM 10, INO 10, ION 11]: an extremely rapid increase in the temperature of ions in the crystal lattice during return to thermal equilibrium (when electronic temperature equals ionic temperature) in a volume that is quasi-constant due to its inertia generates very high local pressure in comparison to the ambient pressure. This results in radial emission of a compression wave. A significant part of it propagates toward the target core, but one part is equally directed toward the surface, and is reflected, being transformed into a stress wave with reversed propagation direction. When propagating through the crystal phase, this stress wave causes fractures and matter ejection. This spallation phenomenon can also occur when the shockwave is reflected and is superimposed on the stress wave that is still propagating toward the back face;

– by fragmentation: separation of a supercritical fluid into droplets by dilution in vacuum above the substrate [LEV 04, WAN 92, ION 13].

When fluence is high, ablation can be caused by non-thermal phenomena. The rapid excitation of the electrons in the conduction band can lead to crystal lattice instability [ROB 86, ROU 01]. Under these circumstances, the direct transition from

solid to plasma state is possible by optical breakdown [VON 96]. Coulomb explosion is also possible in the case of dielectrics, and it consists of ablation due to electrostatic repulsion among ionized atoms [STO 02].

Contrary to the expansion of the plasma cloud generated by nanosecond pulses, the plasma cone generated by ultrashort pulse is dilated without further heating. Its temperature and pressure decrease rapidly and therefore its lifetime is short.

1.3.4.3. *Plasma expansion under vacuum or low pressure*

The plume expansion under vacuum is considered adiabatic, particles are subjected to few collisions and the expansion regime is free. Energy is dissipated through various radiation loss processes. At the beginning, free electrons lose a part of their kinetic energy when they move through the Coulomb field of a neutral atom or ion (Bremsstrahlung effect). The same can happen through radiative recombination when the electron is captured by an ion. When temperature and density of free electrons have sufficiently decreased, emissions corresponding to electron transitions from various excited states in the neutral or ionized atoms take place. Thermal exchange processes lead the vapor atoms to condense in small aggregates of several hundred atoms, and then by aggregations and coalescence to form nanoparticles.

When low concentration gas is used, the plume expansion is restricted by the compression of ambient gas, and this expansion in turn compresses the ambient gas [HARI 03]. Plasma propagates according to a high pressure shockwave that attenuates until it reaches the ambient air pressure. Plasma expansion is reduced due to the gas presence. In case the gas presents reactive atoms, they can have chemical interactions with the ionized atoms and form new species.

When plasma is generated by a short pulsed laser, there is no interaction between plasma and laser pulse, as plasma only emerges after the pulse ends. Table 1.18 presents several examples drawn from the literature on the fabrication of metal and oxide nanoparticles by laser ablation in a gas medium.

1.3.4.4. *Laser ablation in liquids*

The first works related to laser ablation of solids being immersed in liquids in order to have their surface altered were reported at the end of the 1980s by Patil [PAT 87] and Ogale [OGA 88]. It was only in 1993 that the first works carried out by the teams of Henglein and Cotton on the synthesis of nanoparticles by laser ablation in liquids, in order to prepare nanoparticles free of surface contamination, were published [HEN 93, NED 93].

Metal	Target	Experimental conditions	Gas	d or d_o (nm)	Reference
Al	Al	KrF Excimer, λ: 248 nm, pulse: 20 ns, f: 20 Hz, E: 15 mJ/pulse, 5,000 pulses	$P = 10^{-6}$ Torr	76–2,000	[SIR 11]
Cu	Cu	Ti: Sapphire, λ: 800 nm, f: 1 kHz, pulse 100 fs, F: 4 J/cm^2	$P \leq 10^{-4}$ Pa	0.5–12	[NOE 07]
Mo	Mo	KrF excimer, λ : 248 nm, pulse: 20 ns, f: 20 Hz, E: 15 mJ/pulse, 5000 pulses	$P = 10^{-6}$ Torr	75–2,000	[SIR 11]
Ni	Ni	Nd:Glass, λ: 1,055 nm, pulse: 0.85 ps, E: 4 mJ/pulse, f: 33 Hz, T = 60 min Nd:Double glass, λ: 527 nm, pulse: 0.30 ps, E: 1.3 mJ/pulse, f: 33 Hz, T = 60 min	$P \leq 10^{-5}$ Pa $P \leq 10^{-5}$ Pa	23–56 5–65	[AUS 06]
	Ni	Nd:Double glass, λ: 527 nm, pulse: 300 fs, E: 4 mJ/pulse Nd:Triple glass, λ: 263 nm, pulse: 300 fs, E: 4 mJ/pulse	$P \leq 10^{-7}$ Pa $P \leq 10^{-7}$ Pa	37 17	[AMU 07]
	Ni	Ti:Sapphire, λ: 780 nm, f: 1 kHz, pulse 120 fs, F: 0.3 J/cm², 200 pulses	$P \approx 10^{-5}$ Pa	40 ± 19	[AMU 05a]
Si	Si	Nd:Glass, λ: 1055 nm, pulse: 0.85 ps, E: 4 mJ/pulse, f: 33 Hz, T = 2–60 min Nd:Glass, λ: 527 nm, pulse: 0.30 ps, E: 1.3 mJ/pulse, f: 33 Hz, T = 2–60 min	$P \leq 10^{-5}$ Pa $P \leq 10^{-5}$ Pa	5–39 9–114	[AUS 06]
	Si	ArF Excimer, λ: 193 nm, pulse: 12 ns, F: 1 J/cm^2	He, P = 333 Pa He, P = 665 Pa	d_0 = 13 d_0 = 17	[YAM 96]
	Si	Nd:YAG double λ: 532 nm, pulse: 7 ns, F: 5 J/cm^2	Ar, P = 5 Torr	1.5–3	[MAK 04]
W	W	ArF Excimer, λ: 193 nm, pulse: 15 ns, f: 1–25 Hz, F: 1.4–8.3 J/cm^2, T=15 min	N_2, P = 1 atm	2–110	[LAN 03]
	W	Nd:Double YAG, λ: 532 nm, pulse: 4.5-5.5 ns, f: 20 Hz, F: 1.9–3.8 J/cm^2	He, P = 2.7–90 kPa	10–20	[OZA 01]
	W	KrF Excimer, λ: 248 nm, pulse: 20 ns, f: 20 Hz, E: 15 mJ/pulse, 5,000 pulses	$P = 10^{-6}$ Torr	100–2,000	[SIR 11]
CuO	CuO	Nd:YAG λ: 1064 nm, pulse: 0.5 ms, f: 34 Hz, E: 5,600 W/mm^2	Air, $P = 9 \times 10^4$ Pa	4–26	[YAN 02]
α-Cr_2O_3	Cr	Nd:YAG λ: 1,064 nm, pulse: 0.24 ms, f: 10 Hz, E: 1,100 mJ/pulse	Air + O_2 50 L/min	30–100	[LIN 09b]
γ-Fe_2O_3	Fe	Nd:YAG λ: 1,064 nm, pulse: 0.3–20 ns, f: 5–150 Hz, P: 400W	N_2, P = 0.18 MPa O_2 , P = 0.02 MPa	5–90	[WAN 06a]

Table 1.18. *Metal nanoparticles obtained by laser ablation in gas medium d_0, mean diameter; F, fluence, E, energy deposited per pulse; T, ablation duration; P, emitted power*

Many works have meanwhile evidenced the possibility of producing a very wide variety of nanomaterials, depending on a variety of laser parameters or on the nature of the liquids employed.

1.3.4.4.1. Pulse specificity in the liquid phase

In very general terms, when focusing a given wavelength laser beam on a target immersed in a transparent liquid medium, energy is transferred to the target according to the previously described mechanisms, depending on pulse duration [YAN 07a, BER 97]. When the beam irradiates the surface of the immersed target, a plasma is formed at the solid–liquid interface. Confined within the liquid, this plasma undergoes adiabatic dilation at supersonic rate, which triggers a shockwave that, in turn, induces temperature and pressure increase in the plasma [FAB 90] [BER 99, BER 00]. Compared with expansion in air or under vacuum, plasma expansion in a liquid medium is much smaller [WU 08]. This confinement leads to a much higher density of ablated species than in the case of expansion under vacuum or low gas pressure. But on the other hand, plasma lifetime in a liquid medium is also much shorter. These two phenomena have a conflicting effect in terms of size of the particles formed. The first phenomenon tends to facilitate the coalescence of nanoparticles due to the high density of species that are present, while the short lifetime of plasma involves a reduction of the time available, within it, for the reactions of coalescence and agglomeration to last sufficiently and to influence the size of the particles formed [SAI 02].

Finally, the liquid located at the plasma–liquid interface vaporizes and gives rise to bubbles that coalesce and form a cavitation bubble [PAR 96]. The species present in this bubble are dissociated, ionized and mixed with the present species, thus enabling new chemical reactions. Metal ablation in water leads to the formation of metal hydroxides [LIA 04], while if carried out in carbon-rich solvents, it produces carbides [PRO 97]. This bubble will expand its volume and size and will in the end implode. During its implosion, a second shockwave is generated [TSU 07, SAS 05] and all the species present in the plasma will be ejected in the solvent.

As nanoparticles continue to be generated, they accumulate in the liquid phase and interact with the incident beam. Due to absorption and diffusion phenomena, beam transmission in the medium is significantly reduced. This results in an important reduction of efficiency as a function of time [TSU 02]. Several strategies can be deployed as remedy. The first solution consists of using only a small thickness of liquid above the target, but it results in low product quantities, as the liquid volume gets rapidly saturated in particles. The second solution consists of using a steady stream cell that allows us to recover particles as they are produced, while maintaining a flow of liquid free of most of its particles in suspension [BES 10, SAJ 10b]. On the contrary, this reduces the interactions between the beam and the colloids in suspension and consequently the fragmentation and growth phenomena induced by laser pulse irradiation of a colloidal solution [PAN 14, PYA 14].

Thus various types of metal nanoparticles, metal oxides or semiconductor particles such as silicon [SEM 10], have been produced by laser ablation of an immersed massive target [YAN 08] or by fragmentation of particles with sizes of several micrometers placed in suspension in the liquid [PAN 14].

Tables 1.19 and 1.20 report a certain number of examples in the literature referring to metal and oxide nanopowders that have been obtained.

Metal	Target	Experimental conditions	Liquid	d or d_o (nm)	Reference
Al	Al	Nd:YAG, λ: 1.06 µm, *f*: 10 Hz, *T*: 1 h, pulse: 30 ps, *F*: 4 J/cm^2	Ethanol + H_2	30	[VIA 10]
	Al	Ti:Sapphire, λ: 800 nm, pulse: 200 fs, *f*: 1 kHz, *F*: 0.4 J/cm^2, *T*: 10 min Nd:YAG, λ : 1064 nm, pulse: 30 ps, *F*: 8 J/cm^2, *f*: 10 Hz, *T*: 60 min Nd:YAG, λ: 1064 nm, pulse: 150 ps, *F*: 1.5 J/cm^2, *f*: 10 Hz, *T*: 60 min	Ethanol Ethanol Ethanol	10–60 10–250 10–50	[STR 09]
Co	Co	Nd:YAG double, λ: 532 nm, pulse: 3 ns, *F*: 6.37 J/cm^2, *f*: 20 Hz, *T* = 60 min	EG, PVP	22	[ZHA 08]
Cu	Cu	Ti: Sapphire, λ: 800 nm, pulse: 120 fs, *f*: 1 kHz, *F*: 0.2 mJ/pulse, *T*: 60 min	H_2O/ethanol 8/2, PVP	10	[FAN 14]
	Cu	Nd:YAG double, λ: 532 nm, pulse: 5 ns, *E*: 0.2 J/pulse, *f*: 10 Hz, *T* = 10 min	Polysiloxane Mw=240 Mw=1200	 5–20 2–5	[SAI 08]
	CuO	Nd:YAG, λ: 1,064 nm, pulse: 5 ns, *F*: 509 mJ/cm², *f*: 10 Hz, *T* = 5 min	2-propanol	d_o = 28.9	[YEH 99]
Mg	Mg	Nd:YAG, λ: 1,064 nm, pulse: 5.5 ns, *F*: 0.265J/cm^2, *f*: 10 Hz, *T* = 60 min	2-propanol acetone	15–20 50–100	[PHU 08]
Ni	Ni	Nd:YAG double, λ: 532 nm, pulse: 3 ns, *F*: 6.37 J/cm^2, *f*: 20 Hz, *T* = 60 min	EG, PVP	8	[ZHA 08]
	Ni	Nd:YAG double, λ: 532 nm, pulse: 8 ns, *E*: 40 mJ/pulse, *f*: 10 Hz, *T* = 60 min	H_2O	3–5	[MAH 08]
Si	Si	Nd:YAG, λ: 1,064 nm, pulse: 10 ns, *E*: 160 mJ/pulse, *f*: 10 Hz, *T* = 60 min	H_2O, SDS	10–20	[YAN 08]
	Si	Ti : Sapphire double, λ: 387.5 nm, pulse: 180 fs, *f* :1 kHz, *F*: 0.8 J/cm^2	H_2O	d_o = 20	[SEM 10]
	Si	Nd:YAG, λ: 1064 nm, pulse: 60 ps, *f*: 20 Hz, *F*: 0.9–2.7 J/cm², *T* = 60 min, Nd:YAG triple, λ: 355 nm, pulse: 60 ps, *f*: 20 Hz, *F*: 0.4–4.4 J/cm², *T* = 60 min,	H_2O H_2O	40 ± 10 3 ± 1	[INT 14]
	Si	Ti : Sapphire, λ: 800 nm, pulse: 120 fs, *f*:1 kHz, *E*: 1 mJ/pulse, *T* = 30 min	H_2O	d_o = 2.4	[RIO 09]
Zn	Zn	Nd:YAG double, λ: 532 nm, pulse: ns area, *E*: 100 mJ/pulse, *f*: 10 Hz, *T* = 60 min	H_2O, SDS	14.7 ± 8.1	[SIN 07]

Table 1.19. *Metal nanoparticles obtained by laser ablation in liquid medium; EG: ethylene glycol, SDS: sodium dodecylsulfate, PVP: polyvinylpyrrolidone, d_0 mean diameter, F: fluence, E: energy deposited per pulse, T: ablation duration, Mw: average molecular weight*

Oxides	Target	Experimental conditions	Liquid	d or d_o (nm)	Reference
Al_2O_3	Al_2O_3	Ti:Sapphire, λ: 800 nm *f*: 10 Hz, pulse: ≤ 130 fs, *F*: 0.462 J/cm^2, *T*: 90 min,	H_2O Ethanol	60 80	[ALN 13]
	Al_2O_3	λ: 1,064 nm f: 4 kHz, pulse: 40–55 ns, *F*: 14–50 J/cm², *T*: 5 min	H_2O	29	[SAJ 10a]
Bi_2O_3	Bi_2O_3	Ti/Sapphire, λ: 800 nm, pulse: 120 fs, *f*: 1 kHz, *F*: 0.5 mJ/pulse, *T*: 60 min	Ethanol	10–60	[LIN 10]
	Bi	Nd:YAG, λ: 1.06 μm, pulse: 10 ns, *f*: 1 Hz, *F*: 21 J/cm², *T* = 200 min	H_2O	56.81	[ISM 14]
Co_3O_4	Co	Nd:YAG, λ: 1,064 nm, pulse: 4 ns, *f*: 10 Hz, *E*: 330 mJ/pulse, *T* = 15 min Nd:YAG, double, λ: 532 nm, pulse: 4 ns, *f*: 10 Hz, *E*: 165 mJ/pulse, *T* = 15 min	H_2O H_2O	10–14 13–22	[HU 14b]
CuO	Cu	Nd:YAG double, λ: 532 nm, pulse: 90 fs, *f*: 1 Hz, *T* = 30 min, *F*: 9J/cm²	H_2O	25–200	[NAT 11]
Cu_2O	Cu	Nd:YAG, λ: 1,064 nm, pulse: 10 ns, *f*: 10 Hz, *E*: 80 mJ/pulse, *T* = 60 min	H_2O, PVP	15–60	[LIU 11]
Cr_3O_4	Cr	λ: 800 nm, pulse: 90 fs, *f*: 1 kHz, *T* = 35 min, *F*: 102 J/cm²	H_2O	6.8	[SEM 14]
	Cr	Nd:YAG, λ: 1,064 nm, pulse: 240 μs, *f*: 10 Hz, *E*: 1100 mJ/pulse, *T* = 10 min	H_2O	10–30	[LIN 09a]
Fe_2O_3	Fe_2O_3	Nd:YAG, λ: 1,064 nm, *E*: 40 mJ/pulse, *f*: 10 Hz, *T* = 60 min	H_2O H_2O, CTAB	28–33 10.7–15.6	[PAN 14]
	Fe_2O_3	Nd:YAG triple, λ: 355 nm, pulse: 10 ns, *E*: 40 mJ/pulse, *f*: 30 Hz, *T* = 60 min	Ethanol H_2O Acetone	3–50, 5–30 4–28	[MAN 13]
$Mg(OH)_2$	Mg	Nd:YAG triple, λ: 355 nm, pulse: 7–8 ns, *E*: 100 mJ/pulse, *f*: 10 Hz, *T* = 60 min	H_2O, SDS	*L* > 200 Φ = 10– 30	[LIA 04]
	Mg	Nd:YAG, λ: 1,064 nm, pulse: 5.5 ns, *F*: 0.265J/cm^2, *f*: 10 Hz, *T* = 60 min	H_2O H_2O, SDS	*L* = 150, Φ = 5–10 20–30	[PHU 08]
NiO	Ni	CW, P: 250 W, λ: 1,070 nm, *T*: 1s, Spot: 40 μm	H_2O, SDS	13 ± 9	[LIU 09]
TiO_2	Ti	CW, P: 250 W, λ: 1,070 nm, *T*: 1s, Spot: 40 μm CW, P: 250 W, λ: 1,070 nm, T: 1s, Spot: 40 μm	H_2O, SDS H_2O H_2O, SDS	17 ± 7 27 ± 11 40 ± 18	[LIU 09, ABD 08]
	Ti	Nd:YAG triple, λ: 355 nm, pulse: 7 ns, *E*: 150 mJ/pulse, *f*: 10 Hz, *T* = 60 min	H_2O, SDS	2–6	[SAS 04]
Sb_2O_3 fibers	Sb	Nd:YAG double, λ: 532 nm, pulse: 5 ns, *E*: 140 mJ/pulse, *f*: 10 Hz, *T* = 10 min	H_2O H_2O, SDS	35	[MEN 13]
SnO_2	Sn	Nd:YAG triple, λ: 355 nm, pulse: 7 ns, *E*: 100 mJ/pulse, *f*: 10 Hz, *T* = 60 min	H_2O, SDS	2–6	[SAS 04]

	Sn	Nd:YAG triple, λ: 355 nm, pulse: 7 ns, *E*: 100 mJ/pulse, *f*: 10 Hz, *T* = 60 min	H_2O, SDS	2.5 ± 0.6	[LIA 03]
*H_2WO_4 flakes	W	Nd:YAG double, λ: 532 nm, pulse: 10 ns, *E*: 300 mJ/pulse, *f*: 10 Hz, *T* = 30 min	H_2O	10	[XIA 12]
*H_2WO_4	W	Nd:YAG λ: 1064 nm, pulse: 10 ns, *E*: 80 mJ/pulse, *f*: 10 Hz, *T* = 120 min	H_2O	1	[ZHA 14, [ZHA 12b]
WO_3	W	Nd:YAG double λ: 532 nm, pulse: 5 ns, *F*: 1–7 J/cm^2, *f*: 10 Hz, *T* = 30 min	H_2O	2–6	[BAR 11]
ZnO	Zn	Nd:YAG double, λ: 532 nm, pulse: ns, *E:* 60 mJ/pulse, *f*: 10 Hz, *T* = 60 min	H_2O, SDS, O_2	13.7 ± 5.8	[SIN 08]
	Zn	Nd:YAG triple, λ: 355 nm, pulse: 7 ns, *E*: 100 mJ/pulse, *f*: 10 Hz, *T* = 20 min	H_2O, CTAB	10–25	[HE 08]
	Zn	Nd:YAG triple, λ: 355 nm, pulse: 7 ns, *E*: 100 mJ/pulse, *f*: 10 Hz, *T* = 60 min	H_2O pH : 5.36 pH:11.98 pH: 7.51 NaCl	 15 ± 6 20 ± 8 23 ± 11 26 ± 15	[HE 07]
ZnO nanorods	Zn	Nd:YAG triple, λ: 355 nm, pulse: 7 ns, *F*: 3.2 J/cm^2, *f*: 10 Hz, *T* = 40 min	H_2O, 80°C	*L* = 500–600 Φ = 200	[ISH 06]

*WO_3 precursor before calcination at 800°C, 4 h.

Table 1.20. *Metal nanoparticles obtained by laser ablation in liquid medium. SDS; sodium dodecylsulfate; CTAB, cetyltrimethylammonium bromide; PVP, polyvinylpyrrolidone; d_0, mean diameter; F, fluence; E, energy deposited per pulse; T, ablation duration*

1.3.4.5. *Effect of laser parameters*

1.3.4.5.1. Effect of number of pulses

Several authors have shown that when the number of pulses increased, the mean diameter and the size dispersion decreased. Notable examples in this sense include the works of Mahfouz *et al.* [MAH 08] related to the fabrication of nickel oxide nanoparticles in water or those of Prochazka *et al.* [PRO 97] referring to colloidal silver nanoparticles. These researchers have shown that the size of the particles formed decreased when the number of pulses increased and, moreover, irradiating the colloidal solution with only one laser pulse resulted in a reduction of particle size.

Works conducted by Mafuné *et al.* [MAF 01] on the synthesis of silver nanoparticles have evidenced that the abundance of nanoparticles formed increases linearly as a function of the number of pulses, up to a limit of around 50,000 pulses beyond which the increase slows down. Slope reduction beyond the 50,000 pulses

could be explained by weak absorption of the wavelength by the silver nanoparticles that contribute to the attenuation of the laser beam that penetrates the solution above the metal plate. As the energy that reaches the surface of the target is lower, the formation of nanoparticles loses efficiency.

1.3.4.5.2. Effect of pulse duration

Compared with longer pulses, of the nanosecond type [YAN 08], the use of short picosecond [INT 14] or femtosecond [RIO 09] pulses leads to obtaining smaller diameter particles with low polydispersity. This can be due to non-thermal ablation, such as Coulomb explosion for a dielectric, when radiation energy is low. On the other hand, the femtosecond pulse ends well before plasma starts to emerge. This generates a plume of lower intensity and the lifetime of the cavitation bubble is shorter. This tendency increases in the case of ablation in the liquid phase or for adequate pressure of ambient gas. Under femtosecond regime, the growth of nuclei is thus limited, which leads to the production of smaller nanoparticles [SYL 05].

On the other hand, the yield of nanoparticle production can be made up for by using a higher repetition frequency for femtosecond lasers: this is of the order of kilohertz, while for the nanosecond lasers, the repetition frequencies are of the order of hertz or a dozen hertz.

1.3.4.5.3. Effect of wavelength

The rate of metal ablation tends to increase when laser wavelength diminishes [VLA 08, TSU 01]. On the one hand, this is due to higher radiation absorption by the metals when the wavelength is shorter. On the other hand, wavelength reduction generally leads to lower absorption of plasma by inverse Bremsstrahlung [BOG 05].

Furthermore, the secondary interaction between laser and the nanoparticles produced becomes stronger with shorter wavelengths [ZHE 07]. This secondary interaction normally leads to reduced size of the colloids that are fragmented by laser [TSU 02].

The use of shorter wavelengths generally results in a reduction of the mean size of the particles formed [TSU 02, NIC 06a].

1.3.4.5.4. Effect of fluence

Under fixed focus conditions, the mean size increases with pulse energy [SYL 05, KAB 03, AMU 05b]. This is caused by two phenomena. The first arises because of the higher concentration of matter in the plasma plume, which will facilitate coalescence and aggregation during cooling. In particular, Kabashin has shown that during the synthesis of gold colloids in water with a femtosecond laser, he obtained a linear log-normal correlation between the size of nanoparticles and

laser fluence [KAB 03]. When fluence exceeds a certain threshold that depends on the nature of the irradiated metal, a second phenomenon emerges, which generates large size particles. These result from the ejection of molten metal drops from the irradiated surface [YAH 10, FIS 06]. In effect, the largest particles formed (several dozen nanometers) during the use of high fluences are due to the phase explosion taking place at the target surface [ACA 10, AME 09, NIC 06b, KAB 03]. An increase in the size of particles is likewise obtained when defocused radiation is used [PET 09, PYAT 04, MAF 00a].

1.3.4.5.5. Effect of gas pressure

During the ablation in gas medium, the increase in ambient pressure limits the expansion of plasma plume and therefore that of ablated species. This results in weaker dilution that depends on time, and facilitates the growth of particles within plasma as the latter gets cooler [SUZ 12, BAR 07]. There are two mechanisms that govern the formation of different nanoparticles. Small nanoparticles mainly result from evaporation followed by condensation. As for larger particles, they result from a phase explosion process at the surface of the target, caused by laser radiation. As described in section 1.3.4.5.4, this last phenomenon depends on the fluence used [OZA 01].

1.3.4.5.6. Effect of solvent nature

Metal powders can be produced by laser ablation in a solvent. For example, ethylene glycol was used as reducing agent for obtaining nickel nanoparticles [ZHA 08]. The use of ethanol alone or in the presence of hydrogen dissolved by bubbling enables the production of titanium [SIM 04] or aluminum [VIA 10] nanopowders. Using water as solvent generally leads to the formation of metal oxides.

1.3.4.5.7. Effect of surfactants

When basic or acidic salts [SYL 04a, HE 07] or surfactants [SAS 04, PAN 14] [LIU 11] are introduced in the liquid medium before laser ablation, dramatic changes may occur in the distribution, nature [MAF 01], form [LIA 04] and/or aggregation density of nanoparticles obtained at given laser parameters.

Mafuné *et al.* have established that the presence of certain surfactants, such as SDS, could slow down or stop the oxidation of zinc particles in water [SIN 07, HAI 05]. Upon plasma extinction, the zinc clusters formed come in contact with the solvent and surfactant molecules present in solution, and this puts in competition the chemical reactions of oxidation and encapsulation of the particles. When the surfactant concentration is low, the first effect is the reduction of the aggregation of zinc clusters; oxidation phenomena are dominant and lead to the formation of zinc

oxide nanoparticles. When the surfactant concentration increases, the encapsulation effect becomes dominant and prevents zinc oxidation. This protection against oxidation is a phenomenon that has not been evidenced for other metals.

The use of surfactants influences the morphology of magnesium hydroxide crystallites produced in solutions of deionized water. SDS directs the growth of crystallites either along an axis that privileges fibrous morphologies or along two axes, which results in a platelet-analogous form. The growth mode depends on the surfactant concentration [YAN 07b, LIA 04].

In all cases, the increase in the stabilizer concentration results in decrease in the mean size of nanoparticles [MAF 00b, MAF 03, SYL 04b, SYL 04a].

1.3.4.5.8. Effect on colloids in suspension

When particles, either in suspension in gas or in solution, absorb the beam energy, the result may be fragmentation [TAK 99, INA 05, BES 06, SVR 11, YAM 06], growth [YEH 99, ZHE 07, BES 09], or modifications of the form of particles [AGU 04, PYA 07, WAN 10].

In liquid medium, these phenomena have been studied either by direct exposure to radiation of colloidal solutions of nanoparticles [GIAM 10, WER 11, PYA 09] or during the generation of nanoparticles by laser ablation of a solid target [MUT 08, MAF 01, VAN 13].

These works show that laser fragmentation of microparticles allows us to obtain nanoparticles with production yields that are higher than those obtained by laser ablation of the surface of a massive target [YEH 99, ZHA 03, KAW 06]. The nanoparticles produced by this method generally feature lower size polydispersity. Two possible models that explain these phenomena are reported in the literature. The first one relies on thermal transfer [PYA 13]. The energy deposited at the surface of the particle causes an increase in its temperature followed by melting and surface evaporation, which leads to a decrease in particle size [TAK 99] and also a change in form [PYA 07]. The second model, developed by Kamat *et al.* [KAM 98], proposes the Coulomb explosion phenomenon as cause of the observed size reduction. These two models are not mutually exclusive and enable a description of reality depending on the laser emission conditions. Strong fluence facilitates the fragmentation of nanoparticles by Coulomb explosion, while exposure to lower energy radiation facilitates fragmentation by thermal transfer.

1.3.4.6. *Conclusion*

To conclude, this technique offers the possibility of optimizing favorable effects in order to obtain small size particles, with low levels of polydispersity and

aggregation. To this purpose, it is preferable to use low laser fluences, low pulse widths, short wavelength and also long ablation durations. Finally, the use of surfactants facilitates particle size decrease and reduces particle aggregation [YAN 07a]. While small sizes, of the order of several nanometers, and weak polydispersity are obtained, the production yield remains at modest levels.

1.3.5. *Pyrotechnic synthesis*

1.3.5.1. *Detonation synthesis*

The originality of the synthesis by detonation resides in using a phenomenon that is commonly considered destructive to form nanosized grains of matter and "freeze" them while in divided state. Matter dispersion upon detonation allows for the formation of powders, in which elementary nanoparticles are less strongly agglomerated than those prepared in solution or by milling. Due to their small size, but also to the relative independence of the nanoparticles they are made up, the materials synthesized by detonation can be dispersed in liquids for which they have affinity. The formation of colloid suspensions constitutes the most important stage in the formulation of a nanothermite, regardless of whether it has been prepared by simple physical mixture of powders in suspension or by a proper assembly method.

From a historical perspective, nanodiamond was the first detonation synthesized material. Its presence in the secondary explosive detonation products was for the first time observed in July 1963 by Soviet scientists working in the field of nuclear weapons. The first tests conducted in 1962 consisted of the compression of graphite or carbon black contained in spherical or cylindrical storage ampoules due to a detonation shock. Graphite had been afterward incorporated in a cylindrical charge composed of trotyl (TNT) and hexogen. A test conducted in the absence of graphite had at that time shown that nanodiamonds were formed starting from the carbon content of explosive molecules [DAN 04]. The size of nanodiamonds resulted from explosive detonation ranges between 4 and 10 nm. Recent works have shown that the detonation of nanostructured hexolite (TNT/RDX) allowed to produce smaller nanodiamonds and, at the same time, to significantly increase their proportion in the detonation products [PIC 13]. As shown by the carbon phase diagram given by Bundy, at ambient air temperature and atmospheric pressure diamond is a metastable material [BUN 62]. When temperature increases, diamond transforms into graphite or oxidizes depending on the nature of the atmosphere it is exposed to. Diamond is the highest density form of carbon at ambient temperature ($d = 3.52$ g/cm^3) and one of the best heat conductors known [FIE 92]. Moreover, its oxidation energy is close to 33 kJ/g (or 116 kJ/cm^3), which recommends it as a reducing agent of choice for pyrotechnic compositions. The use of nanodiamond as fuel in energetic

compositions based on potassium chlorate ($KClO_3$) has been reported by Comet *et al.* [COM 09]. These compressed compositions feature continuous or intermittent combustion, depending on the proportion of nanodiamond they contain and on their porosity. The study of these original energetic materials has allowed us to estimate the rate of oxidation of the nanodiamond resulted from a detonation at 0.8 mm/s and to show that nanodiamond powders have a thermal conductivity that is four orders of magnitude smaller than that of massive diamond [COM 14a]. The small size of diamond nanoparticles and the presence of oxygen functional groups at their surface [SCH 12] render them easier to oxidize than massive diamond. Nanodiamond however remains a much less reactive fuel with respect to other fuels that are for nanothermite formulation, such as aluminum, boron or red phosphorus. This means that the oxidizability of nanodiamond is too low for this material to be used as fuel in nanothermites. However, detonation synthesized nanodiamond was used by Pichot *et al.* as an additive in order to significantly increase the threshold of sensitivity to friction and electrostatic discharge of a nanothermite based on bismuth oxide (Bi_2O_3) and aluminum. For this purpose, nanodiamond is first deposited on the surface of submicron Bi_2O_3 particles starting from a suspension in acetonitrile. The resulting composite material is then physically mixed with nanosized aluminum powder [PIC 15].

The use of detonation synthesis to produce various types of nanomaterials has been proposed by Eidelman and Altshuler. According to these authors, the detonation waves generate plasmas with high energy density, which can be effectively used to produce nanomaterials. The detonation of the most common explosives, which are formed of carbon, hydrogen, oxygen and nitrogen, results in nanostructured carbonaceous phases whose nature depends on the charge composition and on the environment in which it is fired. Depending on the experimental conditions, the detonation of more exotic explosives, containing boron, results in boron oxide (B_2O_3) or nitride (BN). Nanostructured metals are formed by the detonation of metal azides or acetylides. Finally, the incorporation of metal halides into classical explosive charges would be a method to nanostructure some metals such as iridium, plutonium, rhenium, tungsten, vanadium or titanium. Detonation synthesis offers the unique possibility to obtain stable polymorphous products at high pressure due to the drastic cooling triggered by the rapid quenching of the detonation products [EID 93].

There are two approaches to the detonation synthesis of nanostructured powders. The first is the *top-down method*, which consists of the fragmentation of inert matter under the action of the detonation shockwave. The second is the *bottom-up technique*, which consists of building nanoparticles starting from a reactive precursor.

Gibot *et al.* have used the top-down approach for the fragmentation of silicon carbide (SiC) particles that are initially of micrometer size (40–100 μm). To do so, the SiC particles are first coated with polyurethane in order to limit the friction between carbide and the explosive charge. The coated particles are afterwards mixed with trinitrotoluene and a wax; the charge results from the compression of this mixture. SiC particles are miniaturized by detonation, but their size distribution is very wide (0.01–10 μm) [GIB 11c]. This result indicates that the detonation wave impact does not allow to fragment the whole refractory matter contained by the charge. Dividing the small size primary particles into even smaller size secondary particles requires matter to be submitted to high stress. This experimental observation should be considered in connection with the concept of atom, which has for a long time been presumed an indivisible unit of elementary matter, whose fragmentation is only possible by employing significant energies developed by nuclear reactions. Silicon carbide is a ceramic that cannot be used as a reactive component of nanothermites. However, miniaturized particles of silicon carbide could serve as additives in nanothermites, rendering them sensitive to shock, by the conversion of crushing as result of impact into friction force. SiC particles would thus play the original role of pyrotechnic transducer.

Beloshapko *et al.* have subjected aluminum powders composed of petal-shaped particles of submicron thickness (0.25–0.5 μm) and micron planar size (20–30 μm) to the detonation of various explosive compositions. Aluminum is not incorporated in the explosive charge, but set in contact with it. The particles resulted according to this original variant of the top-down approach have spherical geometry and their composition depends on their size. The smaller particles are essentially composed of α alumina (corundum), while the larger particles contain mostly δ alumina and AlN. To explain the transformation of matter, the authors propose an interesting mechanism: due to the compression of the aluminum powder by the shockwave, the metal melts and evaporates. Aluminum then gets oxidized in contact with the oxygen contained in the firing chamber or/and in the explosive charge. The increase in temperature generated by the reaction causes the dispersion of oxide in a liquid state by evaporation or ablation. The growth of particles takes place through a mechanism of coalescence of liquid droplets [BEL 90]. Obviously, the ceramic nanoparticles obtained by Beloshapko cannot be used to formulate nanothermites, but they testify to the effect of the detonation shockwave on micro-sized aluminum. Metal vaporization through shock may allow for explaining the detonating properties of hybrid formulations [THI 11], in which synergy exists between the detonation of an explosive and the aluminothermic reaction.

A method for the detonation-based preparation of chromium oxide (Cr_2O_3) nanoparticles, which is relevant for both top-down and bottom-up approaches, was reported by Comet *et al.* [COM 11c]. This method consists of fragmenting, melting and dispersing a spongy matrix of chromium oxide by the simultaneous action of

detonation of an explosive (RDX) solidified in the oxide porosity and a hexolite charge serving as reactive confinement to the nanocomposite material RDX@Cr_2O_3 (see Figure 1.7).

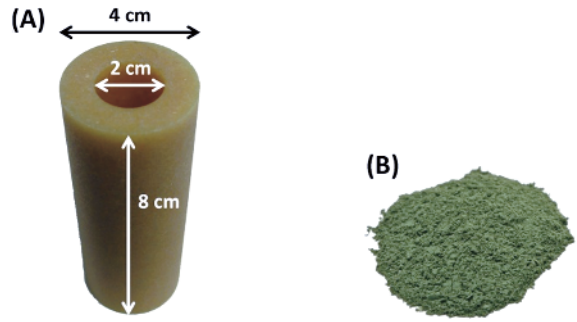

Figure 1.7. *Tubular charge of hexolite (A) used as container for the nanocomposite material RDX@Cr_2O_3 (B) used as precursor for the formation of Cr_2O_3 nanoparticles by detonation [COM 11c]*

Detonation products (see Figure 1.8(a)) contain Cr_2O_3 nanoparticles of spherical or slightly oblong form (5–50 nm) and carbonaceous species, nanodiamonds and graphite particles of crescent form, and also several impurities resulted from the erosion of the walls of the detonation chamber. Carbonaceous phases, which are a major component of detonation soots, are eliminated through an oxidation treatment (air, 500°C), which allows us to recover chromium oxide nanoparticles (see Figure 1.8(b)).

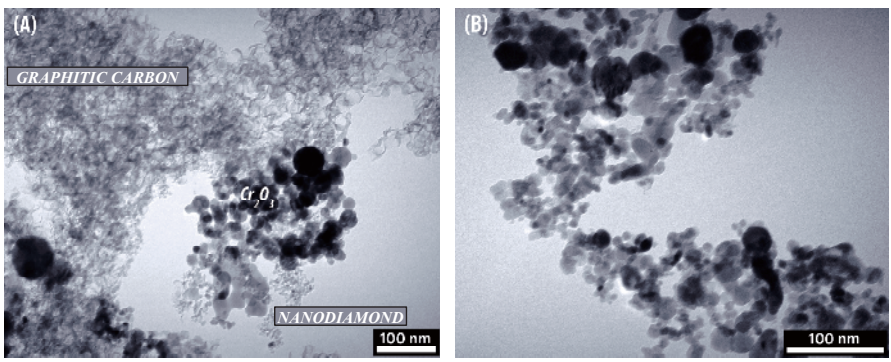

Figure 1.8. *Observation with transmission electron microscope (TEM) of products resulting from the detonation of nanocomposite material RDX@Cr_2O_3: raw soots (A) and Cr_2O_3 nanoparticles extracted from soots after purification (B) [COM 11c]*

Calculation according to Scherrer equation of the mean size of Cr_2O_3 elementary crystallites shows that these are smaller in the Cr_2O_3 of origin (19.4 nm) than in the detonation structured oxide (49.6 nm). This result is confirmed by specific surface area measurements and observations using the scanning electron microscope (see Figure 1.9), which show that Cr_2O_3 primary particles grow larger as a result of detonation. According to Fedoroff *et al.* [FED 60], TNT and RDX detonation temperatures reach 3,450 and 4,500 K, respectively. Therefore, during detonation, Cr_2O_3 is exposed to a temperature between these limits. The detonation temperature is probably closer to that of RDX, insofar as the oxide is in direct contact with this explosive within the nanocomposite material RDX@Cr_2O_3. On the other hand, according to the literature, the melting and boiling temperatures of Cr_2O_3 are 2,539 and 4,273 K. The oxide droplets formed are projected and exposed to rapid quenching in contact with the water in which the charge is fired. This explains why Cr_2O_3 elementary particles produced by detonation are larger than the oxide particles they result from.

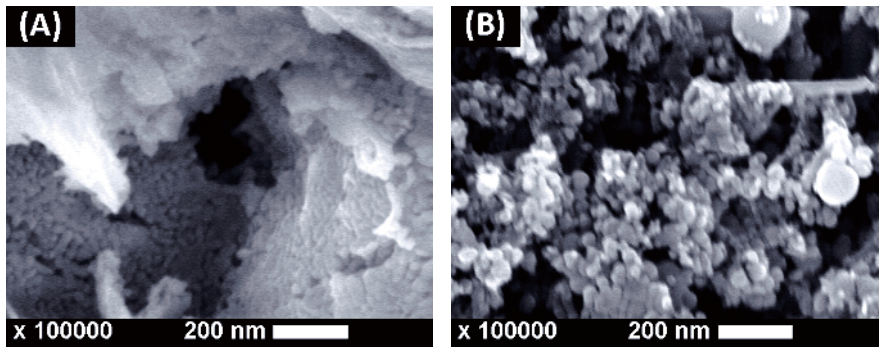

Figure 1.9. *Observation with scanning electron microscope of the morphologies of original Cr_2O_3; a) and detonation produced Cr_2O_3; b); the specific surface areas of these materials are 44.2 and 20.4 m^2/g, respectively [COM 11c]*

Granulometric measurements carried out on aqueous suspensions of detonation structured chromium oxide show that they contain a population of "free" particles of submicron and nanometric size. Moreover, the aggregates of elementary particles are smaller than those observed in the porous chromium oxide suspension (see Figure 1.10). These results show that the Cr_2O_3 particles formed by detonation are more easily dispersible than those of porous chromium oxide, though these are thinner.

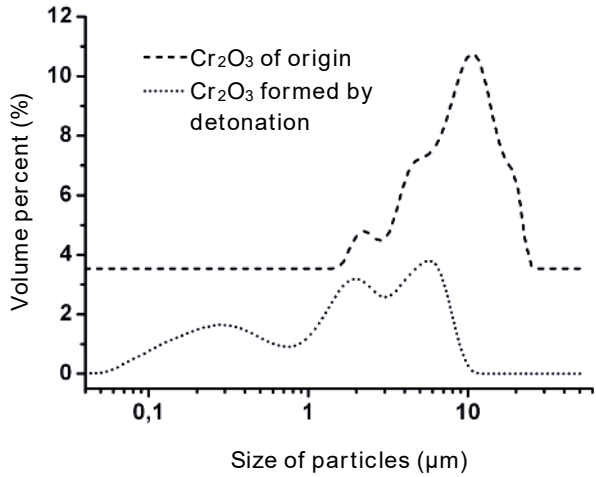

Figure 1.10. *Comparison between the size distribution of Cr_2O_3 of origin and that of Cr_2O_3 formed by detonation [COM 11c]*

Under the same compression conditions, Cr_2O_3/Al nanothermites formulated starting from chromium oxide produced by detonation densify easier than those prepared with porous oxide. This result is an additional illustration of the fact that oxide particles produced by detonation are less agglomerated. The reduction of porosity is also reflected by lower sensitivity to ignition and more regular combustion.

Sphere-shaped (5–25 nm) titanium dioxide (TiO_2) nanoparticles have been produced by the detonation of a charge composed of hexogene and ammonium nitrate containing titanyl hydroxide [QU 11]. In this case, detonation ensures dehydration and dispersion of the precursor. The formed oxide particles contain two allotropic varieties of TiO_2, rutile (65.2%) and anatase (34.8%). The authors use thermodynamic calculation to show that under the given experimental conditions, the reaction temperature obtained (2,577 K) is higher than the melting temperature of rutile (2,153 K). In their opinion, only rutile should form under these circumstances, while the presence of anatase cannot be fully explained by the detonation theory. However, according to Hanaor, rutile is the only thermodynamically stable phase of TiO_2. The formation of anatase, whose structure is less constrained than that of rutile, is facilitated by kinetics [HAN 11]. Thus, it does not seem surprising that anatase forms during the drastic quenching of the molten TiO_2 droplets dispersed by detonation. There is limited interest in the titanium dioxide as far as nanothermite formulation is concerned, since its reaction with nanosized aluminum is one of the weakest known [VAL 03].

Detonation synthesis according to the bottom-up approach consists of the formation of nanoparticles starting from a precursor taking part in the detonation reaction. Thus, nanodiamonds are produced by detonation form starting from the surplus carbon in the explosive. Anisichkin has used isotope marking to show that carbon atoms coming from the TNT molecule are preferentially transformed into diamond [ANI 07]. Frank *et al.* describe the detonation synthesis of the hexagonal variety of gallium nitride (GaN), under the form of small size (2–24 nm) nanoparticles. A primary explosive, triazidogallium, stabilized by various ligands from the trialkylamine family, was used for this purpose [FRA 98]. Many works report on the detonation synthesis of ceramics starting from nitrate-fuel types of compositions. Compositions based on ammonium nitrate have a low temperature of explosion [BÜC 00] and produce a significant quantity of gas. These two effects are particularly important for the production of materials by detonation, since they contribute to limiting the growth of nanoparticles structured by this technique. Zhi-wei Han *et al.* have thus synthesized CeO_2 nanoparticles (55 nm), intended for catalyzing the decomposition of ammonium perchlorate, by using an explosive emulsion in which the dispersed phase consisted of cerium and ammonium nitrates and the continuous phase of paraffin and an emulsifier [HAN 14]. Nitrate-based emulsions have also been used by Neves *et al.* to prepare aluminum-doped zinc oxide (ZnO) nanoparticles (AZO). The observation of formed powders by electron microscope indicates that they are composed of nanoparticles with various morphologies: spheroids, rodlets and platelets. The specific surface areas and the sizes of crystallites do not vary much with aluminum content, which distinguishes detonation synthesis from conventional methods, in which the doping level influences the size of particles. In-depth examination by scanning transmission electron microscopy shows that aluminum is uniformly distributed in the AZO particles formed, both in the ZnO structure where it replaces Zn^{2+} cations, and in the form of a mixed oxide, the gahnite ($ZnAl_2O_4$). Nanoparticles are associated as brittle agglomerates, which are dissociated by milling, using microballs. By this treatment, the specific surface area grows significantly, from 8 to 12 m^2/g [NEV 14]. Zinc oxide nanoparticles (20–50 nm) have been fabricated by detonating a complex nitrate-based emulsion containing 2% epistatic polystyrene microspheres [XIE 06a]. Due to its stability, zinc oxide cannot be used as oxidizer in nanothermites. Nevertheless, an advantage could be drawn from its piezoelectric properties [WAN 06b] in order to increase the shock sensitivity of nanothermites by transforming the energy gained by impact into electrical discharge that can initiate the reaction.

Mixed oxides have been produced by the detonation of compositions containing mixtures of metal nitrates. Thus, Xie *et al.* have prepared primary nanoparticles (20–60 nm) of lithium manganate ($Li_{1+x}Mn_2O_4$) starting from lithium and manganese nitrates. These elementary nanoparticles assemble into spherical secondary particles (1–2 µm) [XIE 06b]. Manganese ferrite ($MnFe_2O_4$) nanoparticles with sizes ranging between 5 and 30 nm have been prepared by the detonation of a complex

composition, containing iron (III), manganese (II) and ammonium nitrates. These authors propose that the material forms by a mechanism in two stages, as follows: first, nitrates are decomposed into oxides, and second, oxides associate and form the mixed oxide [WAN 08]. The use of nanostructured mixed oxides as an oxidizing phase in nanothermites seems to have been little studied until present. The association of two reactive oxides ($MnFe_2O_4$) within the same crystal structure or that of a reactive and an inert oxide provides an additional parameter, which could be used for adjusting the performances of nanothermites.

Luo *et al.* have studied an original method, which consists of the introduction of urea as ligand to the metal cation of iron (III), cobalt and nickel nitrates in order to transform these oxidizing salts into intrinsic energetic compositions. These substances are associated with secondary explosives whose role is to reinforce and support detonation. Nanoparticles (5–30 nm) of various natures have thus been produced starting from modified nickel nitrate, hexogen and paraffin. The addition of paraffin allows us to lower the oxygen balance of the explosive charge, and to define the nature of the products formed by detonation. When the oxygen balance is gradually diminished, the phases formed are nickel oxide (NiO), nickel coated with NiO and amorphous carbon, nickel coated with graphite and finally particles that contain a mixture of nickel and nickel carbide (Ni_3C) [LUO 12a]. Similar charges prepared starting from urea complexed ferric nitrate allow us to produce, by progressively lowering the oxygen balance, the following: iron oxides (25–55 nm), a mixture of iron oxide and iron, face-centered cubic iron nanoparticles (6–35 nm), then body-centered cubic iron nanoparticles (6–40 nm) [LUO 12b]. In the absence of paraffin, detonation results in nanoparticles composed of metal cores of cobalt or nickel (10–25 nm) coated with carbon layers of nanosize thickness (3–5 nm) [LUO 10a]. The nanoparticles produced starting from a ferric precursor have a core composed of iron or iron carbides (Fe_2C or Fe_3C) coated with carbon layers [LUO 10b]. Finally, Guilei *et al.* have used the detonation of a mixture of hexogen and cobalt naphthenate to produce nanoparticles of this metal. These nanoparticles have a metal core (22–56 nm) covered by a thick carbon shell (8–41 nm) [SUN 09].

"Pyrohydrolysis" induced by detonation of titanium tetrachloride ($TiCl_4$) has been studied by Ouyang *et al.* It consists of using water resulting from the detonation of a stoichiometric gas mixture of hydrogen and oxygen, initiated by electrical discharge, in order to hydrolyze the droplets of titanium tetrachloride ($TiCl_4$) sprayed in an explosion chamber. The titanium dioxide produced by this method has a mass composition of 12% anatase and 88% rutile. The material contains many nanoparticles (10–30 nm) and also highly agglomerated small particles. SEM observation of this material shows that it is composed of micron and submicron-sized particles that appear to be highly aggregated. The explanation that the authors advance for the presence of large size particles is that they are formed during the transition of the gas mixture from deflagration to detonation [OUY 08].

More recently, Yan *et al.* have used this method to prepare very small nanoparticles (1–10 nm) and non-agglomerated tin dioxide (SnO_2), starting from gaseous tin tetrachloride ($SnCl_4$). To this purpose, the explosion chamber is maintained at a temperature above the boiling temperature of $SnCl_4$ (YAN 13). Tin dioxide is obtained in a pure state, since the second product of the reaction (HCl) is a gas. This preparation mode has many advantages, which could be used in order to prepare oxides of intermediate stability, such as those composing nanothermites, in the form of weakly agglomerated ultimate size nanoparticles.

Nature	Examples	Interest
Reactive oxides	TiO_2; Cr_2O_3; Fe_xO_y; SnO_2	Moderately reactive nanothermites
Mixed oxides	$Li_{1+x}Mn_2O_4$; $MnFe_2O_4$	Adjustment of performances
Ceramics with specific properties	SiC; ZnO CeO_2	Pyrotechnic transduction Catalysis
Oxide@carbon composites	NiO@C	Desensitization
Metals@carbon composites	Fe@C; Co@C; Ni@C	Precursors of free metal oxide nanoparticles
Carbonaceous materials	Nanodiamond	Desensitization

Table 1.21. *Nature of the materials elaborated by detonation and their possible uses for nanothermite formulation*

1.3.5.2. *Deflagration synthesis*

The deflagration of confined explosive compositions, triggered by slow heating (10–20 K/min), is equally used for producing nanomaterials of various natures. This preparation mode, which is often inappropriately termed “detonation synthesis”, often leads to nanosized tubular objects, whose formation is catalyzed by metal species.

Lu *et al.* use the decomposition of picric acid for the thermolysis of ferrocene and formulation of iron nanoparticles (5–20 nm) covered by a graphite shell that effectively protects the metal core against oxidation under harsh conditions. Carbon nanotubes have also been observed in the reaction products of the ferrocene-poorest charge [LU 05]. Iron carbide (Fe_7C_3) nanocrystals encapsulated in an amorphous carbon coating have been produced by the reaction of an explosive composition consisting of a nitrated coal pitch and ferric nitrate [WU 03]. Carbon nanotubes can be produced by the explosion of compositions with a nitroaromatic compound associated with an organic metal salt. Multiwall carbon nanotubes are formed, for example, in the explosion of a mixture of picric acid and cobalt (II) acetate. The reaction of picric acid alone gives few solid products; the latter are exclusively

composed of amorphous carbon nanoparticles [LU 02]. Nanotubes having a bamboo structure have also been produced by the explosion of this same composition, in which hydrocarbons such as benzene or paraffin had been incorporated [LU 04]. The deflagration of mixtures based on dinitrobenzene (DNB) and cobalt acetate or nickel formate generates multiwall carbon nanotubes and carbon-encapsulated nanoparticles. The highest yields of nanotubes are obtained with high charging densities and DNB/cobalt acetate molar ratios [LU 03]. Finally, carbon nanobulbs have been produced by blowing of carbon nanotubes, resulting from the explosive reaction of a mixture of picric acid and nickel formate [ZHU 04]. Siegert *et al.* have proved that hollow carbon fibers with an inner diameter of about 40 nanometers could serve to desensitize MnO_x/Al ($x \approx 1.9$) nanothermites to friction, by physically separating manganese oxide from aluminum [SIE 10]. The tubular carbon structures with relatively large diameter produced by deflagration could serve for this purpose. More generally, the deflagration of explosive could be used for coating metal oxide nanoparticles with a carbon film in order to formulate nanothermites that are less sensitive to friction and electrostatic discharge.

1.3.5.3. *Combustion synthesis*

For thousands of years, man has been using fire to extract metals from ores and to process metals and ceramics. The use of the "internal fire" produced by the reaction of combustion of a substance to form a material with defined chemical nature and morphology has been studied for the first time by Berzélius in 1825, upon the discovery of the pyrophoric character of zirconium powder. There is however in nature a very common example of this method, namely wood combustion. The pyrolysis of biopolymers, cellulose and lignin produces the porous carbon structure of charcoal. The ashes resulted from complete oxidation of charcoal are nanostructured materials, composed of a cocktail of mineral oxides. Moore and Feng [MOO 95] offer an interesting chronology of the history of combustion synthesis from its start to 1995.

Various modes of combustion synthesis have been reviewed by Patil *et al.* who distinguish four types of methods: (1) self-propagating high temperature synthesis (SHS), (2) solid state metathesis reactions, (3) synthesis by flame pyrolysis and (4) synthesis starting from redox compounds or mixtures [PAT 97].

The conventional SHS method is not adapted to the production of nanomaterials, as it involves the reaction of highly heterogeneous combustible compositions, made up of particles with sizes ranging between 10 and 100 µm. Metathesis reactions serve to prepare ceramics for electronics and have to be carried out under rigorously inert atmosphere.

The synthesis by flame pyrolysis is a method used in industry for producing pyrogenated silicas such as Cab-O-Sil® or Degussa P25 titanium dioxide. This

method has been used to produce certain oxides (V_2O_5, Fe_2O_3, SnO_2, WO_2) of interest for the nanothermites [ROT 07]. According to Patil *et al.* flame pyrolysis can be used to prepare boron or refractory metal (Ti, Ta, Zr, Hf, Nb) particles that could serve as fuels for nanothermites. These materials are produced by the displacement of metal halide by an alkaline or alkaline earth metal in gas state [PAT 97].

In an updated literature review, Patil *et al.* mention catalysts and nanomaterials synthesis by solution combustion [PAT 02] and offer examples of refractory oxides that are pure, mixed or doped with metal elements elaborated by this method. Still more recently, Mukasyan *et al.* have described the specific advantages of combustion synthesis for producing nanostructured materials. First, the initial reaction medium is in liquid state, which means that reagents are homogeneously mixed at molecular scale. Second, reaction temperatures are high, which leads to pure and well-crystallized products. This specificity allows to avoid the thermal treatment, which is almost always necessary for purifying or crystallizing nanomaterials elaborated through other methods. Finally, the rapid transformation of matter and the dispersion of products in the condensed phase in the surrounding gas species contribute to limiting the particle growth, stabilizing them in divided state. The nature and morphology of the phases formed in the synthesis by solution combustion depend on the following: (1) fuel/oxidant ratio, (2) nature of the atmosphere in which it is carried out and (3) the chemical nature of the fuel and oxidant [MUK 07]. Today, the synthesis by solution combustion had been used to prepare more than one thousand complex oxides in the form of fine powders. Thin powders of pure oxides are often prepared by combustion of metal nitrates mixed with various fuels. Metal nitrates generally contain a high number of molecules of water of constitution.

The synthesis by solution combustion has been used by Lima *et al.* to produce chromium (III) oxide. Ammonium dichromate is used as precursor; it is associated with urea or glycine to form fuel-rich compositions. The proportion of oxygen in these compositions is increased by adding ammonium nitrate, so as to define fuel-rich, stoichiometric or oxidant-rich compositions. Under optimized conditions, obtained with glycine and oxygen in excess compared to the stoichiometry, Cr_2O_3 nanoparticles with a mean size of around 20 nm have been produced [LIM 06]. Yu *et al.* have nanostructured manganese oxide (ε-MnO_2) by combustion of mixtures of manganese nitrate ($Mn(NO_3)_2$) and probably of glycine ($C_2H_5NO_2$). Combustion of an excessively oxygenated mixture produces platelets with a diameter of 50–150 nm and thickness of 20–25 nm. The reaction of an insufficiently oxygenated mixture leads instead to the formation of spherical particles with a diameter of around 60 nm. In both cases, the electron micrographs presented suggest a quite strong agglomeration of ε-MnO_2 nanoparticles [YU 10]. Nagabhushana *et al.* have prepared α-MoO_3 nanoparticles by the combustion of a solution of peroxopolymolybdic acid

and sucrose, and by the combustion of another solution of ammonium heptamolybdate and DL-malic acid [NAG 14]. The observation of these materials using the scanning electron microscope shows that they are both macroporous, but the first appears to be far less agglomerated than the second. The characterization using the transmission electron microscope of the first material shows that it is formed of primary nanoparticles of small diameter (2–10 nm) that seem relatively independent one from another. However, the specific surface area of this material (≈ 4.97 m^2/g) is much lower than it would be expected, given the size of particles it is formed of. Contrary to what the authors state, it therefore seems that α-MoO_3 particles are relatively agglomerated. By using iron nitrate as oxidizer with various fuels, such as glycine, hydrazine or citric acid, Deshpande *et al.* have produced various types of iron oxide nanoparticles: α-Fe_2O_3, γ-Fe_2O_3 and Fe_3O_4, pure or in mixture. The specific surface areas of these materials (50–175 m^2/g) show that they are formed of small size primary particles, but the analysis of their morphology using the scanning electron microscope shows a strong agglomeration of these nanoparticles [DES 04]. One of the most reactive nanothermites was produced starting from bismuth oxide (Bi_2O_3) nanoparticles prepared by combustion. To this purpose, Martirosyan *et al.* have conceived an original variant of synthesis by liquid combustion, which consists of mixing pentahydrated bismuth nitrate and molten glycine. The reaction is initiated by introducing the solution in an oven that was preheated at 250°C. Nanosized (18–95.8 nm) Bi_2O_3 crystallites are formed starting from excessively oxygenated compositions, with a glycine content of only 0.05–0.4 times the stoichiometry. The lower and upper limits of fuel content are defined by non-flammability and explosibility of the solution, respectively. The crystallinity and size of Bi_2O_3 particles increase with fuel content, which is a logical consequence of the reaction temperature increase [MAR 09a].

1.3.5.4. *Conclusion*

A presentation of the characteristics of the three modes of pyrotechnic synthesis of materials of interest for the synthesis of nanothermites is provided in Table 1.22. *Detonation* synthesis allows us to form nanoparticles of refractory materials in a weakly agglomerated state. Chemical and thermal treatment is necessary in order to purify the detonation soots, which contain impurities produced by the erosion of the detonation chamber, and nanostructured carbon species resulting from partial gasification of the explosive charge. The *deflagration* of explosive compositions provides mixtures of carbon materials in various forms, which seem difficult to separate. *Combustion* synthesis allows us to produce a wide range of either pure or mixed nanosized metal oxides, under much suitable conditions than the other two methods. The low temperatures involved in the combustion synthesis seem to be best adapted to the synthesis of thermally vulnerable oxides (Bi_2O_3, CuO, MnO_2, MoO_3).

	Detonation	Deflagration	Combustion
Materials	Little reactive oxides and refractory ceramics	Carbon materials for desensitization	Pure or mixed reactive oxides
Conditions	Very rapid reactions (< 0.1 μs) Detonation chamber	Rapid reactions Manometric chamber	Slow reactions (1–100 s) Glassworks device
Advantages	Independent nanoparticles, brittle agglomerates	Polymorphic materials: metal/carbon tubes, bulbs, onions	Polyvalence, high purity materials
Drawbacks	Presence of various impurities	Mixture of phases, difficult separation	Relatively agglomerated nanoparticles

Table 1.22. *Comparison of pyrotechnic methods for the preparation of precursors that are part of the composition of nanothermites*